T.C.
DOKUZ EYLÜL ÜNİVERSİTESİ
İZMİR ULUSLARARASI BİYOTIP
VE GENOM ENSTİTÜSÜ

INVESTIGATION OF THE MOLECULAR ROLE OF *RUVBL1* GENE IN MALIGNANT PLEURAL MESOTHELIOMA

MEDİNE ZEYNEP
GÜNGÖR

DEPARTMENT OF GENOMICS AND MOLECULAR BIOTECHNOLOGY

MASTER THESIS

IZMIR-2023

Thesis Code: DEU.HSI.MSc- 2019850038

T.C.
DOKUZ EYLÜL ÜNİVERSİTESİ İZMİR
ULUSLARARASI BİYOTIP VE GENOM
ENSTİTÜSÜ

INVESTIGATION OF THE MOLECULAR ROLE OF *RUVBL1* GENE IN MALIGNANT PLEURAL MESOTHELIOMA

DEPARTMENT OF GENOMICS AND MOLECULAR BIOTECHNOLOGY

MASTER THESIS

MEDİNE ZEYNEP GÜNGÖR

Adviser: Assoc. Prof. Şerif ŞENTÜRK

(This Thesis supported by The Scientific and Technological Research Council of Turkey (TUBITAK) with grant number 221Z170.)

Thesis Code: DEU.HSI.MSc -2019850038

T.C.
DOKUZ EYLÜL ÜNİVERSİTESİ
İZMİR ULUSLARARASI BİYOTIP VE GENOM ENSTİTÜSÜ

YÜKSEK LİSANS TEZ SAVUNMA SINAVI TUTANAĞI

Dokuz Eylül Üniversitesi İzmir Uluslararası Biyotıp ve Genom Enstitüsü Genom Bilimleri ve Moleküler Biyoteknoloji Anabilim Dalı Moleküler Biyoloji ve Genetik Yüksek Lisans Programı 2019850038 numaralı öğrencisi Medine Zeynep GÜNGÖR "Investigation of the Molecular Role of RUVBL1 Gene in Malignant Pleural Mesothelioma" konulu Yüksek Lisans tezini 26.01.2023 tarihinde yapılan savunma sınavı sonucunda başarılı / ~~başarısız~~ olmuştur.

BAŞKAN
Doç. Dr. Şerif ŞENTÜRK

JÜRİ ÜYESİ
Dr. Öğr. Üyesi Yavuz OKTAY

JÜRİ ÜYESİ
Doç. Dr. Hasan Akbaba

TABLE OF CONTENTS

LIST OF TABLES **V**

LIST OF FIGURES **VI**

ABBREVIATION **IX**

ACKNOWLEDGEMENT **X**

ABSTRACT **1**

ÖZET **2**

1. AIM OF THE STUDY **3**

2. INTRODUCTION **3**

2.1. Malignant Pleural Mesothelioma (MPM) **3**

2.1.1. Histological Subtypes of MPM 4

2.1.2. MPM Epidemiology 5

2.1.3. Genetics of MPM 6

2.2 Functional Studies **8**

2.3 *RUVBL1* Gene **9**

3. TYPES OF RESEARCH **11**

4. TIME AND PLACE OF RESEARCH **11**

5. MATERIALS & METHODS **11**

5.1. Materials **11**

5.1.1. Cell Lines and Cell Culture Consumables 11

5.1.2. Plasmids 12

5.1.3. Oligonucleotides 16

5.1.4. PCR Reagents and Primers 16

5.1.5. Enzymes and Buffers for Molecular Cloning Experiments 18

5.1.6. Bacterial Strains and Reagents 18

5.1.7. Western Blot Reagents and Antibodies 18

5.1.8. Comet Assay Reagents 20

3.1.9. BrdU Assay Reagents 21

5.1.10. Senescence-Associated β-Galactosidase (SA-β-Gal) Assay 21
5.1.11. Other Chemicals, Consumables and Commercial kits 22
5.1.12. Machines and Hardware 23
5.2. Methods 24
5.2.1. Cell Culture Methods 24
5.2.2. Overexpression and gRNA Vectors Construction 25
5.2.2.1. gRNA Vectors Construction 25
5.2.2.2. pLV-EF1a-IRES-Puro Construction 26
5.2.3. Transformation of Ligated Products 26
5.2.4. Colony PCR 27
5.2.5. Mini Culture and Plasmid Isolation 27
5.2.6. Transfection and Virus Production 27
5.2.7. Infection 28
5.2.8. Competition Assay 28
5.2.9. RNA Isolation 28
5.2.10. cDNA Synthesis 29
5.2.11. Quantitative Real-Time Polymerase Chain Reaction (qRT-PCR) 29
5.2.12. Western Blot 29
5.2.12.1. SDS Gel Preparation 30
5.2.13. Immunofluorescent Staining (IF) 32
5.2.14. BrdU Assay 32
5.2.15. MTT Assay 33
5.2.16. Cell Cycle Analysis 33
5.2.17. SA-β-Gal Staining 34
5.2.18. Comet Assay 34
5.2.19. FACS Analysis and Apoptotic Assay (Annexin V) 35
5.2.20. Wound Healing 35

5.2.21. Transwell Invasion and Migration Assay 35
5.2.22. 2D and 3D Colony Formation Assay 36
5.2.23 Gene Set Enrichment Analysis (GSEA) 37
5.2.24. Study Plan and Calendar 37
5.2.25. Data Evaluation 38
5.2.26. Limitation of the Study 38
5.2.27. Ethics Committee Approval 38
6. RESULTS 38
Chapter 1
6.1. Selection of *RUVBL1* Gene and Cell Lines 38
6.2. Knockout of *RUVBL1* by CRISPR/Cas9 System 43
6.3. *RUVBL1* Depletion Reduces the Proliferation and 2D Growth Capacity of MPM Cells 43
6.4. *RUVBL1* Knockout Attenuates 3D Anchorage-Independent Growth of MPM Cells 46
6.5. *RUVBL1* Depletion Reduces Cell Proliferation and Growth via Multiple Mechanisms 47
6.6. The Impact of *RUVBL1* Depletion on Cancer Aggressive Phenotypes: Motility, Invasion and Migration Capacity 55
6.7. Overexpression of *RUVBL1* in MPM Cell Lines 57
6.8. Overexpression of *RUVBL*1 does not Affect the Proliferation of MPM Cells 59
6.9. RUVBL1 Overexpression Augments 3D Anchorage-Independent Growth of MPM Cells 59
6.10. Upregulation of RUVBL1 Enhances Cell Motility and Invasion Capacity of MPM Cells 61
6.11. Upregulation of RUVBL1 is Associated with Epithelial Mesenchymal Transition 62
6.12. CB-6644 Inhibits the Proliferation and 2D Growth Capacity

of MPM Cells **66**

6.13. CB-6644 Reduces Cell Proliferation and Induces the Apoptosis of MPM Cells **69**

6.13. CB-6644 Inhibits Cell Migration and Invasion Capacity of MPM Cells **71**

6.14. Development of RUVBL1 gRNA Resistant MPM Cells **73**

6.14.1. Engineering of Mutant RUVBL1 (mRUVBL1) Construct 73

6.14.2. Validation of mRUVBL1 in MPM Cells 74

6.14.3. gRNA Resistant MPM Cells Display Rescued 2D Growth Capacity 75

Chapter 2

6.15. Validation of Inducible System **76**

6.15.1. Obtaining Cell Clones That Express Inducible Cas9 77

6.15.2. Obtaining RUVBL1 Knockout Cell Clones 77

6.15 3. Validation of the Inducible Cas9 Expressing and RUVBL1 Knockout Clones 79

7. DISCUSSION **82**

8. CONCLUSION AND FUTURE PERSPECTIVES **86**

9. REFERENCES **87**

10. APPENDIX **93**

LIST OF TABLES

Table 1. List of the cell culture consumables 12

Table 2. List of the Plasmids 12

Table 3. List of the oligonucleotides used in this study 16

Table 4. PCR and cDNA Synthesis Reagents 17

Table 5. qRT-PCR Primers List 17

Table 6. Enzymes and Buffers used in Molecular Cloning Studies 18

Table 7. Chemical Reagents used for Bacterial Experiments 18

Table 8. RIPA Buffer Recipe 19

Table 9. Antibodies used in western blot experiments 19

Table 10. Reagents and consumables used in western blot 20

Table 11. Reagents used in Comet Assay 20

Table 12. Buffer Recipes 20

Table 13. Reagents and Antibodies for BrdU assay 21

Table 14. List of reagents used in SA-β-Gal assay 21

Table 15. Staining Solution Recipe 22

Table 16. List of Consumables 22

Table 17. List of the machines used in this study 23

Table 18. Separating gel recipe 30

Table 19. Stacking gel recipe 31

LIST OF FIGURES

Figure 1. Molecular mechanisms underlying the MPM pathogenesis 6

Figure 2. Genetic alterations of BAP1, NF2, TP53, and LATS2 genes in the TCGA cohort of MPM patients (n = 87). Data were downloaded from the cBioPortal for Cancer Genomics. 7

Figure 3. Schematic of the PAQosome Structure. Schematic representation of the PAQosome (green), known adaptors (on arrows), and client complexes (right). 9

Figure 4. pLV-EF1α-IRES-Puro vector map 13

Figure 5. pLentiCRISPR v2 vector map 14

Figure 6. lentiGuide-Hygro-dTomato vector map 14

Figure 7. pCDNA-3XFLAG-Pontin vector map 15

Figure 8. pCW-Cas9 vector map 15

Figure 9. Survival analysis results of the RUVBL1 gene in MPM, LUAD, LGG and LIHC datasets. LUAD: lung adenocarcinoma, LGG: lower-grade glioma, LIHC: liver hepatocellular carcinoma 39

Figure 10. RUVBL1 gRNA scores in H2052 and H2452 cell lines. The lower Log2 Fold Change (FC), the more depleted the gene. 40

Figure 11. RUVBL1 CRISPR gene effect of MPM cell lines. Data were taken from DepMap portal. 41

Figure 12. Competition assay results in H2052 and H2452 cells. 42

Figure 13. Western blot results of clones infected with Control gREN or RUVBL1 gRNAs. 43

Figure 14. Comparison of the viability of H2052 and H2452 cells infected with gREN and RUVBL1 gRNAs. 44

Figure 15. BrdU labeling results of H2052 and H2452 cells infected with gREN and RUVBL1 gRNAs. 45

Figure 16. Cell survival results reflected by colony formation assay. 46

Figure 17. Effect of RUVBL1 depletion on Anchorage-independent growth of MPM cells. 47
Figure 18. Cell cycle distribution of RUVBL1 depleted and control MPM cells. 48
Figure 19. Gene set enrichment analysis of MYC and E2F hallmark targets in RUVBL1 high and low MPM samples. 48
Figure 20. Senescence-associated-β-galactosidase (SA-β-gal) staining of RUVBL1-depleted and control MPM cells. 49
Figure 21. Apoptosis measurement of apoptosis by flow cytometry. 51
Figure 22. Immunofluorescent (IF) Staining of γH2AX. 53
Figure 23. Alkaline Comet Assay of RUVBL1 depleted or Control MPM cells. 55
Figure 24. Wound healing assay of RUVBL1 knockout or control MPM cells. 56
Figure 25. Representative images and quantification of Migration and invasion capacity of RUVBL1 knockout and control MPM cells. 57
Figure 26. Western blot results of clones infected with Venus or RUVBL1 inserted vector. 58
Figure 27. Western blot results of clones infected with RUVBL1 inserted vector with 4 different dilutions. 58
Figure 28. BrdU labeling results RUVBL1 overexpressing and control MPM cells. 59
Figure 29. Effect of RUVBL1 overexpression on Anchorage-independent growth of MPM cells. 60
Figure 30. Wound healing assay of RUVBL1 overexpressed and control MPM cells. 61
Figure 31. Representative images and quantification of invasion capacity of RUVBL1 upregulated and control MPM cells. 62
Figure 32. Representative images of RUVBL1 upregulated and control MPM cells. 63
Figure 33. Immunofluorescent staining of RUVBL1 upregulated or control MPM cells with Phalloidin. 64

Figure 34. The expression level of Vimentin and N-cadherin in cells with and without upregulation of RUVBL1. 64
Figure 35. Relative fold change representation of gene expression of EMT marker genes by qRT-PCR analysis. 65
Figure 36. Gene set enrichment analysis of target genes regulating the EMT phenotype in RUVBL1 low and high MPM samples. 66
Figure 37. Half maximal inhibitory concentration (IC50) values of CB-6644 in H2052 and H2452 cell lines. 67
Figure 38. Demonstration of the inhibitory effect of different doses of CB-6644 on MPM cell proliferation by BrdU assay. 67
Figure 39. Cell survival results of CB-6644 treated cells reflected by colony formation assay. 69
Figure 40. Cell cycle distribution of CB-6644 treated and control MPM cells. 69
Figure 41. Apoptosis measurement of apoptosis by flow cytometry. 70
Figure 42. Representative images and quantification of Migration and invasion capacity of CB-6644 treated and control MPM cells. 72
Figure 43. Schematic representation of the generation of RUVBL1 g2-resistant MPM cells. 74
Figure 44. Validation of RUVBL1 g2-resistant H2052 and H2452 clones by Western blot. 75
Figure 45. Colony formation analysis of gRNA resistant MPM cells. 76
Figure 46. Validation of inducible Cas9 expressing cells by western blot analysis. 77
Figure 47. Comparison of the viability of H2052 and H2452 cells infected with gREN and RUVBL1 gRNAs. 78
Figure 48. Cell survival results of RUVBL1 gRNAs or gREN infected cells reflected by colony formation assay. 78
Figure 49. Western blot analysis of time-dependent change of RUVBL1 expression in gREN or RUVBL1 gRNAs infected cells. 79
Figure 50. Validation of inducible Cas9 expressing cells by western blot analysis. 80

Figure 51. Western blot analysis of RUVBL1 expression in gREN or RUVBL1 gRNAs infected MPM cells. 80

Figure 52. Western blot analysis of time-dependent change of RUVBL1 expression in gREN or RUVBL1 gRNAs infected cells. 81

ABBREVIATION

MPM: Malignant Pleural Mesothelioma

RUVBL1: RuvB Like AAA ATPase 1

gRNA: Guide RNA

CRISPR: Clustered Regularly Interspaced Short Palindromic Repeats

Cas9: CRISPR Associated Endonuclease 9

TERT: Telomerase Reverse Transcriptase

CDK: Cyclin Dependent Kinase

RNAi: RNA Interference

SA-β-Gal: Senescence-Associated β-galactosidase

BrdU: Bromodeoxyuridine

IF: Immunofluorescent

NMD: nonsense mediated decay

MTT: 3-(4,5-Dimethylthiazol-2-yl)-2,5-Diphenyltetrazolium Bromide

qRT-PCR: Quantitative Real Time Polymerase Chain Reaction

PI: Propidium Iodide

GSEA: Gene Set Enrichment Analysis

Dox: Doxycycline

ACKNOWLEDGEMENT

Firstly, I would like to thank my supervisor, Assoc. Prof. Serif SENTURK. He has always been more than a mentor to me. I would like to thank him not only for his academic contributions but also for always making me feel his support in my 3-year adventure, helping me find my motivation when I lost it, and knowing that he was always ready to listen to me. I am grateful for making me deserve this degree.

My other thanks are not to my Lab friends, but to my family in Izmir because they became my family. Thank them for being the people I can trust endlessly. My expectation from the master's degree was not to make excellent friends but it happened (bonus). Ecü Reis (Ece Cakıroglu) is the sanest person in our lab. The person I didn't get a "don't know" answer to any of the questions I asked. With her calmness and wisdom, she became not only the first person I consulted but also my older sister. Thank her for being involved in this period of my life. I hope she can reach the places she deserves in the continuation of her academic life. Sude (Sude Eris) and Merve (Merve Uysal), I couldn't think of them separately. I bored them so much with my problems and sometimes with my tears. But I can only take down my walls beside people I feel really close to. Thank them for making me feel this warmth, trust, sincerity, and love. I also thank them for opening the doors of their homes to me during the thesis writing process. I hope they can achieve what they desire deepest. P.S. They deserve the best. I would like to thank my older sister Beng (Bengisu Uluata Dayanc), who never lost her kindness in the face of any situation, for her unsparing and unconditional love and a huge heart. I hope she always meets people like her in life and achieves everything she aims for. The fragile pole of our lab, Minenur Kalyoncu, quickly put everything in order and made our work easier. Her delicious pastries and ravioli deserve a special thanks. I wish her to reach the days when she can eat whatever she wants as soon as possible. Buse Akdemir, who is the newest of us, I just wish her less stress and more calmness. And I have a question for her: "Did your father also use to make revision?" And special thanks to dear Dilara Demirci, who is the person I learned almost everything. Maybe she is not aware of it, but I learned from her to take decisions calmly in the most critical moments, how to plan, and think systematically. It was a great opportunity for me to work with her. I wish her a happy life with her nuclear family as she rides high in her career life. Last but not least, I would like to thank to ‘Aybük

the Cat Mom' (Fatma Aybüke Mazı). She was not only my lab mate, but also my home mate for 2 years. I wish her a quieter life far from Turkey and with plenty of cats.

My next thanks go to my dear friends Ülkü Akpınar, Berivan Çelik and Tuğba Karaman. Their presence has always made me feel stronger. They have made me feel their support in every aspect so I cannot thank them enough. My dear Berivan, I would like to also thank her for her endless motivational speeches, her mother's stuffed leaves, and her sister's cakes.

I cannot thank the AHBAP İzmir family enough for making my time worthwhile in my 3 years of adventure in İzmir. I would like to thank to all Ahbap İzmir Management and volunteers, especially Yeşim Fitoz, for making me feel that there is always a hand supporting me on my shoulder. It was an honor for me to be among them.

Of course, the foremost thank is to my dear family, who were my biggest moral supporters during my master's and then my thesis writing process. When I don't want to hear negative comments, the first name I call my dear mother and my dear brothers and sisters who make me laugh the most, I couldn't have done it without them. I love them very much.

My final thanks to my best friend and confidant diary. I am writing to it only when I am unhappy, but I promise I will try to write good things from now on. Thank it for the years I spent and will spend with it.

Investigation of the Molecular Role of *RUVBL1* Gene in Malignant Pleural Mesothelioma

Medine Zeynep Güngör, Dokuz Eylul University Izmir International Biomedicine and Genome Institute, zeynep.gungor@ibg.edu.tr

ABSTRACT

Malignant pleural mesothelioma (MPM) is an aggressive and rarely treatable fatal tumor. Since no effective treatment has yet been found for MPM, which constitutes approximately 90% of all mesotheliomas, the survival time of patients is approximately 1 year after diagnosis. The mechanisms underlying the highly heterogeneous MPM carcinogenesis are not fully known. These mechanisms need to be investigated to develop effective treatment methods for MPM. In this study, the molecular role of *RUVBL1* (RuvB Like AAA ATPase 1) in MPM, which is one of the target genes we identified in the whole genome CRISPR/Cas9 screening study, which enables the elucidation of signaling pathways and mechanisms that we associate with cell survival and proliferation in MPM carcinogenesis, was investigated. Many studies on the function of RUVBL1 in cancer, known for its ATPase and ATP-dependent helicase activities, have revealed that it may have different cancer-specific functions. However, there are no studies on its molecular role in MPM carcinogenesis. As a result of the CRISPR/Cas9 screen, the 2 cell lines -H2052 and H2452- with the highest score of *RUVBL1* gRNAs were selected. The molecular functions of the *RUVBL1* gene in selected cell lines were investigated by CRISPR/Cas9-mediated depletion with the RUVBL1 gRNA and increasing the expression level. Finally, the effects of pharmacological inhibition on cell survival and aggressive phenotypes were investigated. Our findings suggested that altered RUVBL1 expression level is associated with MPM cell proliferation and cancer aggressive phenotypes. In addition, our overexpression experiments showed that increased expression level of RUVBL1 may be associated with EMT. All these studies have shown that RUVBL1 can be targeted in the treatment of MPM with further supportive research.

Key Words: MPM, RUVBL1, CRISPR/Cas9, Pharmacological Inhibition

RUVBL1 Geninin Malign Plevral Mezotelyomadaki Moleküler Rolünün Araştırılması

Medine Zeynep Güngör, Dokuz Eylul University Izmir International Biomedicine and Genome Institute, zeynep.gungor@ibg.edu.tr

ÖZET

Malign plevral mezotelyoma (MPM), agresif ve nadiren tedavi edilebilen ölümcül bir tümördür. Tüm mesotelyomaların yaklaşık 90%'ını oluşturan MPM'e yönelik etkili bir tedavi henüz bulunamadığı için hastaların hayatta kalma süresi tanıdan sonra yaklaşık 1 yıl kadardır. Oldukça heterojen özellikte olan MPM karsinogenezinin altında yatan mekanizmalar tam olarak bilinmemektedir. MPM'e yönelik efektiv tedavi yöntemlerinin geliştirilebilmesi için bu mekanizmaların araştırılması gerekmektedir. Bu çalışmada MPM karsinogenezinde özellikle hücre sağ kalımı ve çoğalmasıyla ilişkilendirdiğimiz sinyal yolakları ve mekanizmaların aydınlatılmasına olanak sağlayan, tüm genom CRISPR/Cas9 taraması çalışmasında tespit ettiğimiz hedef genlerden biri olan *RUVBL1*'in (RuvB Like AAA ATPase 1) MPM'deki moleküler rolu incelenmiştir. ATPaz ve ATP-bağımlı helikaz aktiviteleriyle bilinen RUVBL1'in kanserdeki işleviyle ilgili pek çok çalışma kanser-spesifik farklı fonksiyonları olabileceğini ortaya koymuştur. Bununla birlikte, MPM karsinogenezindeki moleküler rolü üzerine herhangi bir çalışma bulunmamaktadır. CRISPR/Cas9 taraması sonucunda *RUVBL1* gRNA'larının en yüksek skor verdiği 2 hücre hattı -H2052 ve H2452- seçilmiştir. RUVBL1 geninin CRISPR/Cas9 aracılı susturulmasıyla ve ekspresyon seviyesi arttırılarak seçilen hücre hatlarındaki moleküler fonksiyonları araştırılmıştır. Son olarak farmakolojik inhibisyonunun hücre sağ kalımı ve agresif fenotipleri üzerindeki etkileri incelenmiştir. Bulgularımız, değiştirilmiş RUVBL1 ekspresyon seviyesinin, MPM hücre proliferasyonu ve kanser agresif fenotipleri ile ilişkili olduğunu göstermiştir. Ayrıca, aşırı ekspresyon deneylerimiz, RUVBL1'in artan ekspresyon seviyesinin EMT ile ilişkili olabileceğini gösterdi. Tüm bu çalışmalar, RUVBL1'in MPM'e yönelik tedavi geliştirilmesinde hedeflenebileceğini göstermiştir.

Anahtar Kelimeler: MPM, RUVBL1, CRISPR/Cas9, Farmakolojik inhibisyon

1. AIM OF THE STUDY

Today, the identification of cancer cell models and high-throughput functional genomic screening methods has provided the appropriate environment for the discovery of new therapeutic targets. However, studies to identify genes involved in MPM survival are very limited. With this study, we aimed to investigate the molecular role of RUVBL1 in MPM carcinogenesis, which was first identified in Senturk laboratory with the CRISPR/Cas9 whole genome negative-selection screening method and predicted to be associated with survival of the MPM carcinogenesis process. Our objective is to achieve this goal through CRISPR/Cas9-mediated genetic ablation, pharmacological inhibition, and overexpression of the *RUVBL1* gene.

2. INTRODUCTION

2.1. Malignant Pleural Mesothelioma (MPM)

MPM is an aggressive and rarely treatable cancer, arising from the mesothelial lining of the pleura, the most common of malignant mesotheliomas, accounting for approximately 90% of the disease. The incidence of MPM, which is classified as a rare tumor in developed countries, has increased in the last 10 years and is expected to continue to increase in the coming years (1). According to the World Health Organization (WHO) 2020 data; approximately 25 thousand deaths occurred due to mesothelioma (2). Worldwide incidence and mortality rates of MPM vary greatly depending on asbestos use (3,4). In most of Eastern Europe, Asia, South America and Africa, its incidence is anticipated to increase in the upcoming years due to uncontrolled asbestos production and commercial use (5,6). For this reason, it can be predicted that the economic burden of MPM on health sectors will continue in the future.

2.1.1. Histological Subtypes of MPM

Histologically, mesotheliomas are categorized as epithelioid, biphasic, or sarcomatoid. Biphasic mesotheliomas are heterogeneous tumors with varying ratios of epithelioid and sarcomatoid characteristics (7). The morphology of tumor cells identifies this histologic category. Ninety percent of the cells in sarcomatoid tumors have spindle-shape and 90% of the cells in epithelioid tumors have the form of an epithelioid. However, the proportions of the two in biphasic tumors vary. Even though epithelioid MPM is often the most common histologic subtype, the relative incidence of each subtype varies depending on the research population and the kind of specimen used (8,9). It is estimated that epithelioid, biphasic, and sarcomatoid subtypes have overall prevalence rates of 61.5%, 22%, and 16.4%, respectively. Each histologic subtype has distinct characteristics and is a vital independent prognostic factor. Survival is correlated with the level of differentiation for all three categories. When compared to tumors that are well or moderately differentiated, tumors with poor differentiation have a hazard ratio of 2.5 (10).

The most promising prognosis is associated with the epithelioid subtype, the most prevalent kind of MPM (median survival 14.4 months). Both surgery and chemotherapy were proven to be beneficial for patients with epithelioid MPM (11). In rare instances, poor surgical candidates with epithelioid histology and little pleural disease might be studied before turning to chemotherapy (12). At least 10% of the cells in a biphasic tumor must be of the epithelial and spindle-shaped cell types. However, clinical behavior is impacted by the relative abundance of each cell type within biphasic tumors. According to Vigneswaran and colleagues' investigation, biphasic MPM's epithelioid differentiation level is a very reliable predictor of survival (13). Similar to this, Harling and colleagues (2019) showed that lower survival in biphasic tumors was linked to an increase in the sarcomatoid component (14). Compared to epithelioid and sarcomatoid cancers, patients with biphasic tumors have an intermediate overall survival rate (median 9.5 months, (11)). Sarcomatoid histology is connected to more advanced TNM stage and greater tumor size upon diagnosis (15). The median overall survival rate for patients with sarcomatoid tumors is the lowest of the three kinds (median 5.3 months, (11))

2.1.2. MPM Epidemiology

The underlying mechanisms of MPM carcinogenesis are multifactorial. The primary etiological factor of MPM is exposure to asbestos, which is composed of six different silicate minerals with very fine fibers, accounting for more than 80% of cases. A recurrent cycle of tissue injury and healing is generated when asbestos fibers are inhaled and move to the pleura within the pleural space. Free oxygen radicals produced when asbestos fibers are phagocytosed by macrophages result in DNA damage and aberrant repair (16). It is also known that asbestos fibers interfere with mesothelial cells, cause DNA mutations via disrupting mitosis, and alter the chromosomal structure. Inflammatory cytokines such as tumor growth factor-B, platelet-derived growth factor, and Vascular Endothelial Growth Factor (*VEGF*) are secreted by mesothelial cells exposed to asbestos, which promotes the tumor formation.

MPM is a highly heterogeneous disease at the molecular level. Several genomic analyses propose many genetic, epigenetic, and transcriptomic alterations in MPM. Currently, some recurrent genetic or epigenetic changes in MPM are well described. These molecular analyses show that MPM lacks several oncogenic events (such as *PIK3CA*, *KRAS, EGFR* and *BRAF* gene mutations) typical for other tumors, while also losing tumor suppressor genes (17).

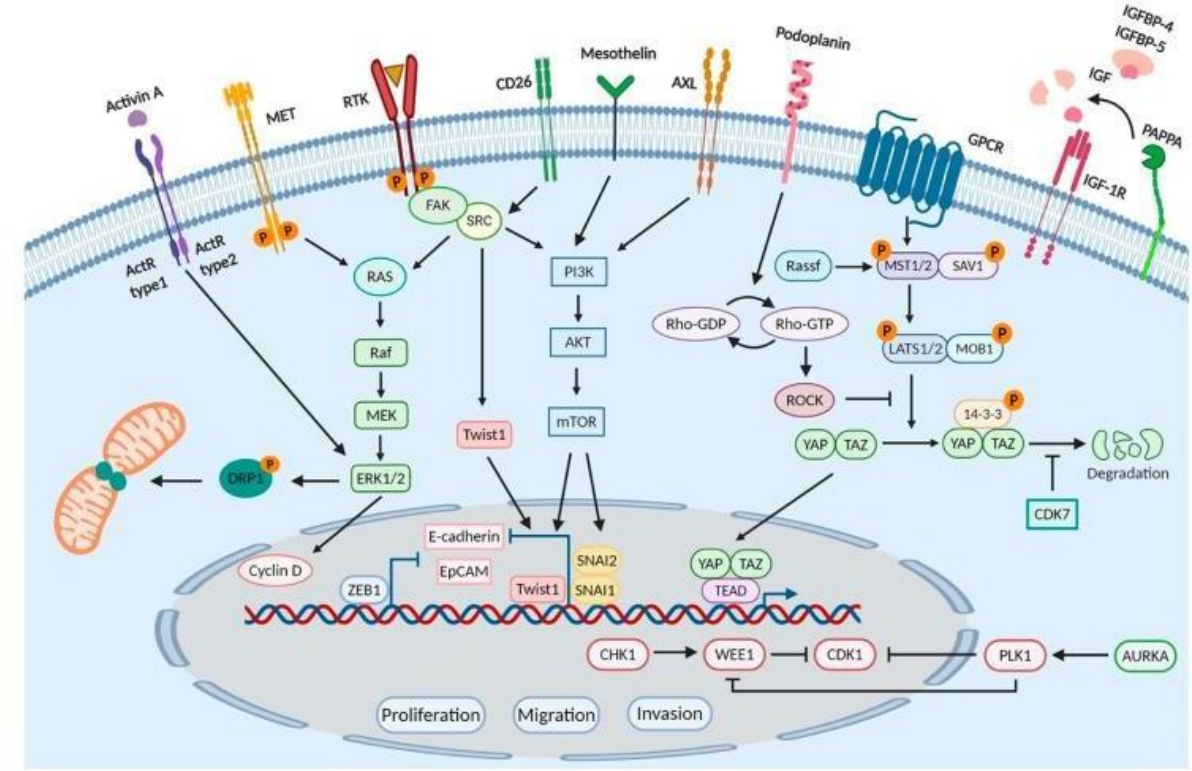


Figure 1. Molecular mechanisms underlying the MPM pathogenesis (18).

2.1.3. Genetics of MPM

In contrast to other cancers that are rich in oncogenic gains, genomic losses are more frequent in MPM carcinogenesis (18). According to preliminary karyotype and comparative genomic hybridization investigations, the most frequent losses were noted in chromosomal regions 1p, 3p, 6q, 9p, 13q, 15q, and 22q in MPM (19). In various subsequent studies, it was reported that the most common low or high-risk genetic changes for MPM were inactivating mutations in BRCA1-associated protein 1 (*BAP1*), *CDKN2A, TP53, LATS2* and *NF2* in these chromosomal regions (Figure 2) (20–24).

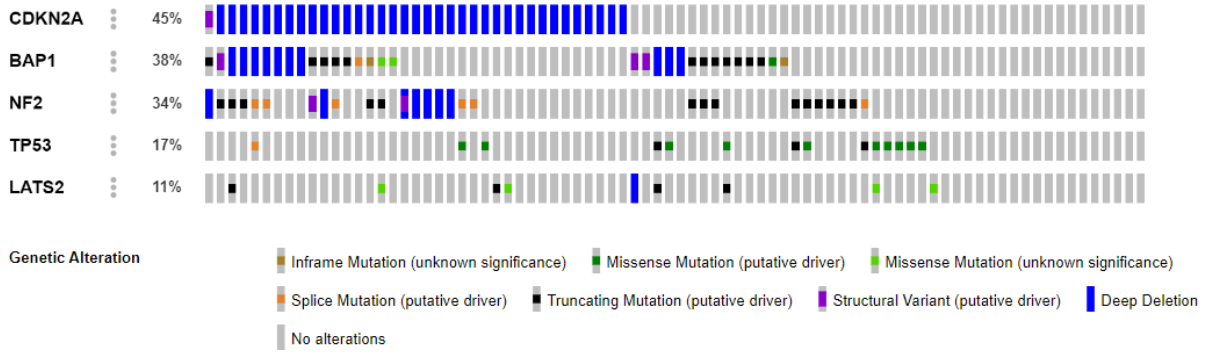


Figure 2. Genetic alterations of CDKN2A, BAP1, NF2, TP53, and LATS2 genes in the TCGA cohort of MPM patients (n = 87). Data were downloaded from the cBioPortal for Cancer Genomics.

Recurrent copy number gains are less common in MPM compared to other cancers (25–27). Chromosomal gains have been reported for numerous MPM genome regions, including 1q, 5p, 7p, 8q, and 17q. It is interesting that the early oncogenic gain of function modifications in MPM include TERT gene (telomerase reverse transcriptase) copy number increases and hotspot promoter mutations, which are typically seen in 10–15% of all cancer types. MPM patients with mutations in the TERT promoter, TP53, and NF2 have a shorter overall survival. Additionally, TERT promoter mutations often occur with CDKN2A inactivation. This makes query whether telomerase inhibitor therapy alone or in conjunction with CDK4/6 inhibitors is clinically effective. Recurrent gains in RPTOR (regulatory associated protein of mTOR complex 1), a gene with recognized oncogenic activities in colorectal cancer, have been reported in one of the most comprehensive investigations of MPM genomics. To confirm a similar biological function in MPM biology, more research is required.

Despite the well-established etiology of MPM, the diagnosis can frequently only be made at a late stage of the disease since the mechanisms underlying carcinogenesis have not yet been fully understood. The treatment of MPM is very difficult and nowadays mostly relies on multimodal (surgery, chemotherapy, and radiotherapy) and palliative treatment. However, due to the aggressive character of the tumors, the average overall survival time is approximately 13 months (28). In summary, therapeutic options beyond first-line therapy are currently very limited and the disease control rate is approximately 30% (29,30). The only next-generation treatment approach approved

in the last 17 years for the treatment of MPM is the combined drug therapy of nivolumab and ipilimumab (30). On the other hand, the last small molecule drug approved by the FDA is injectable pemetrexed, a chemotherapeutic agent similar to folic acid, which was approved in 2004 (https://www.fda.gov/media/144982/download). In a clinical phase III study in patients with advanced MPM, combination therapy of the anti-vascular endothelial growth factor antibody bevacizumab with cisplatin/pemetrexed was associated with significantly longer survival compared with chemotherapy alone. However, the systemic toxicity of this triple therapy has made the current situation a new treatment paradigm for MPM (31).

Eventually, still there is no effective targeted therapy in the treatment of MPM. In this regard, well established molecular mechanisms underlying carcinogenesis and MPM development is necessary for both diagnostic and therapeutic improvements. Therefore, it is undeniable that scientific and clinical research should go on to treat MPM holistically and effectively.

2.2. Functional Studies

High-throughput functional genomics studies are one of the important approaches used in the discovery of genes that play a role in cancer pathogenesis. Thanks to these studies, many cellular and molecular mechanisms have been identified at the gene and signaling pathway level that controls aggressive phenotypes such as cell survival, proliferation, adhesion, migration, and differentiation in different cancers (32). Recent research, using high-throughput RNAi screening for critical gene landscapes, have served to identify new therapeutic targets for the treatment of cancer(33). In mammalian cells, the CRISPR/Cas9 system-based gene-specific editing method is an effective and precise genome editing tool. Be exploiting specific gRNAs with Cas9 nuclease, this system enables the generation of double-stranded DNA breaks that lead to loss-of-function mutations. Further, genome-wide CRISPR/Cas9 screening is an effective method for identifying genes essential for the survival and proliferative ability of cancer cells (34).

2.3. *RUVBL1* Gene

RUVBL1 is an enzyme encoded by the *RUVBL1* gene that is localized mostly in the cell nucleus and has single-stranded DNA-dependent, two ATP-binding sites with ATPase and ATP-dependent DNA helicase (3' to 5') activities (35,36). However, many studies have shown the function of the RUVBL1 protein in complex assembly, indicating that it may also have chaperone-like activity. (37,38). RUVBL1 shows ATPase activity by forming ring-shaped heterohexomers with its paralog protein RUVBL2. Nuclear RUVBL1 participates in large molecular complexes such as the INO80 or PAQosome complexes that are engaged in chromatin remodeling or DNA damage repair. (39,40).

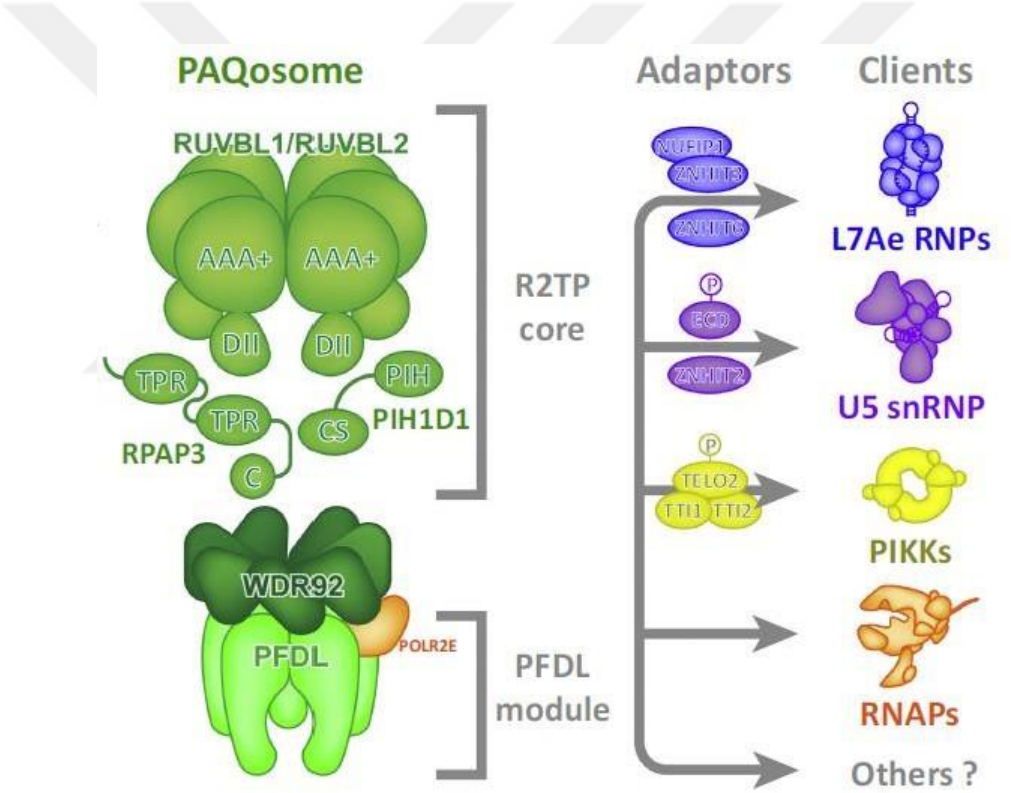


Figure 3. Schematic of the PAQosome Structure. Schematic representation of the PAQosome (green), known adaptors (on arrows), and client complexes (right) (40).

RUVBL1, required for PAQosome maturation and/or dissociation, has a role in regulation of the stability of the PIKK family of proteins as well as biogenesis of small nucleolar ribonucleoproteins and small nuclear ribonucleoproteins via the PAQosome (39). RUVBL1 effects histone acetylation, histone composition, and nucleosome

positioning, respectively, through the proteins TIP60, SRCAP, and INO80 from the INO80 family of chromatin remodelers (41,42). The function of RUVBL1 ATPase activity in these complexes is yet unclear, despite the fact that RUVBL1 appears to be essential for these complexes.

Recent studies show that RUVBL1 also has cytosolic functions such as regulation of nonsense-mediated mRNA decay (NMD). In a study, the impact of RUVBL1 knockdown on the abundance of UHG and GAS5 mRNAs, which are endogenous targets of NMD, suggested that RUVBL1 is required for NMD. This study reveals that RUVBL1 is necessary for NMD via a mechanism distinct from the regulation of SMG-1 (Nonsense Mediated mRNA Decay Associated PI3K Related Kinase) abundance, which is required for NMD (43).

RUVBL1 is involved in many cancer-related cellular processes. Recent studies revealed that RUVBL1 is essential for cellular proliferation and have been implicated as an oncogenic protein in various cancers (44,45). In a study by Yuan et al. in 2016, in a lung adenocarcinoma sample, evidence was presented showing that silencing the *RUVBL1* gene can induce arrest in the G1/S phase of the cell cycle through multiple mechanisms in lung adenocarcinoma cells (46). Yenerall and colleagues, in a comprehensive study on the ATPase activity of the RUVBL1/2 complex, reported a positive correlation between the expression level of this gene and cell proliferation (47). In another study examining the functions of the *RUVBL1* gene in ovarian cancer cells, the expression level of the gene was positively correlated with cell proliferation (48). In a similar study with hilar cholangiocarcinoma cells, siRNA-mediated silencing of the *RUVBL1* gene was shown to decrease the colony forming capacity of the cells (49).

Numerous data suggest that DNA replication stress is a significant trigger of cancer because it results in oncogene-induced DNA damage. Hristova and colleagues proposed a relationship between the changing expression level of the *RUVBL1* gene and DNA replication stress. They demonstrated that both an excess and a deficiency of RUVBL1 cause abnormal transcription dynamics that result in conflicts between replication and transcription (50).

In summary, many studies on the function of RUVBL1 in cancer have revealed that it may have context-dependent functions. Nonetheless, there are no studies on its

molecular role in MPM carcinogenesis. More importantly, the potential anti-cancer effects of this enzyme, which has a commercial inhibitor, in MPM are unknown.

In this study, we examined the effects of altered *RUVBL1* expression levels on aggressive cancer phenotype and survival in MPM cells. Our data indicated that *RUVBL1* is crucial in the aggressive phenotypes of MPM. We analyzed the protein level of *RUVBL1* in MPM cell lines. We demonstrated that *RUVBL1* suppression could significantly suppress the invasive capability of both H2052 and H2452 cell lines in vitro. We showed that overexpression of RUVBL1 can be associated with EMT, accelerate proliferation rate, and increase migration and invasion capacity of the MPM cells. Finally, in our experiments with the pharmacological inhibitor of RUVBL1, we showed that this gene is drug targetable. These results may provide a novel strategy for the development of targeted therapy for MPM.

3. TYPES OF RESEARCH

Type of research in this study is experimental.

4. TIMES AND PLACE OF REASEARCH

The study was conducted in Senturk Functional Cancer Genomics Laboratory at Izmir Biomedicine and Genome Center between August 2021 and January 2023.

5. MATERIALS AND METHODS

5.1. MATERIALS

5.1.1. Cell Lines and Cell Culture Consumables

H2052 (NCI-H2052, Cat. No: CRL5915) and H2452 (NCI-H2452, Cat. No: CRL5946) cell lines were purchased from ATCC. Hek293T Cell Line was kindly provided by Prof. Dr. Nuri Öztürk (Department of Molecular Biology and Genetics, Gebze Technical University). Consumables used in cell culture studies are listed in Table 1.

Table 1. List of the cell culture consumables

Name	Cat. No	Vendor
RPMI	B.L0498-500	BIOWEST
	21875034	Gibco
FBS	10500064	Gibco
	SV301060.03	Hyclone
Penicilin-Streptomycin	15140122	Gibco
PBS (10X)	70011036	Gibco
	SH30258.01	Hyclone
DMSO	472301	Sigma
DMEM	41965039	Gibco
Hexadimethrine bromide (Polybrene)	H9268-5G	Sigma
PEI	23966	Polyscience
Puromycin	ant-pr-1	Invivogen
Minisort Syringe Filter (0,22 um)	16532	Sartoriaus
0,45 um PES Membrane Filter	AND2545	Gilson
0.25% Trypsin-EDTA (1X), phenol red	25200-056	Gibco
TrypLE Express (-) Rhenol Red	12604013	Gibco

Cell culture plates, dishes, sterile falcon, microcentrifuge tubes, serological pipettes, and cryogenic vials were purchased from Sarstedt, Cornomics Life Sciences, Greiner Bio-One, SPL Life Science, or CAPP.

5.1.2. Plasmids

The plasmids (mainly lentiviral vectors) used in this study and their sources are shown in Table 2. In addition, the maps of the vectors used in molecular cloning experiments are shown with restriction sites.

Table 2. List of the plasmids

Name	Source
pECPV	Senturk, S. *et al.*, 2017
pLentiCRISPR v2	Addgene #52961
pLV-EF1α-IRES-Puro	Addgene #85132
pLV-EF1α-Venus-IRES-Puro	Senturk Lab
pCDNA-3xFLAG-Pontin	Addgene #51635
pCW-Cas9	Addgene #50661

pLentiGuide-Hygro-dTomato	Addgene #99376
pMD2.G	Addgene #12259
pSPAX2	Addgene #12260

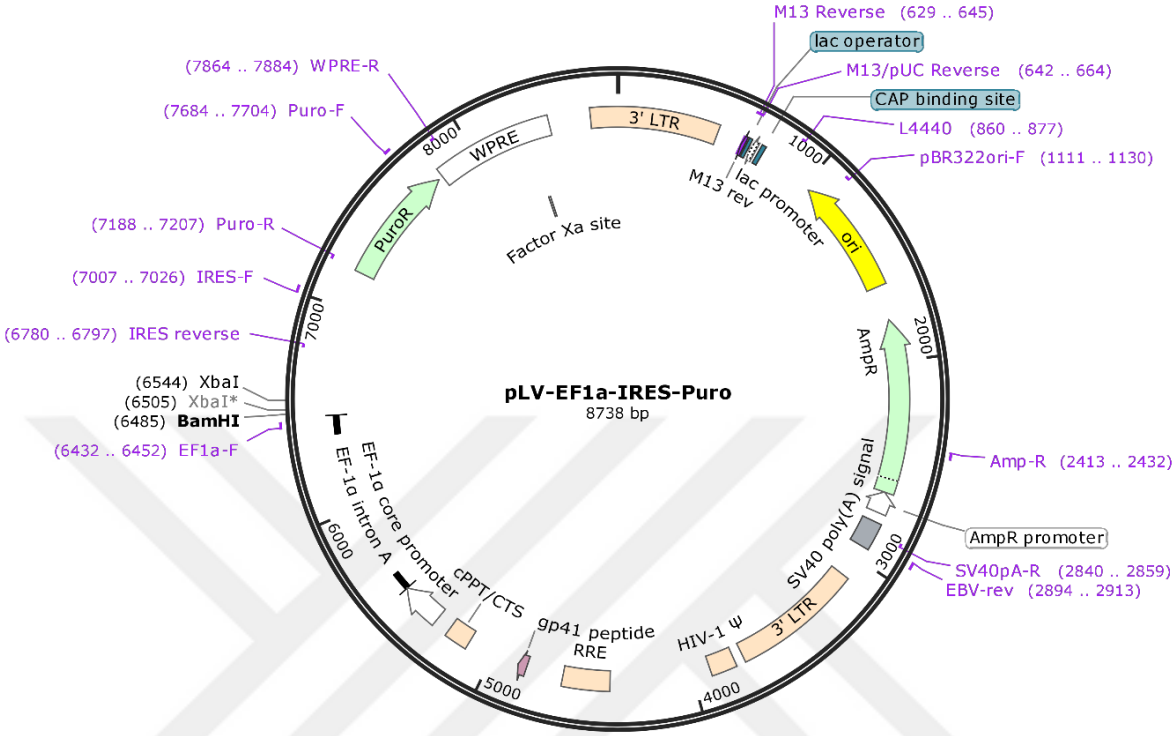


Figure 4. pLV-EF1α-IRES-Puro vector map

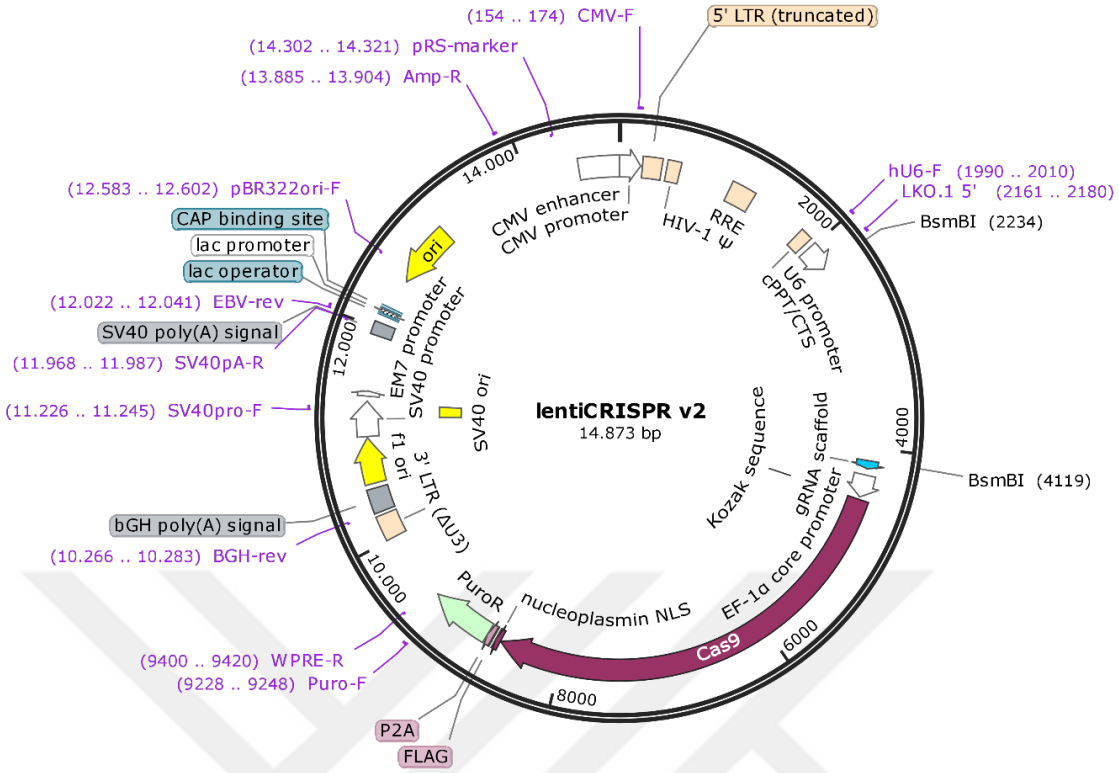


Figure 5. pLentiCRISPR v2 vector map

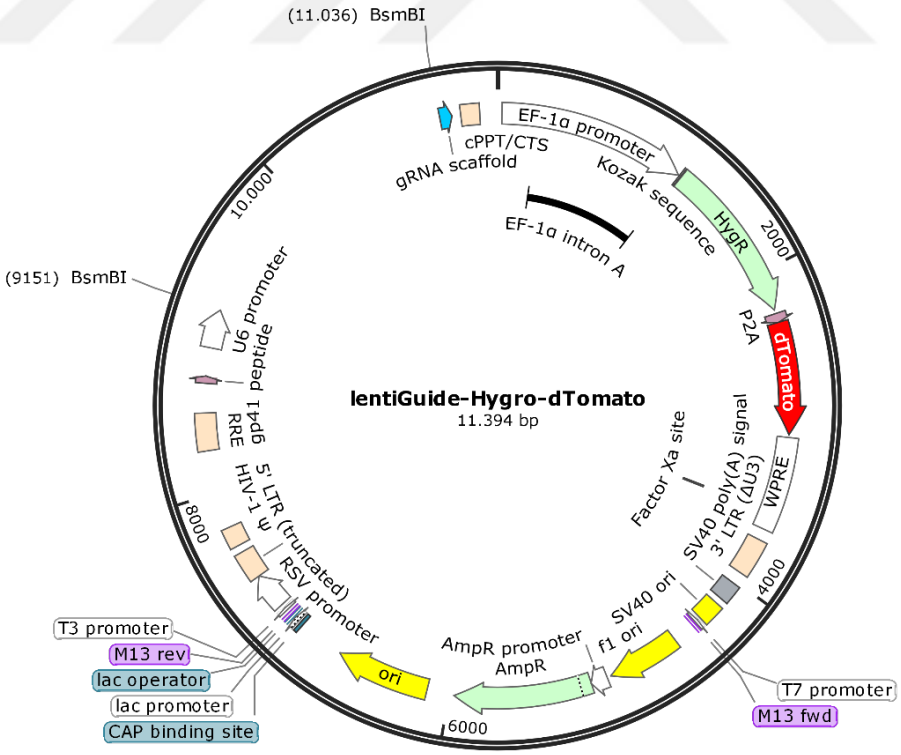


Figure 6. lentiGuide-Hygro-dTomato vector map

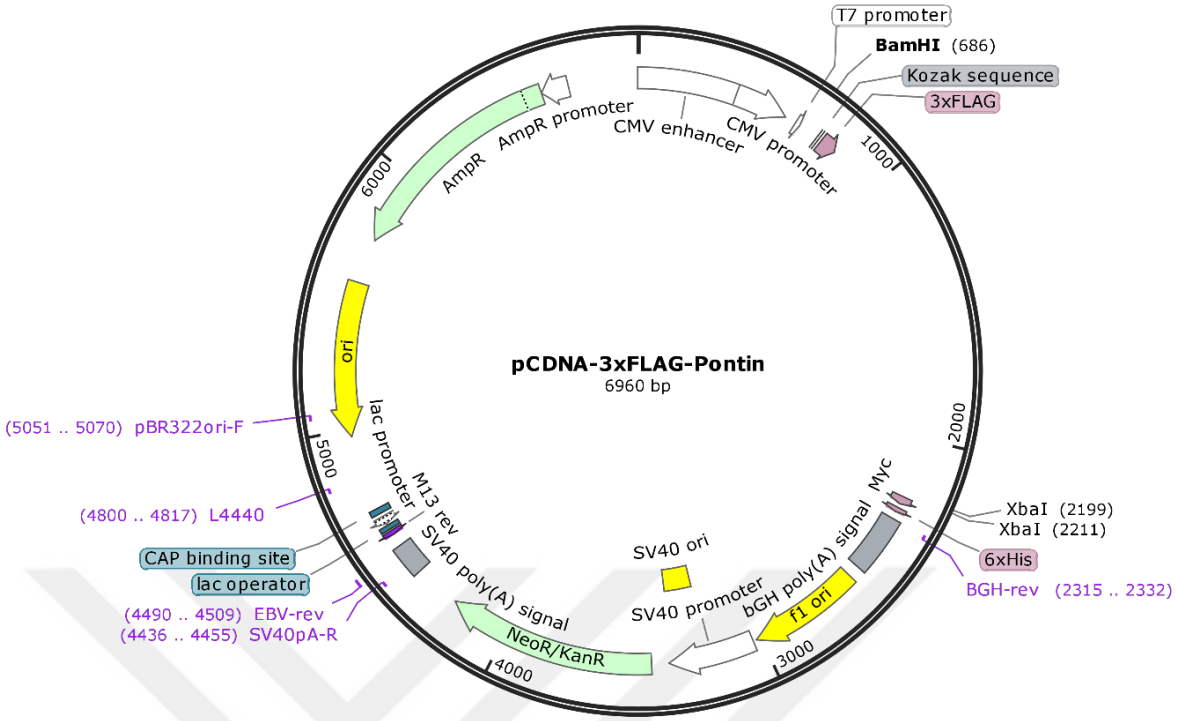


Figure 7. pCDNA-3xFLAG-Pontin vector map

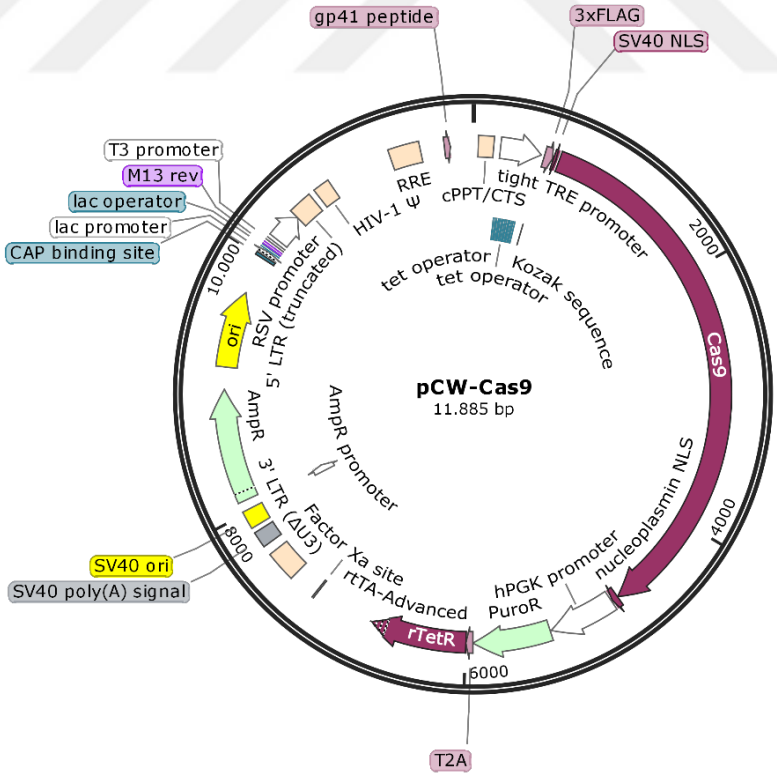


Figure 8. pCW-Cas9 vector map

5.1.3. Oligonucleotides

Oligonucleotides which were used for gRNA cloning in CRISPR/Cas9 knockout studies or rescue experiments were purchased from Macrogen (Seoul, South Korea) or Sentegen (Ankara, Turkey). RUVBL1 specific gRNA sequences were retrieved from the Brunello gRNA library (51). gREN against the Renilla luciferase gene which does not exist in the human genome was used as a negative (non-targeting) control. Oligonucleotide sequences are listed in Table 3.

Table 3. List of the oligonucleotides used in this study.

Name	**Sequence (5' - 3')**
RUVBL1 g1_F	CACCGACTACTTACCAATGGCCCTG
RUVBL1 g1 R	AAACCAGGGCCATTGGTAAGTAGTC
RUVBL1 g2 F	CACCGACTTGGATGTGGCTAATGCG
RUVBL1 g2_R	AAACCGCATTAGCCACATCCAAGTC
gREN_F	CACCGGTAGCGCGGTGTATTATACC
gREN_R	AAACGGTATAATACACCGCGCTACC
RUVBL1 F1	TCGTGAGGATCCACTAGTCCAGT
RUVBL1 R1	TATCTTGTCCCCCCTGGGGGCGTGCATTCGCAACATCCAGGTCATGCAAGGTCACATCTTGG
RUVBL1 F2	CCAAGATGTGACCTTGCATGACCTGGATGTTGCGAATGCACGCCCCCAGGGGGGACAAGATA
RUVBL1 R2	CGGCCCGTCGACTCTAGACTTAA

5.1.4. PCR Reagents and Primers

Reagents used in colony PCR and cDNA synthesis and the nucleotide sequences of the primer pairs used in qRT-PCR experiments are shown in Table 4 and Table 5, respectively. RUVBL1 g1_R, RUVBL1 g2_R and hU6_F (5'-GAGGGCCTATTTCCCATGATT -3') were used for the colony PCR experiment.

Table 4. PCR and cDNA Synthesis Reagents

Name	Cat. No	Vendor
iScript™ cDNA Synthesis Kit	1708891	Bio-Rad
BlasTaq 2X qPCR MasterMix	G891	abmgood
MicroAmp Fast 96 well Reaction Plate	4346906	Applied Biosystems
Dream Taq Hot Start DNA Polymerase	EP1701	ThermoScientific
10X Dream Taq Buffer	B65	ThermoScientific
dNTP Solution mix (10 mM each dNTP)	N0447S	NEB

Table 5. qRT-PCR Primers List

Gene	Sequence	Amplified Fragment Size (bp)
RPL41 F	GAAACCTCTGCGCCATGA	72
RPL41 R	TCTTTCTTCTTTTGCGCTTCA	
VIMENTIN F	CGTCACCTTCGTGAATACCA	169
VIMENTIN R	CCAGAGGGAGTGAATCCAGA	
E-CADHERIN F	CGAGAGCTACACGTTCACGG	162
E-CADHERIN R	GGCCTTTTGACTGTAATCACACC	
N-CADHERIN F	GGACCGAGAATCACCAAATG	141
N-CADHERIN R	AACACTTGAGGGGCATTGTC	
SNAIL F	GAAAGGCCTTCAACTGCAAA	249
SANIL R	TGACATCTGAGTGGGTCTGG	
ZEB1 F	GCCAACAGACCAGACAGTGTT	95
ZEB1 R	TTTCTTGCCCTTCCTTTCTG	
ZEB2 F	TCCTGTCTGTCTCGCAAAAA	193
ZEB2 R	GCCTTGAGTGCTCGATAAGG	
TWIST1 F	GGAGTCCGCAGTCTTACGAG	201
TWIST 1 R	TCTGGAGGACCTGGTAGAGG	
TWIST2 F	CATGTCCGCCTCCCACTA	81
TWIST2 R	CAATGGCAGCATCATTCAGA	
OCLN F	CCAAAGCCAGAAGGTGAAAC	79
OCLN R	GGATTGGATGACACATGCAC	

5.1.5. Enzymes and Buffers for Molecular Cloning Experiments

Consumables used in molecular cloning studies are listed in Table 6.

Table 6. Enzymes and Buffers used in Molecular Cloning Studies

Name	Cat. No	Vendor
BamHI-HF	R3136S	NEB
XbaI	R0145S	NEB
CutSmart Buffer	B7204S	NEB
FastDigest BsmBI	FD0454	Thermo Scientific
Fast AP (Alkalyne phosphatase)	EF0651	Thermo Scientific
10X FastDigest Buffer		Thermo Scientific
10X T4 ligation buffer	B0202L	NEB
T4 Polynucleotide Kinase (3' phosphate minus)	M0236L	NEB
T4 DNA ligase	M0202L	NEB

5.1.6. Bacterial Strains and Reagents

One Shot™ Stbl3™ Chemically Competent Cells (ThermoFisher Scientific; Cat. No:737303) were used in the bacterial transformation experiments. Chemical reagents used for these experiments were listed in Table 7.

Table 7. Chemical Reagents used for Bacterial Experiments

Name	Cat. No	Vendor
Ampicilin	A0166	Sigma
Yeast Extract	MB16401	Nzytech
LB Broth with Agar	L2897	Sigma
Tryptone	1553.03	AppliChem
NaCl	M106404.1000	Merck

5.1.7. Western Blot Reagents and Antibodies

All proteins were lysed with modified RIPA Buffer. BCA Protein Assay Kit (ThermoFisher Scientific, Cat. No: 23227) was used to determine the concentration of the proteins. The recipe of RIPA buffer is listed in Table 8.

Table 8. RIPA Buffer Recipe

for 5 mL RIPA Lysis Buffer:		Final Concentration
Triton X-100 (10%)	500 µl	1%
Na deoxycholate (10%)	250 µl	0.50%
SDS (20%)	25 µl	0.10%
Tris-Cl pH:7,4 (1M)	250 µl	50 mM
NaCl (5M)	150 µl	150 mM
EDTA pH:8 (0.5M)	10 µl	1 mM
EGTA (0.1M)	50 µl	1 mM
β-glycerolphosphate (0.5M)	100 µl	10 mM
NaF (0.5M)	100 µl	10 mM
PMSF (0.1M)	50 µl	1 mM
Na Vanadate (0.1M)	100 µl	1 mM
Leupeptin (5mg/ml)	10 µl	10 ug/ml
Aprotinin (5mg/ml)	10 µl	10 ug/ml
Pepstatin (1mg/ml)	50 µl	10 ug/ml
H2O to final volume		

Mini-PROTEAN Tetra Cell system and Mini Trans-Blot Module (Bio-Rad; Cat. No: 1658029) were used in western blot experiments. Antibodies used in western blot analyses are listed in Table 9.

Table 9. Antibodies used in western blot experiments

Antibodies	**Cat. No**	**Vendor**	**Working Dilution**
N-Cadherin (D4R1H) XP® Rabbit mAb	13116	Cell Signalling Technology	1:1000
Vimentin (D21H3) XP® Rabbit mAb	5741	Cell Signalling Technology	1:1000
Pontin/RUVBL1 (D1L8J) XP Rabbit mAb	74775	Cell Signalling Technology	1:2000
B-Actin (8H10D10) Mouse mAb	3700	Cell Signalling Technology	1:5000
Anti-Rabbit IgG (H+L) Dylight 800 4X PEG conjugate	5151P	Cell Signalling Technology	1:20000
Anti-mouse IgG (H+l) Dylight 680 conjugate	5470S	Cell Signalling Technology	1:10000

All other reagents and consumables used in the western blot experiments are shown in the Table 10.

Table 10. Reagents and consumables used in western blot

Name	Cat. No	Vendor
Cell Scraper	70-2180	Biologix
Acetic Acid	21225-2.5L-R	Sigma
APS	1610GR100	BioFroxx
BLUelf Prestained Protein Ladder	PM008/0500	GeneDirex
Bovine Serum Albumin	1126GR100	BioFroxx
β-Mercaptoethanol	8057400250	Merck
Glycine	sc29096A-500g	SantaCruz
Nitrocellulase Membrane (0.2 µm)	10600004	GE Healthcare
Panceau S	P3504-10G	Sigma
Protogel Stacking Buffer	EC-893	National Diagnostic
Protogel (Ultra-Pure) 30%	EC-890	National Diagnostic
SDS	8170341000	Merck
Skimmed Milk Powder	70166-500G	Sigma
TEMED	T22500-100	Sigma
TRIS	T1503-1KG	Sigma
Trıton X-100	T8787-100ml	Sigma
Tween-20	BP337-100	Fisher BioReagents

5.1.8. Comet Assay Reagents

Sodium lauryl sarcosinate (Sigma, Cat. No: L9150) was kindly gifted by Erkek Lab (Izmir Biomedicine and Genome Center). All the reagents and buffer recipes used in Comet assays are listed in Table 11 and Table 12.

Table 11. Reagents used in Comet Assay

Name	Cat. No	Vendor
Na_2EDTA	E5134	Sigma
NaOH	1064981000	Merck
Propidium Iodide	81845	Sigma
NaCl	1064041000	Merck
Biomax Agarose	000320PR	Prona

Table 12. Buffer Recipes

A1 (Alkaline Lysis Solution):
1.2 M NaCl
100 mM Na2EDTA

0.1% Sodium lauryl sarcosinate
0.26 M NaOH (pH > 13)
dH_2O to final volume
A2 (Alkaline Rinse and Electrophoresis Solution):
0.03M NaOH
2mM Na2EDTA
dH_2O to final volume

5.1.9. BrdU Assay Reagents

Reagents and antibodies used in the BrdU Assay are listed in Table 13.

Table 13. Reagents and Antibodies for BrdU assay

Name	Cat. No	Vendor
5-Bromo-2'-deoxyuridine	B5002	Sigma
BrdU (Bu20a) Mouse mAb	5292	Cell Signalling Technology
Dnk pAb to Ms IgG Alexa Flour 488	ab150105	Abcam
Hydrocloric acid fuming 37%	1003172500	Merck
DAPI for mb	1322MG005	Neofroxx
Microscope Cover Glasses 18 mm	111580	Marienfeld
Microscope Cover Glasses 12 mm	111520	Marienfeld

5.1.10. Senescence-Associated β-galactosidase (SA-β-Gal) Assay

Reagents, and the recipe for fixative and staining solutions used in the SA-β-Gal experiment are shown in Table 14 and Table 15, respectively.

Table 14. List of reagents used in SA-β-Gal assay.

Name	Cat. No	Vendor
Glutardialdehyde Solution	820603.1000	Merck
Formaldehyde solution	F1635	Honeywell
Citric Acid Monohydrate	9100461000	Isolab
Sodium phosphate dibasic dihydrate	4272	Sigma
Potassium hexacyanoferrate (II) trihydrate (ferro)	LC-10061.1	Neofroxx
Potassium hexacyanoferrate (III) (ferri)	LC-6423.3	Neofroxx
Sodium Chloride	1064041000	Merck

Magnesium chloride hexahydrate	LC-5041.4	Neofroxx
PBS (1X)	10010-015	Gibco
X-Gal for mb	1168GR001	Neofroxx

Table 15. Staining Solution Recipe

Fixative Solution (for 10 ml solution)	
25% Glutardialdehyde solution	80 µl
37% Formaldehyde	500 µl
PBS (1X)	9420 µl
200 mM citric acid/Na phosphate buffer (for 40ml) pH: 6	
citric acid (0,2 M)	7.37 ml
sodium phosphate dibasic dihydrate (1 M)	5.052 ml
dH_2O to final volume	
Staining Solution (for 10 ml solution)	
200 mM citric acid/Na phosphate buffer	2 ml
100 mM potassium ferrocyanide	500 µl
100 mM potassium ferricyanide	500 µl
2 M NaCl	750 µl
100 mM $MgCl_2$	750 µl
(1 mg) X-gal in dimethyl formamide	250 µl
dH_2O to final volume	5.75 ml

5.1.11. Other Chemicals, Consumables and Commercial Kits

Chemicals, consumables, and commercial kits used in this study are listed in Table 16.

Table 16. List of Consumables

Name	**Cat. No**	**Vendor**
FITC Annexin V Apoptosis Detection Kit with PI	640914	Biolegend
NucleoSpin Gel and PCR Clean-up	740609.50	MN
Monarch Total RNA Miniprep Kit	T2010S	NEB
EZ-10 Spin Column Plasmid DNA Miniprep Kit	BS614.0612R0C	BioBasic
Phalloidin	A22287	Invitrogen
CB-6644/1MG	36125.1MG	CAYMAN
Matrigel® Basement Membrane Matrix, LDEV-free	356234	Corning
Permeable Support for 24-well Plate with 8.0 µm Transparent PET Membrane, Sterile	353097	Falcon

Gel Loading Dye, Purple (6X) - 4,0 ml	B7024S	NEB
Ultrapure Distiled Water 500 ml	10977-035	Invitrogen
Methanol HPLC Grade	20864320	VWR
Crystal Violet	C6158	Sigma
Thiazoly blue tetrazolium bromide (MTT)	1334GR001	Neofroxx
Absolute Ethanol	9200262500	Isolab
2-Propanol	24137	Sigma
Noble Agar, Ultrapure, Thermo Scientific	J10907-100gr	Alfa Aesar
Rnase A	1263MG050	Neofroxx
1 kb DNA Ladder	N3232S	New England Biolabs
10 ml/cc Steril Enjektör		Genject
Polystyrene Round Bottom Tube w/cell-strainer cap	352235	Falcon

5.1.12. Machines and Hardware

Machines and hardware used in this study are listed in Table 17.

Table 17. List of the machines used in this study

Machine	**Vendor**
pH Meter	HANNA Instruments
Toploader Balance 820 g x 0.01g	Sartorius
MicroCL 17 Microcentrifuge (Ventilated) 230V with Hematocrit rotor	ThermoFisher Scientific
SimpliAmp™ Thermal Cycler	Applied Biosystems
Owl™ EasyCast™ B1A Mini Gel Electrophoresis Systems	ThermoFisher Scientific
microwave oven	Beko
mySPIN™ 6 Mini Benchtop Centrifuge	ThermoFisher Scientific
Vortex Mixer	ThermoFisher Scientific
Basic Power Supply	Bio-rad
PowerPac Universal power supply	Bio-rad
Hotplate Stirrer Thermolyne	ThermoFisher Scientific
Waterbath	Nuve
Centrifuge 5810R	Eppendorf
Centrifuge MicroCL 17R	ThermoFisher Scientific
Incubator MaxQ 4000	ThermoFisher Scientific
Confocal Microscopy	Zeiss LSM880
ABI 7500 Fast Thermal Cycler	ThermoFisher Scientific
LI-COR Odyssey Imaging System	LI-COR
NanoDrop 2000	ThermoFisher Scientific
Multiskan GO Microplate Spectrophotometer	ThermoFisher Scientific
BD LSRFortessa™ flow cytometer	BD Biosciences

CKX41 Inverted Microscope	Olympus
BX61 Fully Motorized Fluorescence Microscope	Olympus
Gel Doc XR+ System with Image Lab Software	Bio-rad

5.2. METHODS

5.2.1. Cell Culture Methods

Cell lines were maintained at 37°C and 5% CO_2 culture conditions. Hek293T cells were cultured in High Glucose DMEM supplemented with 10% FBS and 1% penicillin–streptomycin (complete DMEM). H2052 and H2452 cells were cultured in High Glucose Roswell Park Memorial Institute Medium (RPMI) supplemented with 10% FBS and 1% penicillin–streptomycin (complete RPMI).

For thawing, one vial of frozen cells was taken out of the nitrogen tank or 80°C freezer and put in a 37°C water bath until there was only a small piece of ice remaining in the vial. Then, thawed cells were put into a 15-ml Falcon tube with 9 ml of growth media, and spun for two minutes at 1800 rpm in a tabletop centrifuge. After the supernatant was discarded, the cell pellet was resuspended in full growth media and then transferred to the proper cell culture dish. Every cell line was routinely examined for mycoplasma contamination and found to be clear (52).

For subculturing, the medium was suctioned, and cells were washed with 1X PBS. After the trypsinization with TrypLE or trypsin, cells were harvested with the complete medium in a 15 ml falcon tube and centrifuged at 1800 rpm for about 2 min in a tabletop centrifuge. Cells were partied in a proper ratio based on the confluency and seeded in a cell culture plate or dish. If a certain number of cells will be seeded the cell pellet was resuspended in a complete medium and 10 µl of the cell-medium mix was loaded into both chambers of the hemocytometer to be counted. Then, a determined number of cells were seeded into a dish or plate after performing the requisite dilutions.

For cryopreservation, cells grown in 10-cm dishes were rinsed with phosphate-buffered saline (PBS), trypsinized, and collected with 5 ml of RPMI media in a 15-ml Falcon tube. The collected cells were centrifuged in a tabletop centrifuge for two minutes at 1800 rpm and the supernatant was discarded. Next, the pellet was resuspended in a freezing medium prepared in the respective cell culture medium supplemented with

20% FBS and 8% DMSO. Then cells were transferred to cryovial tubes which were stored at −80°C freezer for short-term or liquid nitrogen for long-term storage (52).

5.2.2. Overexpression and gRNA Vectors construction

5.2.2.1. gRNA Vectors construction

The following protocols were applied for the cloning of two different RUVBL1 targeting gRNA sequences, which we selected from the Brunello gRNA library, into lentiviral plasmids pLentiGuide-Hygro-dTomato, pECPV and pLentiCRISPR v2.

Digestion and Dephosphorylation of Plasmids

5 µg of plasmid was digested and dephosphorylated with 3 µL BsmBI and 3 µL FAST AP enzymes in 6 µL 10X Fast Digest Buffer and an appropriate volume of distilled water at 37°C for 2 hours. The products were run on 0.8% agarose gel. The digested plasmids were extracted from the gel by the NucleoSpin Gel and PCR Clean-up kit.

Phosphorylation and Annealing of Oligos

As a result of CRISPR/Cas9 whole genome negative-selection screening, two different *RUVBL1* gRNAs selected from the Brunello gRNA library, with a gRNA score of more than 80% depletion and which we know to be functional, were phosphorylated with 0.5 µL T4 PNK enzyme and 1 µL 10X T4 Ligation Buffer according to the optimized protocol and incubated for ligation of forward (100 µM) and reverse oligos (100 µM) at appropriate temperatures. Thermocycler parameters are shown below. The obtained products were diluted 1/20 and made ready for use for the next ligation step.

Thermocycler parameters:

37°C 30 min

95°C 5 min and ramp down to 25°C at 5°C/min

Ligation of oligo duplex to digested plasmids

50 ng of the digested plasmids were ligated with the annealed gRNA duplexes by incubating them with 0.5 µl T4 Ligase and 1 µl T4 ligation buffer at 25˚C for 2 hours.

5.2.2.2. pLV-EF1a-IRES-Puro construction

Digestion of pCDNA 3x-FLAG Pontin and pLV-EF1a-IRES-Puro plasmids

Both mammalian pCDNA 3x-FLAG Pontin and lentiviral pLV-EF1a-IRES-Puro plasmids were cut with BamHI and XbaI enzymes. Reaction setup for both plasmids is shown below.

BamHI-HF	0.5 µl
XbaI	0.5 µl
CutSmart Buffer	1 µl
Plasmids	2 µg
dH_2O	to 10 µl

The products were run on 1% agarose gel and corresponding bands, 3x-FLAG Pontin and pLV-EF1a-IRES-Puro backbone, were extracted from the gel by the NucleoSpin Gel and PCR Clean-up kit.

Ligation of 3x-FLAG Pontin and pLV-EF1a-IRES-Puro backbone

3x-FLAG Pontin and pLV-EF1a-IRES-Puro backbone were ligated at 25˚C for 2 hours in a 3:1 (insert: vector) ratio with the vector being 50 ng in the reaction. Reaction setup is shown below.

3x-FLAG Pontin (1513 bp)	26.25 ng
pLV-EF1a-IRES-Puro backbone (8679 bp)	50 ng
T4 DNA Ligase	0.5 µl
10X T4 ligation buffer	1 µl
dH_2O	to 10 µl

5.2.3. Transformation of the ligated products

For bacterial transformation, 50 µl of Stbl3 competent E. coli strain and the entire ligated product were incubated on ice for 30 minutes. Then it was incubated at 42˚C for 45-60 seconds (heat shock) and put on ice for 2 minutes again. Then, 1 mL

of LB medium was added to the tube and incubated at 37˚C for 1 hour (recovery). Finally, bacteria were centrifuged, the excess medium was discarded, and pellet was spread on LB Agar containing 100 µg/ml Ampicillin. Plates were incubated for 18-20 hours at 37˚C and at least 3 colonies were picked to perform colony PCR.

5.2.4. Colony PCR

To confirm the cloning efficiency, colony PCR was performed by selecting at least 3 colonies from each LB Agar plate containing the relevant plasmid. For this, the selected colony with the tip was swirled in a reaction tube including 2 µl of 10X Taq Buffer, 0.4 µl of dNTP, 0.8 µl of F+R Primer mix, and 0.1 µl Taq polymerase. Then selected colonies were dropped in 5 ml LB medium with ampicillin and incubated at 37˚C for 18-20 hours. PCR was run with the following parameters and the PCR product was visualized a 2% agarose gel.

Thermocycler parameters:

Step	Temp.	Time	Number of Cycle
Inıtial Denaturation	94°C	5 min	1
Denatturation	94°C	30 sec	
Annealing	60°C	30 sec	30
Extension	72°C	2 min	
Final Extension	72°C	5 min	1

5.2.5. Mini Culture and Plasmid Isolation

Colonies were grown in 5 ml LB media with ampicillin for 18-20 hours at 37˚C and 225 rpm shaker. Bio Basic EZ-10 Spin Column Plasmid DNA Miniprep Kit protocol was followed for plasmid DNA isolation.

5.2.6. Transfection and Virus Production

Hek293T cells were used to package the lentiviral particles. At t=0h cells were transfected with target vector and helper plasmids by using PEI transfection reagent. For each target vector, PEI reagent protocol was performed. Total of 6 µg plasmid were

mixed with 1X PBS. In another tube PEI and 1X PBS were mixed in a microcentrifuge tube in a 1:10 ratio, respectively. PEI+1X PBS and DNA+1X PBS mixtures were both 300 µl in final volume. Two tubes were mixed and incubated at room temperature for 25 minutes. Hek293T cells that were 80% confluent in a 60 mm dish were rinsed with 1X PBS and 2.4 ml of complete DMEM was added. Following incubation, 600 µl mixture was added, drop by drop, to the 60 mm dish. At t=48h the medium of Hek293T cells (3 ml) was collected and filtered by using 0.45 µm PES membrane filter, then stored at -80˚C. For lentivirus production, psPAX2 and pMD2.G vectors were used as a helper. The target vector, psPAX2, pMD2G vectors were mixed in a 4:2:1 ratio, respectively, for a total of 6 µg DNA.

5.2.7. Infection

150,000 cells were seeded into appropriate cell culture dish or plate. 8 µg polybrene was added after the virus-containing medium had been diluted in a 1:5 ratio. This medium was added to the cells to be infected. Cells were exposed to the virus for 48h. After that cells were rinsed twice with 1X PBS and selection medium containing 2 µg/ml Puromycin was added to the cells. After 3 days, the selection medium was removed, and complete medium was added. The emerging Puromycin resistant cells were cultivated, and the cell stocks were taken.

5.2.8. Competition Assay

gREN, RUVBL1 g1, and RUVBL1 g2 gRNAs were cloned into the pECPV backbone and virus packaging was performed. Then, H2052 and H2452 cells were infected with virus particles (virus dilution: 1/10) and Venus positivity was measured by flow cytometry on days 0 (day 5 post-infection), 4, and 8. The percentage of Venus+ cells on day 0 was normalized to 100% and the measurements of the following days were normalized accordingly.

5.2.9. RNA Isolation

Trypsinized cells were collected in the 1.5 ml tubes and centrifuged at 1800 rpm for 2 minutes. After the medium was discarded and the pellet was rinsed with 1X PBS, the centrifugation step was repeated. RNA isolation was performed using the Monarch

Total RNA Miniprep Kit. Concentrations of isolated RNAs were measured using Nanodrop and diluted to a concentration of 100 ng/µl for each sample.

5.2.10. cDNA Synthesis

cDNA synthesis from the RNA was performed by iScript cDNA synthesis kit. For each reaction, a mixture of 4 µl iScript reaction mix (5X), iScript reverse transcriptase, 5 µl nuclease-free water, and 10 µl RNA (1µg) was prepared. The mixtures were placed in the thermal cycler to synthesize cDNA in the conditions shown below. Samples were diluted 4.2X by nuclease-free water and stored at -20˚C.

Application	Duration	Temperature
Priming	*5 min*	*25 ˚C*
Reverse Transcription	*20 min*	*46 ˚C*
Reverse Transcriptase Inactivation	*1 min*	*95 ˚C*

5.2.11. Quantitative Real-Time Polymerase Chain Reaction (qRT-PCR)

Reaction mixes were prepared with 5 µl SYBR Green Master mix (2X), 0.4 µl forward primer (10 µM), 0.4 µl reverse primer (10 µM), and 4.2 µl cDNA (1 µg) for each sample. Prepared mixtures were loaded onto MicroAmp Fast 96 well Reaction Plate as 3 technical replicates of each sample. The qRT-PCR experiment was performed at the Applied Biosystems 7500 Real-Time PCR System. C_t values of genes of interest were used to calculate relative gene expression to the internal control (RPL41). Calculation is shown below (52).

Relative gene expression = 2 ^ (-ddCt)

5.2.12. Western Blot

For protein isolation, cells were taken on ice and rinsed once with ice-cold 1X PBS. Appropriate amount of RIPA lysis buffer was added to the plates and the cells were scraped with a scraper. Samples collected in 1.5 ml Eppendorf tubes were incubated on ice for 30 minutes, vortexing every 10 minutes. Following the incubation, the samples were centrifuged at maximum speed at +4˚C for 30 minutes. The supernatant was transferred to new tubes and placed at -80˚C for long-term storage.

For determination of protein concentration, BCA assay was performed by using BCA Protein Assay kit. Firstly, the albumin standards were prepared via serial dilution with RIPA buffer following concentrations: 1000, 500, 250,125, 62.5, 31.25 µg/ml. To a 96-well plate, 2 µl were added in triplicate from each sample, starting with Albumin standards. RIPA lysis buffer was used as blank. Then, 50 µl of solution b: solution a mixture prepared at a ratio of 1:50 was added to each sample, including the blank. Plate covered with aluminum foil to protect from light was incubated at 37˚C for 30 min. At the end of the incubation, absorbance was measured at 562 nm using the Multiskan GO Microplate Spectrophotometer. After the absorbance of Blank was removed from all samples, a standard curve was plotted according to the absorbance values of albumin at different concentrations at 562 nm. According to the standard curve, the concentrations of each sample were determined by the Varioskan software.

Samples whose concentrations were determined were equalized with RIPA buffer to the one with the lowest concentration. An equal amount of 5X Laemmle buffer was added to all samples and boiled at 95˚C for 5-10 minutes. Prepared samples were used immediately for western blot or placed at -20˚C for short-term storage.

5.2.12.1 SDS Gel Preparation

The contents and recipes of the stacking gel, and separating gel were prepared according to the molecular weight of the protein which will be checked are shown in Table 18 and Table 19.

Table 18. Separating gel recipe

Components (for 5 ml)	**6%**	**8%**	**10%**	**12%**	**15%**
Protogel (ml)	1	1,35	1,65	2	2,5
dH_2O (ml)	3.375	3.025	2.725	2.375	1.875
Main gel buffer (ml)	0.625				
10% APS (µl)	25				
TEMED (µl)	5				

Table 19. Stacking gel recipe

Components (for 2 ml)	
Protogel (ml)	0.25
ddH_2O (ml)	1.25
Protogel stacking buffer pH:6.8 (ml)	0.5
10% APS (µl)	12.5
TEMED (µl)	2.5

After the separating gel was prepared according to the recipe in Table 18, it was filled between western glasses, and 60% isopropanol was added to polymerize it in a flat line. After the gel was frozen, the isopropanol was removed, and the western glasses were thoroughly dried with a napkin. Stacking gel prepared according to Table 19 was filled on the separating gel and a comb was placed between the western glasses. After the stacking gel polymerized, the comb was removed, and the running system was set up. After the system was filled with Running buffer, 20 µg of sample was loaded into each well of the gel with the protein ladder in the first well.

The samples were run at 90 V for about 20-30 minutes until they were passed to the separating gel. The voltage was then set to 120V and continued to be running until the protein ladder was properly opened. After the running process, the stacking part of the gel was discarded and a sandwich system was prepared with the separating part of the gel, nitrocellulose membrane, filter paper, and sponges. This sandwich was placed in the tank and 1X transfer buffer containing 20% ethanol was added. The transfer was completed in 90 minutes at 350 mA. After the transfer process was completed, the membrane was stained with Ponceau S, and it was confirmed whether the transfer was successful.

For blocking, the membrane was incubated in 5% milk powder dissolved at 1X tbs for 1 hour at room temperature by shaking at 20 rpm. Then the membrane was rinsed 3 times with 1X TBS-T and the milk powder was completely removed. For blotting, the membrane was incubated overnight with the antibody prepared at appropriate dilution in 1% BSA and 1X TBS at +4˚C. At the end of the blotting, the membrane was washed 3 times for 10 minutes with 1X TBS-T by shaking at 50 rpm. Then, it was incubated in the dark with the secondary antibodies prepared in the appropriate dilution at room

temperature for 1 hour. Finally, the membrane was washed 3 times with 1X TBS-T and 1X TBS was added and imaged at 700 and/or 800 channels on a LI-COR device.

5.2.13. Immunofluorescent Staining (IF)

15,000 cells were seeded in triplicate on 12 mm coverslips placed in each well of 24-well cell culture dishes on post infection day 10. After 2 days, the medium was removed, and the cells were washed 2 times with 1X PBS. Then, the cells were fixed by incubating with 4% formaldehyde prepared in 1X PBS for 10 minutes. After fixation, cells were washed with 1X PBS 3 times for 5 minutes and incubated for permeabilization with 0.5% Triton-100 in 1X PBS for 5 minutes with shaking. It was then incubated with 5% BSA in 1X PBS for 1 hour at room temperature with shaking, and the washing step was repeated. 12 µl of γH2AX primary antibody prepared at a 1:500 ratio with 1% BSA and 1X PBS was added to the coverslips and incubated at room temperature for 1 hour. Then, the washing steps were repeated and 12 µl of secondary antibody prepared at a ratio of 1:500 with 1X PBS containing 1%BSA was added to each coverslip and incubated at room temperature for 1 hour. After incubation, cells were washed again 3 times with 1X PBS and stained with DAPI for 1 min. Finally, the cells were rinsed with dH_2O, and the coverslips were mounted on the slide. Confocal Microscope was used to visualize cells.

5.2.14. BrdU Labeling

An appropriate number of cells were seeded in triplicate on coverslips placed in each well of 24-well cell culture dishes and labeled with 30 µM BrdU for 12 hours. To perform BrdU staining, cells were washed with 1X PBS two times and fixed on ice with 70% cold ethanol for 10 minutes. After fixation, cells were washed again with 1X PBS 3 times for 5 minutes followed by incubation with 2N HCl for 20 minutes to facilitate DNA denaturation. After the washing steps were repeated the coverslips were incubated with the anti-BrdU primary antibody (1/1000 dilution) for 2 hours at room temperature. After PBS washes, cells were incubated with a secondary antibody, anti-mouse Alexa Fluor 488, at room temperature for 1 hour. Finally, cells were stained with DAPI for 1 minute and the coverslips were mounted on a slide and viewed under a fluorescent microscope (52). The percentage of proliferative cells was calculated as

the number of BrdU labeled cells over the total number of DAPI-positive nuclei in min 8 fields randomly counted in the microscope field (magnification, 200X).

5.2.15. MTT Assay

On the post-infection day 7, RUVBL1 knockout cells (2000 cells/well in 200 µl RPMI) were seeded in 6 replicates in 4 separate 96-well cell culture dishes, and MTT analysis was performed in 2-day periods, with the first analysis 48 hours after cell seeding. 200 µl medium was used as blank. For MTT analysis, firstly, the medium in the wells was discarded and 200 µl of fresh medium containing 20 µl MTT was added. Plate covered with aluminum foil to protect from light was incubated at 37°C for 4 hours. Then the medium was suctioned, 100 µl DMSO was added to each well, and the plate was incubated at room temperature for 30 minutes, protected from light. At the end of the incubation, absorbance was measured at two different wavelengths, 570 and 720 nm, using the Multiskan GO Microplate Spectrophotometer, and the calculations were made on these two values. In this way, proliferation rate of cells was determined as a result of 4 measurements made with an interval of 2 days.

5.2.16. Cell Cycle Analysis

On post-infection day 10, 100,000 cells were seeded into 6 cm cell culture dishes. After 2 days, cells were collected by trypsinization and pelleted by centrifugation. Using 2.5 ml of 100% ice-cold ethanol (the final ethanol concentration is 70%), cells that had been resuspended in 1 ml of PBS were fixed. Cells were incubated for 15 minutes on ice for fixation. Then, fixed cells were harvested by centrifugation (1200 rpm, 15 minutes, 4°C) and resuspended in 70 µl of PI solution (25 µg/ml propidium iodide, 0.1 mg/ml RNase A and 0.05% Triton X-100 in PBS). Cells were incubated for 40 minutes at 37°C by vortexing every 10 minutes. After centrifugation at 6000 rpm for 5 minutes in a tabletop centrifuge, the stained cells were resuspended in 100 µl of PBS, transferred to polystyrene tubes equipped with cell strainer caps, and analyzed on the LSR Fortessa Flow Cytometer. Cell cycle profile was determined using FlowJo software version 10 (52).

5.2.17. SA-β-Gal Staining

20,000 cells were seeded into each well of 12-well plate on post infection day 10. After 48 hours incubation cells were washed with 1X PBS two times and fixed with fixative solution containing 3.7% formaldehyde for 5 minutes. Cells were rinsed with 1X PBS 3 times and SA-β-Gal staining solution was added to wells. After 12 hours of incubation at 37°C in a CO_2-free incubator, the blue color became apparent. After the blue color had fully developed, the cells were washed with PBS and 8 random fields were counted under the microscope.

5.2.18. Comet Assay

To prepare 1% agarose gel, 1 g of agarose was dissolved in 100 ml of distilled water, in the microwave. Slides were dipped into 1% agarose and wiped on one side clean. Agarose was air-dried to a thin film. Mechanical dissociation or enzyme disaggregation was used to prepare a single-cell suspension. On post-infection day 12, cells were trypsinized and harvested with RPMI. After centrifugation at 1800 rpm for 2 minutes, cell density was adjusted to about 20,000 cells/ml in 1X PBS. 0.4 ml of cells were transferred into a 15 ml Falcon and 1% agarose at 40°C was added. Agarose-cell suspension was mixed and pipetted onto the agarose-covered slide rapidly. Slides were incubated to solidify agarose for 2 minutes. After the agarose has gelled, slides were placed in the A1 Lysis buffer-containing dish and incubated overnight at 4°C in the dark. Slides were removed and submerged in the A2 rinse solution for 20 minutes at room temperature. This step was repeated 2 times and ensured the removal of all salt and detergent. Slides were placed in the tank and electrophoresis was performed in solution A2 for 25 minutes at 18V (0.6 V/cm), 250 mA. Slides were removed from the tank and rinsed with distilled dH_2O. 100 µl of a 10 µg/ml stock solution of propidium iodide was pipetted directly onto the slide and incubated for 20 minutes. Slides were rinsed with distilled water again to remove excess stain. Cells were analyzed by examining at least 50 comet images from each slide. ImageJ-OpenComet tool was used for analysis.

5.2.19. FACS Analysis and Apoptotic Assay (Annexin V)

Cell apoptosis was investigated by dual staining of MPM cells with Annexin V and Propidium Iodide (PI), using Annexin V Apoptosis Detection kit. 100,000 MPM cells were seeded into a 6-well plate. After 24 hours of incubation, cells were then detached by Trypsin, washed with PBS, and suspended in 36 µl of Annexin V binding buffer containing 4 µl PI and 2 µl of Annexin V. After 15 minutes of incubation at room temperature, samples gently mixed with 120 µl of Annexin V binding buffer were transferred to FACS tubes and placed on ice for analysis by Flow Cytometry. Data was analyzed by FlowJo. In all FASC analysis, the four quadrants (Q1, Q2, Q3, and Q4) are marked. Cells that tested positive for Annexin V only (Q3), or double positive for both Annexin V and PI (Q2) were defined as apoptotic cells (Q2 + Q3); cells that tested positive for PI only (Q1) were defined as necrotic cells; and cells negative for both Annexin V and PI (Q4) were defined as live cells.

5.2.20. Wound-Healing

150,000 cells/well were seeded in 6-well plates on post-infection day 10. Once the cells were confluent, the wound area was opened using 200 µl pipette tips, washed with 1X PBS, and incubated in RPMI containing 2% FBS. Wound closure was monitored at 0, 24, and 48 hours post-scratch using the Olympus CKX41 inverted light microscope (8 random pictures were taken per wound, at least 4 wounds/conditions). Scratch area was measured at 0, 24, and 48 hours using ImageJ, and the results are expressed as the percentage of the healed wound area of the mean value of at least 8 independent measurements.

5.2.21. Transwell Invasion and Migration Assay

The invasion of cells was investigated using Transwells placed in 24-well plates. First, 50 µl of Matrigel was added to each well, incubated for solidification at 37°C for 2 hours, and excess matrigel was removed. H2052 and H2452 cells were suspended in uncomplete RPMI on post-infection day 10. 250 µl of cell suspension (50,000 cells) was added to the upper chamber covered with Matrigel and 400 µl of RPMI containing 10% fetal bovine serum was added to the lower chamber. After 48 hours of incubation at 37°C, the wells were washed twice with 1X PBS and fixed for 2 minutes with 3.7%

formaldehyde. Cells were then permeabilized by incubation with 100% methanol for 20 minutes and washed twice with 1X PBS. Then the cells were stained with Crystal violet for 15-20 minutes, washed with 1X PBS and the cells on the upper surface of the filter were removed with a cotton swab. Images were taken under a light microscope (Olympus CKX41) at x100 magnification on five random fields per well. ImageJ was used for cell counting. Each experiment was performed in duplicate. For the migration assay, 25,000 cells were seeded in matrigel-free transwells. After 48 hours, the staining protocol was followed.

5.2.22. 2D and 3D Colony Formation Assay

For 2D colony formation assay, 1000 cells per well were seeded in triplicates in six-well plates on post-infection day 7. The cells were then incubated at 37°C, 5% CO_2, for 10 days changing medium twice a week. End of the 10 days, cells were washed with 1X PBS three times and fixed with 3.7% formaldehyde for 10 minutes. Then cells were rinsed with 1X PBS and stained with Crystal Violet (0.1% Crystal Violet and 20% EtOH in dH_2O) for 45 minutes. Plates were washed with water, dried overnight, and next day imaged on a LI-COR device.

For 3D colony formation assay, 0.5 g agar was solved in sterile 25 ml PBS to get 2% final concentration in the microwave oven. 2% agar and complete RPMI heated to 43°C were mixed thoroughly to obtain 0.5% agar. 1 ml soft agar was poured per well. The mix was solidified in the hood at room temperature for ~30 minutes. The left 2% agar was melted in the microwave oven for ~20-30 sec to fully dissolved. 2% agar was placed into the water bath, at 43°C to cool down for ~1 minute. The appropriate volume of 1X PBS and 2% agar were mixed to get a 1.4% final concentration. Cells were trypsinized and obtained 10,000 cells/ml concentration in RPMI. 750 µl of cell suspension and 250 µl of 1.4% soft agar were mixed and added to the top of the 0.5% agar layer. The plate was left at room temperature for 30 minutes to solidify of agar. Then 1 ml RPMI was added to each well and the plate was placed in the incubator for 3 weeks changing medium twice a week. Images were taken under a light microscope (Olympus CKX41) at x100 magnification on five random fields per well and bigger than 50 µm diameter of colonies were counted.

5.2.23. Gene Set Enrichment Analysis (GSEA)

To correlate the RUVBL1 expression level with EMT, E2F and MYC targets gene set enrichment in MPM samples, the GSE2549, GSE51024 and GSE163722 datasets were analyzed. GSE2549 dataset consists of 42 MPM tumor tissues and 5 normal pleura tissues: GSE51024 dataset consists of 51 MPM tumor tissues and 41 normal paired lung parenchyma tissue and the GSE163722 dataset contains 131 MPM tumor tissues. All datasets were individually divided into two cohorts based on the median value of RUVBL1 expression. These cohorts were represented as RUVBL1 High and RUVBL1 Low groups. Differentially expressed genes (DEGs) from “High” vs. “Low” expression groups were evaluated for enriched gene sets using the GSEA tool from the Broad Institute (Subramanian et al., 2005). As for the GSEA, a list of DEGs with phenotype labels “High” vs. “Low” was uploaded to the GSEA tool, and false discovery rates (FDR), nominal p-values (p), and normalized enrichment scores (NES) were computed after 500 or 1000 random permutations of the gene set. FDR<0.25, $p < 0.05$, and an NES > 1 were statistically significant.

5.2.24. Study Plan and Calendar

August 2021-September 2021	Literature Search and Gene Selection gRNA Cloning (pECPV) and Validation Experiments
September 2021 - January 2022	Inducible System Validation Experiments
September 2021 - September 2022	gRNA Cloning (pLentiCRISPR v2) Knockout experiments
March 2022 - October 2022	RUVBL1 Overexpression Cloning Overexpression Experiments
May 2022 - October 2022	Determining IC50 of CB-6644 CB-6644 Experiments
August 2022 - January 2023	Rescue Experiments

5.2.25. Data Evaluation

To perform all statistical analyses, GraphPad Prism 8 software was used. Student's t-test and Multiple t-test were used to compare two independent groups. ANOVA was used to compare the multiple groups. Significance was calculated by using the Two-stage linear step-up procedure of Benjamini, Krieger and Yekutieli. P-value< 0.05: *, p-value< 0.01: **, and p-value< 0.001: *** represent the significance.

5.2.26. Limitation of the Study

Although all our results were reproducible, the inducible system could not be fully developed, causing knockout experiments not to be performed with a single cell clone. Therefore, knockout experiments within the scope of this thesis were carried out with 3 different infections of polyclonal cells.

5.2.27. Ethics Committee Approval

This study was approved by the IBG local ethics committee with ethics protocol number 2021-033.

6. RESULTS

Chapter 1

6.1. Selection of *RUVBL1* Gene and Cell Lines

Ece Çakıroğlu, a doctoral student at Senturk Functional Cancer Genomics laboratory, conducted a whole genome CRISPR/Cas9 screening study to elucidate the molecular mechanisms (primarily focusing on genes and signaling pathways associated with cancer cell survival and proliferation) that may have an important role in MPM carcinogenesis. This study identified genes with a common depletion score in H2052, H2452, and H28 cell lines infected with the sgRNA pool library and expressing Cas9. The CRISPR/Cas9 screen experiments conducted by Dr. Ece Çakıroğlu are

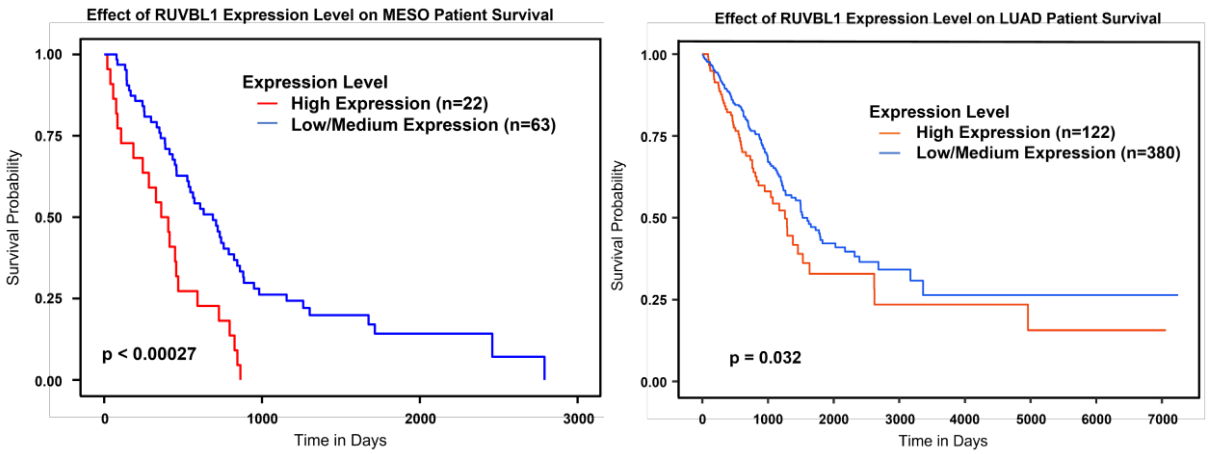
detailed in the PhD thesis coded DEU.HSI.PhD-2016850041. On the basis of the CRISPR screen results, we evaluated these genes according to the criteria:

(1) having an inverse correlation between gene expression and overall survival of MPM patients,

(2) having an enzymatic function, and

(3) being druggable with commercially available small chemical molecules.

First, we assessed the association of relevant genes with MPM patient survival on the TCGA MPM dataset using UALCAN (http://ualcan.path.uab.edu/ (53)) and GEPIA (http://gepia.cancer-pku.cn/ (54)) tools. Accordingly, we found that increased expression of many genes in MPM may be inversely correlated with patient survival. Next, we evaluated the genes against the second criteria which is; to function as an enzyme and to have a commercially available small molecule inhibitor. As a result of all these evaluations, we reduced the number of candidate genes to 4 (four). Among these, elevated expression of the *RUVBL1* gene is negatively correlated with Mesothelioma survival (Figure 9). Moreover, this association is also seen in other cancer types (i.e., LUAD, LGG, LIHC) (Figure 9).



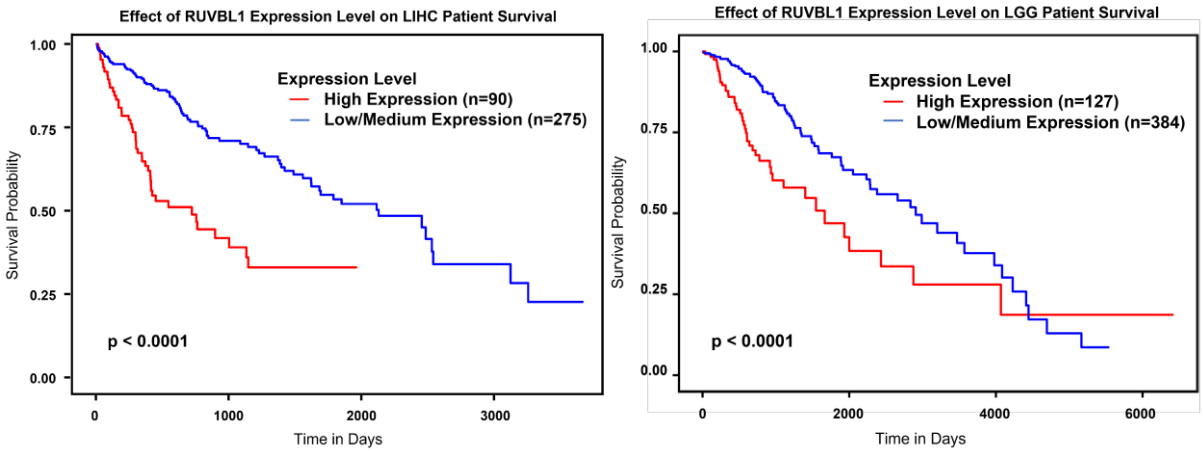
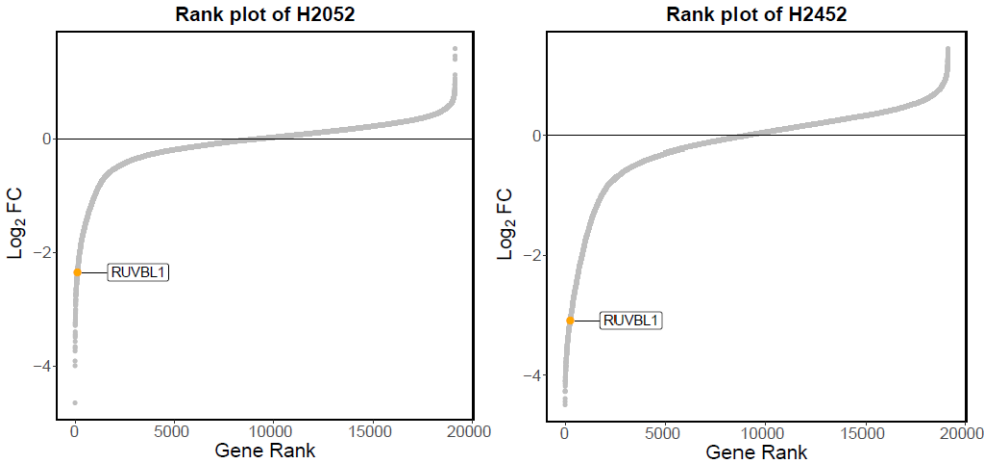


Figure 9. Survival analysis results of the RUVBL1 gene in MPM, LUAD, LGG and LIHC datasets. LUAD: lung adenocarcinoma, LGG: lower-grade glioma, LIHC: liver hepatocellular carcinoma

This analysis provided primary insights that the *RUVBL1* gene may play an important role in MPM carcinogenesis. Accordingly, we prioritized the *RUVBL1* gene for further molecular studies. Notably, CRISPR/Cas9 screen identified higher depletion scores in H2052 and H2452 cell lines, thus the molecular studies were performed with these two cell lines (Figure 10a). We randomly selected 2 of the high-scoring gRNAs in all cell lines (Figure 10b).

a)



b)

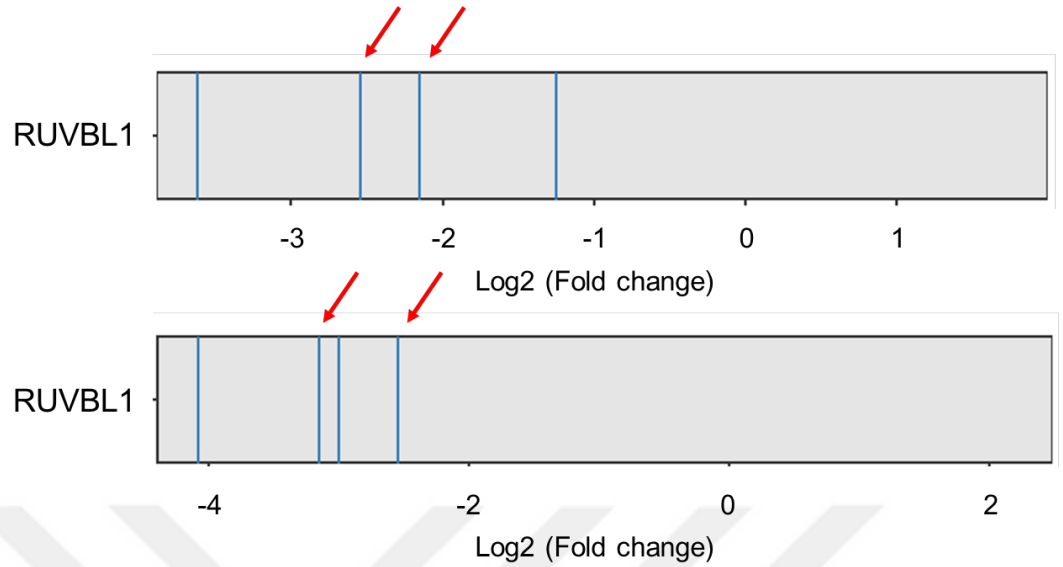
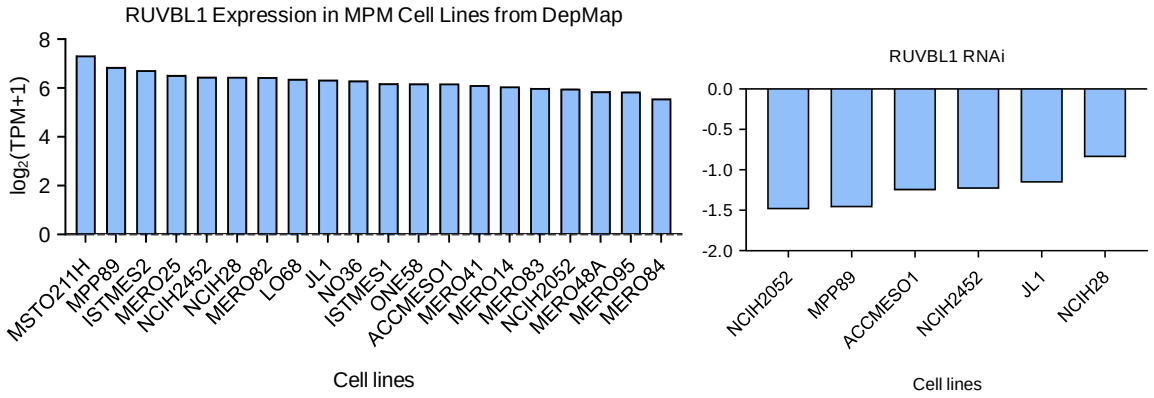


Figure 10. RUVBL1 gRNA scores in H2052 (top) and H2452 (bottom) cell lines. The lower is the Log2 Fold Change (FC), the more depleted is the gene.

Next, we investigated the broad impact of RUVBL1 depletion on the survival of other MPM cell lines using the DepMap portal's CRISPR, RNAi, and Achilles project data. We observed that RUVBL1 depletion had a negative effect on the survival of all MPM cell lines tested in the DepMap project. In addition, RUVBL1 expression levels were analyzed in MPM cell lines tested in the DepMap project. (Figure 11).



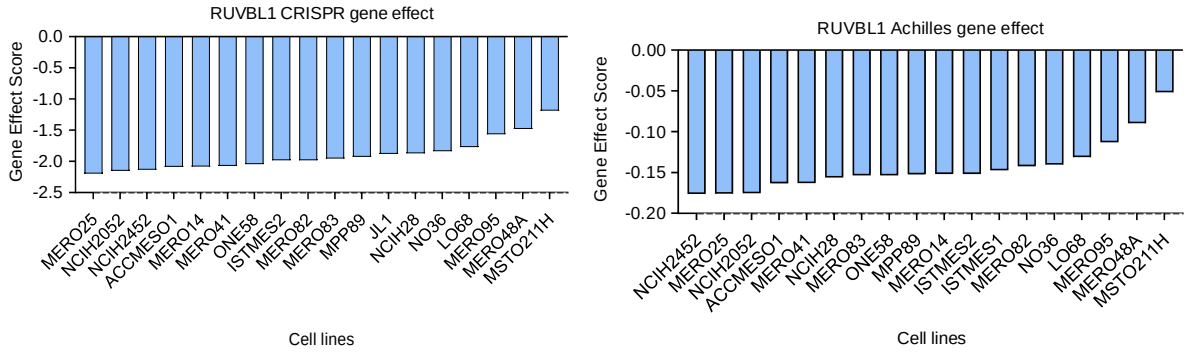


Figure 11. RUVBL1 CRISPR gene effect of MPM cell lines. Data were taken from DepMap portal.

In continuation of our preliminary work, we validated the CRISPR screen findings using the competition assay. To this end, we first cloned two different RUVBL1 targeting gRNA sequences (RUVBL1 g1 and RUVBL1 g2) into the pECPV (pEFS-Cas9-P2A-Venus) vector that we previously derived from the lentiCRISPR v2 backbone (55). In this experiment, we used the Renilla luciferase gene-specific gRNA sequence (gREN) as a negative non-targeting control. gREN is known to have no specific target in the human genome. Next, we performed virus packaging of the respective vectors and infected the H2052 and H2452 cell lines with virus particles, aiming to achieve partial transduction. For competitive detection - using flow cytometry analysis - we examined the distribution of cells over time for Venus (YFP variant) positivity every 4 days (Figure 12).

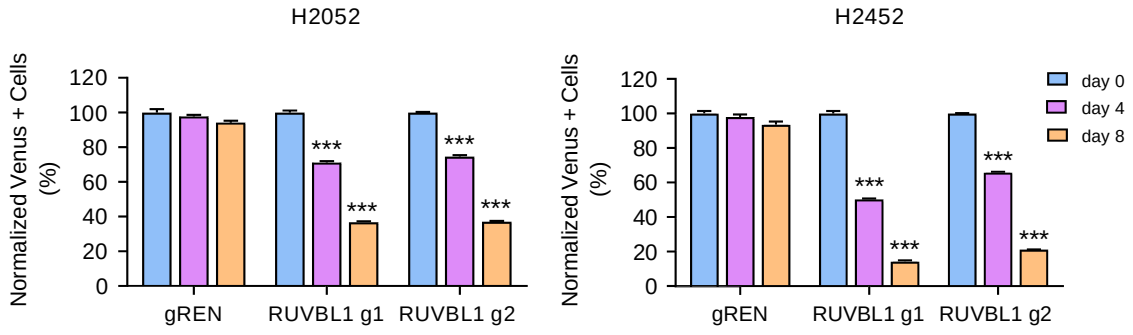


Figure 12. Competition assay results in H2052 and H2452 cells. While no significant change was observed in the percentage of Venus+ cells in the control group, gREN, the percentage of Venus+ cells significantly decreased after 8 days of follow-up in cells infected with both gRNAs targeting RUVBL1. The Venus percentage was normalized to 100 for the start time (day 0) of each sample.

We observed a significant decrease in the percentage of infected Venus-positive (+) cells (excluding the Renilla control group) over time. These data strongly suggested that the RUVBL1 gene plays a role in MPM cell proliferation or cell survival and possibly other cancer phenotypes.

6.2. Knockout of *RUVBL1* by CRISPR/Cas9 System

After preliminary studies in which we demonstrated the association of *RUVBL1* with MPM cell survival, we then focused on studying the molecular functions of this gene in MPM carcinogenesis. In line with this goal, we first cloned gREN, RUVBL1 g1 and g2 sequences into the pLentiCRISPR v2 vector. Then, we performed the infection of virus particles to H2052 and H2452 cell lines following virus packaging, selected with puromycin to generate clones with polyclonal nature. Western blot analysis with the lysates harvested at day 9 post infection validated the efficiency of knockout (Figure 13).

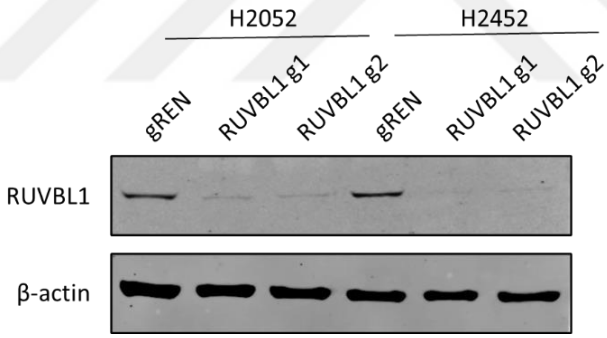


Figure 13. Western blot results of clones infected with Control gREN or RUVBL1 gRNAs.

6.3. *RUVBL1* Depletion Reduces the Proliferation and 2D Growth Capacity of MPM Cells

To examine the potential implication of *RUVBL1* in MPM cell proliferation and growth, we analyzed cell proliferation rates and colony-forming patterns via the MTT test, BrdU assay, and colony formation assay, respectively, in control and *RUVBL1* knockout cells.

First, we performed the MTT test (with 2-days intervals) with infected cells seeded in 4 different 96-well cell culture dishes. As expected, *RUVBL1* depleted H2052 and H2452 cells displayed significantly lower viability rates than gREN-infected control cells (Figure 14). We noted a significant decrease in cell viability in *RUVBL1* depleted cells, especially from day 13 of infection (8 days from completion of puromycin selection), suggesting that RUVBL1 depletion results in a rapid loss of cell viability. This prompted us to perform further studies on post-infection days 9-15 when the effect was most visible.

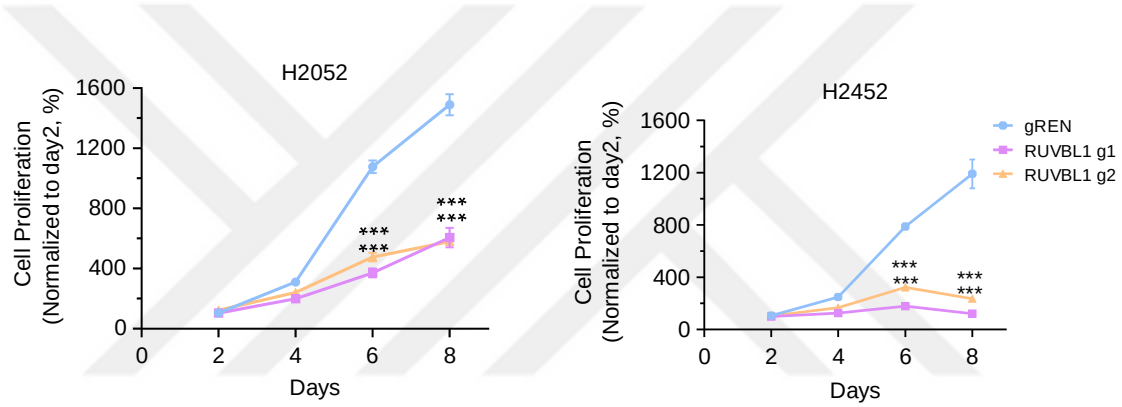


Figure 14. Comparison of the viability of H2052 and H2452 cells infected with gREN and RUVBL1 gRNAs. The first measurements were made after 2 days of cell seeding and these values were normalized to 100. The following days' measurement results were proportioned to the first day. The experiment was performed in 6 technical replicates.

To measure proliferation index, we labeled the cells seeded in 24-well cell culture dishes with BrdU reagent. 12 hours after the labeling, we assessed the BrdU incorporation rates of each clone. BrdU, a Thymidine analog, incorporates into the DNA during the replication. In this context, BrdU serves as a marker of DNA synthesis and is used for counting mitotic cells. Once incorporated into nuclear DNA, BrdU can be detected by immunohistochemical methods (56). Similar to the MTT results, the proliferation rate of RUVBL1 depleted cells was significantly lower than the cells infected with gREN (Figure 15).

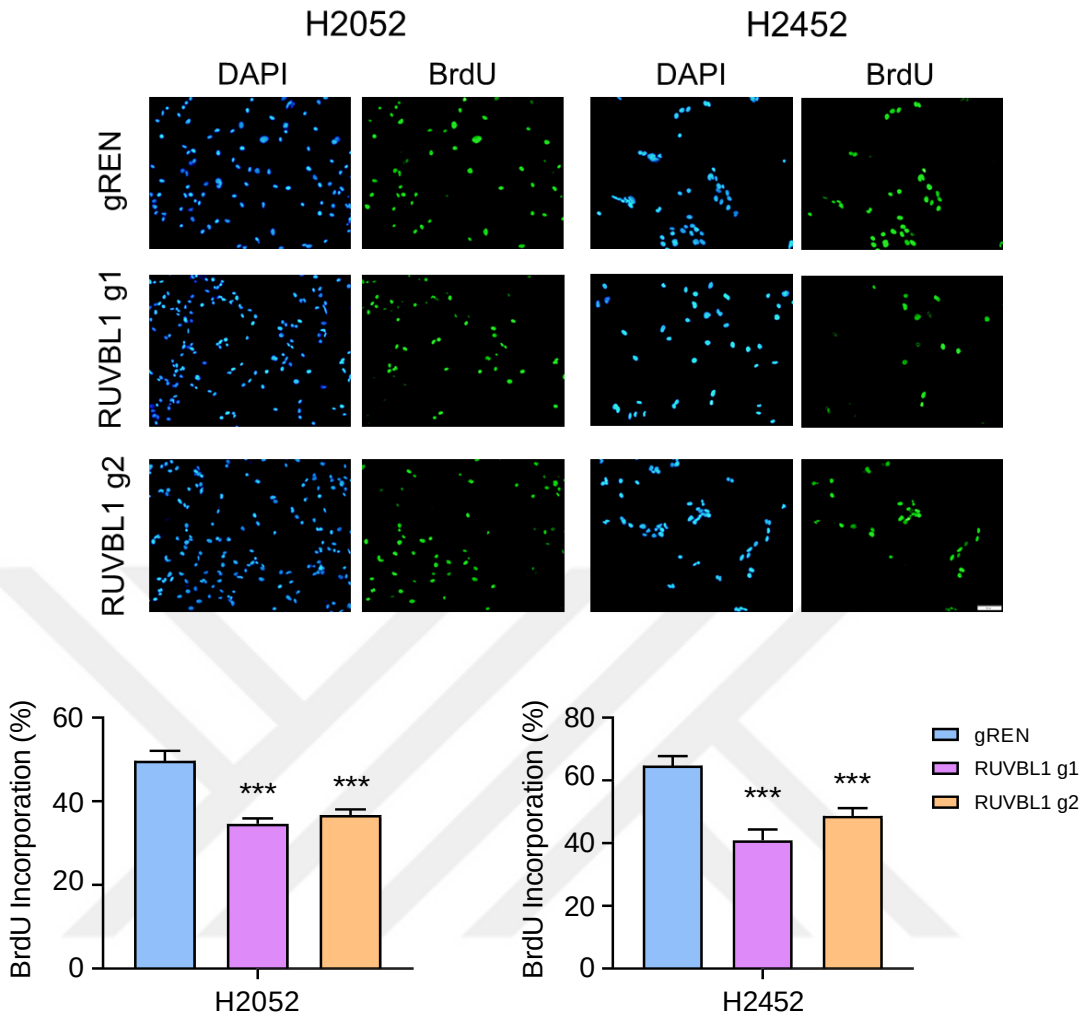


Figure 15. BrdU labeling results of H2052 and H2452 cells infected with gREN and RUVBL1 gRNAs. From cells labeled with 10 mM BrdU for 12 hours, cells stained with DAPI and/or BrdU in 6 randomly selected regions for each condition were counted. The number of BrdU-labeled cells was proportioned to cells stained with DAPI. 20X magnification, scale bar represents 50 µm.

Finally, to determine the effect of RUVBL1 knockout in colony-forming capacity we performed two-dimensional (2D) colony formation assay. For this, we seeded 1000 cells in each well of 6-well cell culture dishes and incubated for 10 days (changing media every 3 days). We have shown that cells infected with gREN have a higher colony-forming capacity than RUVBL1 gRNA-targeted cells (Figure 16).

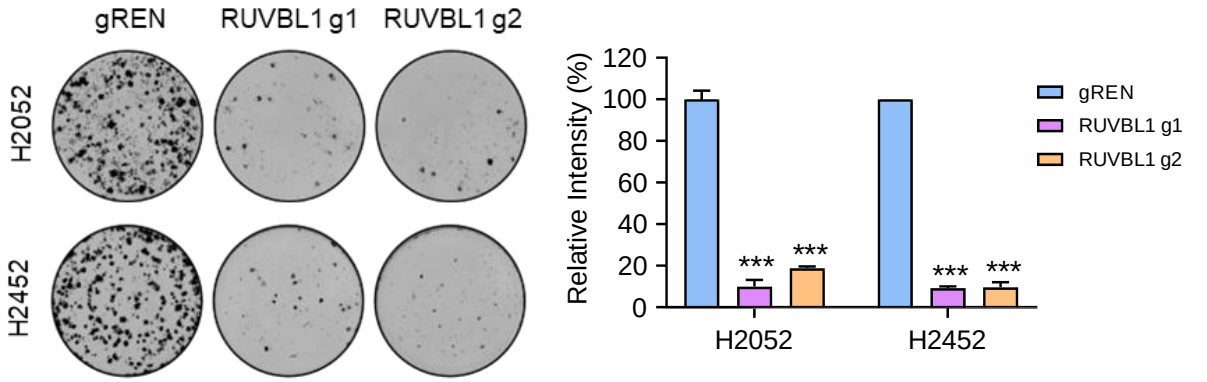


Figure 16. Cell survival results reflected by colony formation assay. RUVBL1 gRNA-infected cells were proportioned to control cells. The experiment was performed in 3 technical replicates.

6.4. *RUVBL1* Knockout Attenuates 3D Anchorage-Independent Growth of MPM Cells

On the basis of our findings in 2D cell culture, we sought to evaluate the effect of *RUVBL1* depletion on the three-dimensional (3D) anchorage-independent growth capacity of MPM cells. To this end, we performed the Soft Agar Colony formation assay. Experimentally, we seeded the cells in 12-well cell culture dishes in Noble agar and incubated the plates for 21 days, under normal cell culture conditions. By the end of 21 days, we examined the colonies under a light microscope. We randomly photographed 5 areas (10X magnification) from each cell group that we infected with *RUVBL1* gRNAs and the gREN. We then determined the size of the colonies with the ImageJ program and counted the number of colonies larger than 50 µm diameter (57). In both cell lines, we found that *RUVBL1* knockout significantly attenuated 3D colony-forming capacity of MPM cells (Figure 17).

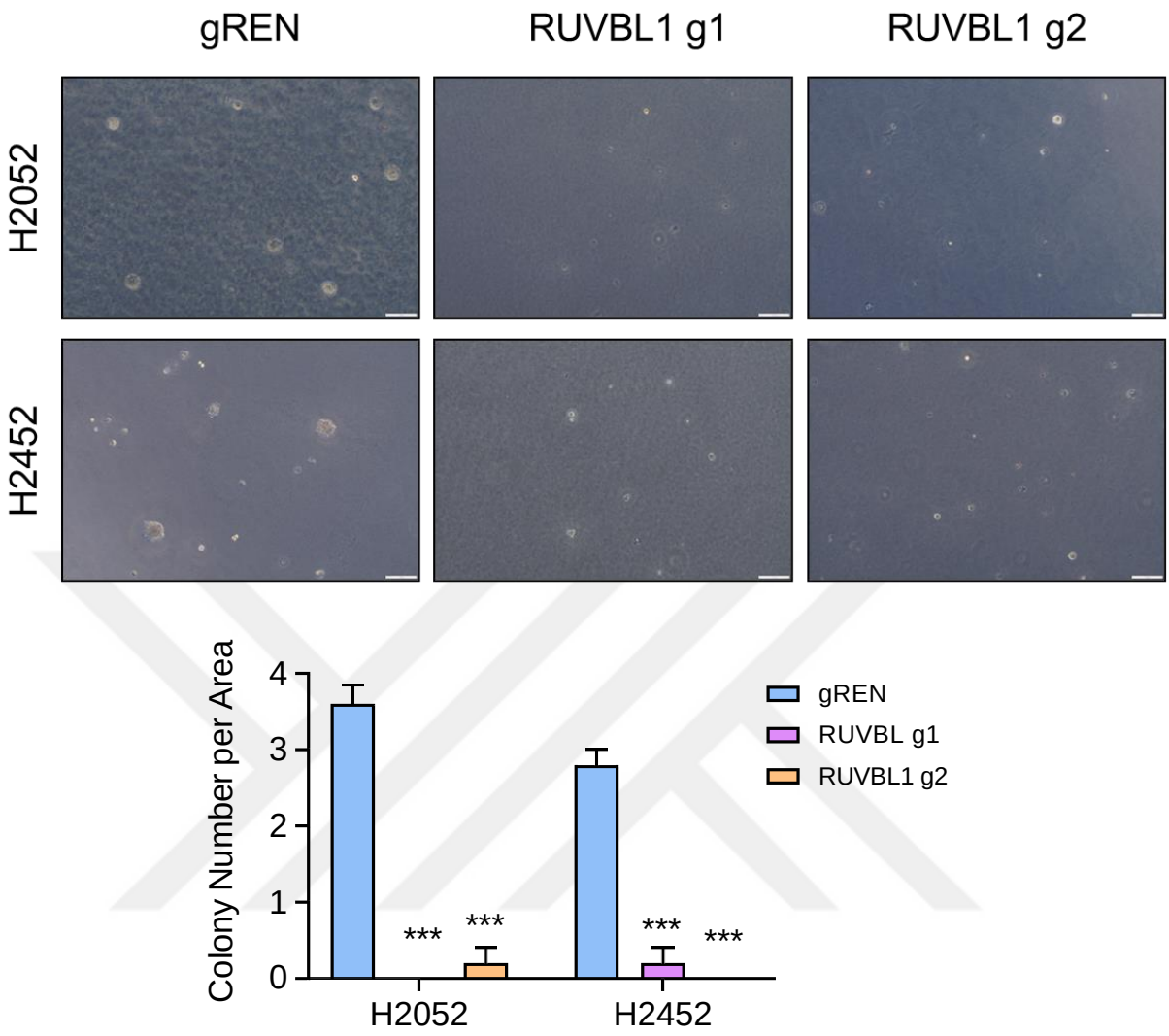
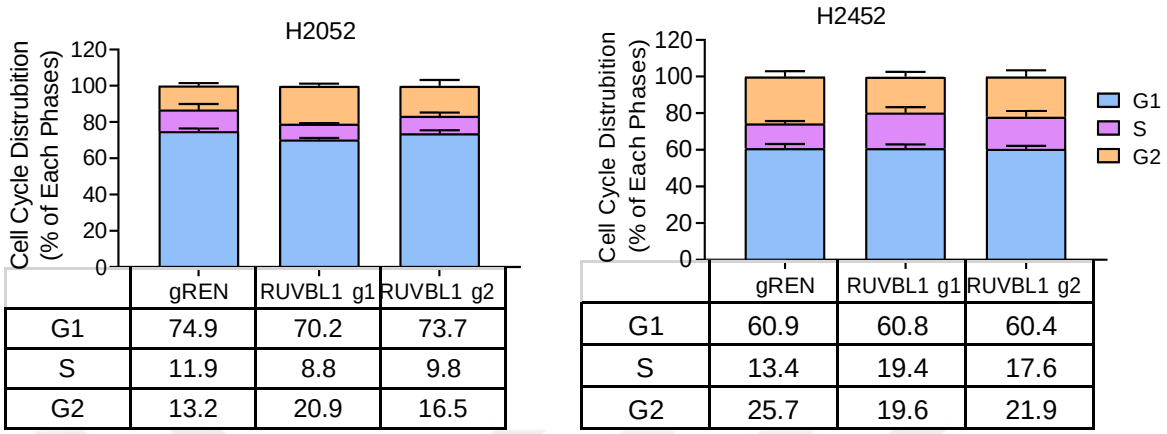


Figure 17. Effect of RUVBL1 depletion on Anchorage-independent growth of MPM cells. Images were taken 21 days after the cell seeding. Randomly selected 5 areas were photographed by light microscope (10X magnification). Colonies were measured by ImageJ and colonies with a diameter larger than 50 µm were counted. Scale bar represents 100 µm.

6.5. *RUVBL1* Depletion Reduces Cell Proliferation and Growth via Multiple Mechanisms

To elucidate the mechanisms associated with reduced MPM cell proliferation and growth, we first examined the cell cycle profiles and apoptosis rates of MPM cells infected with RUVBL1 gRNAs. H2052 cells with lower *RUVBL1* expression displayed cell cycle arrest in the G2 phase as determined by cell accumulation in G2 phase and a reciprocal reduction in the S phase. In contrast, H2452 cells with low *RUVBL1*

expression had cell cycle arrest in S phase as evidenced by cell accumulation in S phase and a reciprocal decrease in G2 phase (Figure 18).

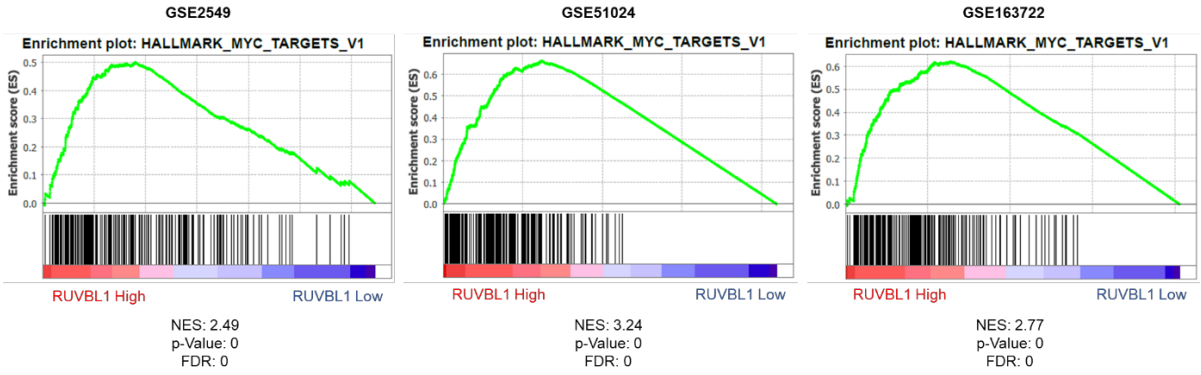


	gREN	RUVBL1 g1	RUVBL1 g2
G1	74.9	70.2	73.7
S	11.9	8.8	9.8
G2	13.2	20.9	16.5

	gREN	RUVBL1 g1	RUVBL1 g2
G1	60.9	60.8	60.4
S	13.4	19.4	17.6
G2	25.7	19.6	21.9

Figure 18. Cell cycle distribution of RUVBL1 depleted and control MPM cells. The experiments were performed in 3 biological replicates. The average of biological replicates was shown below the graph.

We hypothesized that tumors with a high RUVBL1 expression level would have enriched expression of cell cycle-related pathways. To test this hypothesis, we examined the tumor expression of the MYC and E2F Hallmark targets in three distinct GEO dataset samples using the gene set enrichment analysis (GSEA) method. GSEA identified a significant and postivie correlation between RUVBL1 and the expression of the transcription factors E2F and MYC which are important for the G1/S transition (Figure 19).



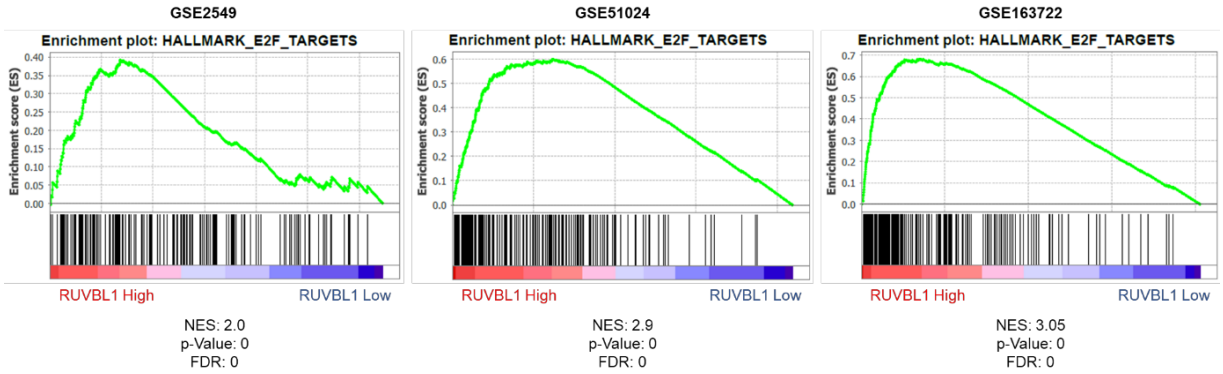
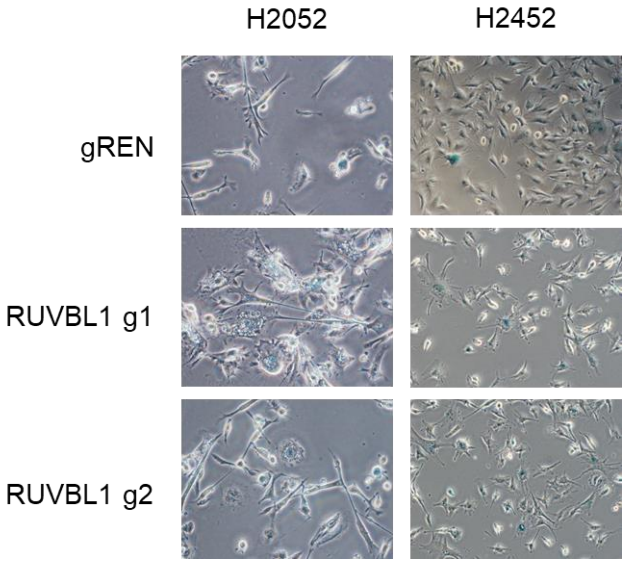


Figure 19. Gene set enrichment analysis of MYC and E2F hallmark targets in RUVBL1 high and low MPM samples. The median value of the scores was used to divide cohorts into high and low groups within each cohort. Enrichment plots along with normalized enrichment score (NES) and false discovery rate (FDR) are shown for both Hallmark gene sets for which enriched expression is observed in the high compared to the low group in GEO Datasets.

Based on the cell cycle profiles and BrdU results, we hypothesized that MPM cells would undergo cellular senescence upon downregulation of the *RUVBL1* gene. To test this, we seeded cells into 24-well plates and incubated for 2 days. We then carried out the SA-β-Gal staining assay for 12 hours (Figure 20). Senescent cells in culture are detected by histochemical staining of senescence-associated beta-galactosidase (SA-β-gal) in cells using the artificial substrate X-gal (58).



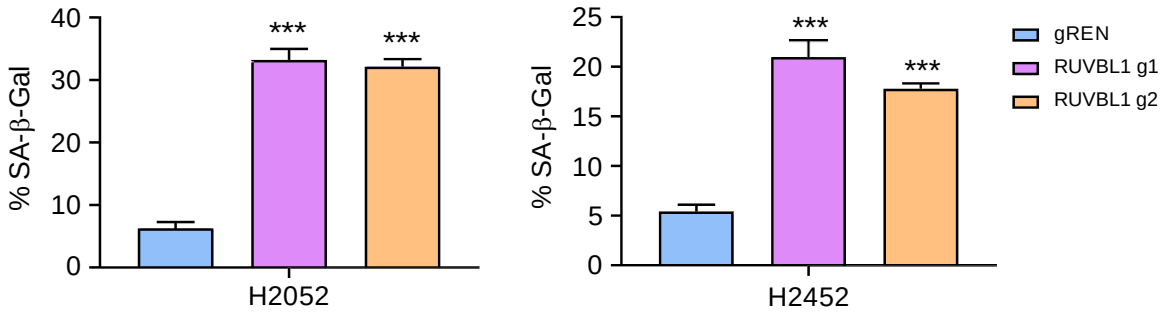
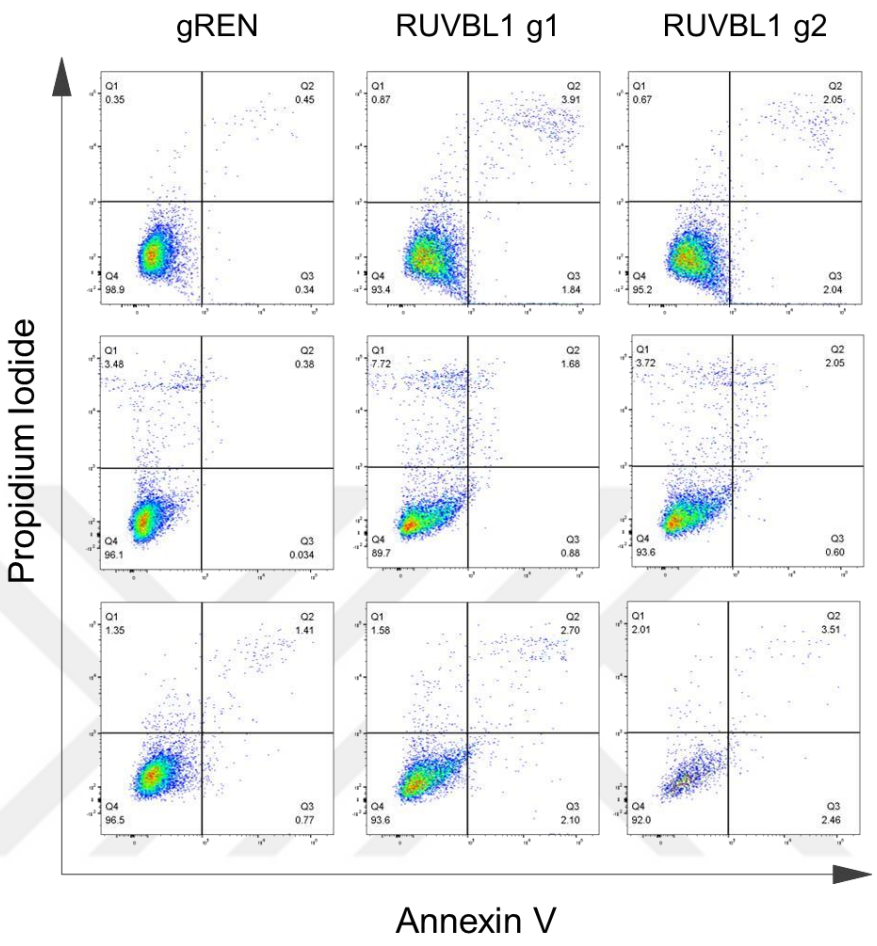


Figure 20. Senescence-associated-β-galactosidase (SA-β-gal) staining of RUVBL1-depleted and control MPM cells. Cells were counted with ImageJ software and the number of SA-β-gal-positive cells was compared to the total cell number. Randomly selected 8 areas were photographed by light microscope with 10X magnification.

As we expected, control cells in both cell lines had approximately 5% staining, while *RUVBL1* knockout cells showed intense blue staining as they showed senescence phenotype. When we examined it in detail, we revealed that the rate of senescent cells increased from ~6% to ~30% in the H2052 cell line, while it increased from 5% to ~20% in the H2452 cells.

To examine if *RUVBL1* depletion causes apoptosis in MPM cells, we analyzed the cells against an apoptotic phenotype using the Annexin V/propidium iodide. As a result of the experiment that we performed in 3 biological replicates, we observed an increase in the rate of apoptotic cells after *RUVBL1* depletion in both cell lines. However, due to the deviation between the biological repeats in the H2452 cell line, the results were not significant (Figure 21).

H2052


gREN
RUVBL1 g1
RUVBL1 g2
Propidium Iodide
Annexin V
Q1 0.35
Q2 0.45
Q4 98.9
Q3 0.34
Q1 0.87
Q2 3.91
Q4 93.4
Q3 1.84
Q1 0.67
Q2 2.05
Q4 95.2
Q3 2.04
Q1 3.48
Q2 0.38
Q4 96.1
Q3 0.034
Q1 7.72
Q2 1.68
Q4 89.7
Q3 0.88
Q1 3.72
Q2 2.05
Q4 93.6
Q3 0.60
Q1 1.35
Q2 1.41
Q4 96.5
Q3 0.77
Q1 1.58
Q2 2.70
Q4 93.6
Q3 2.10
Q1 2.01
Q2 3.51
Q4 92.0
Q3 2.46

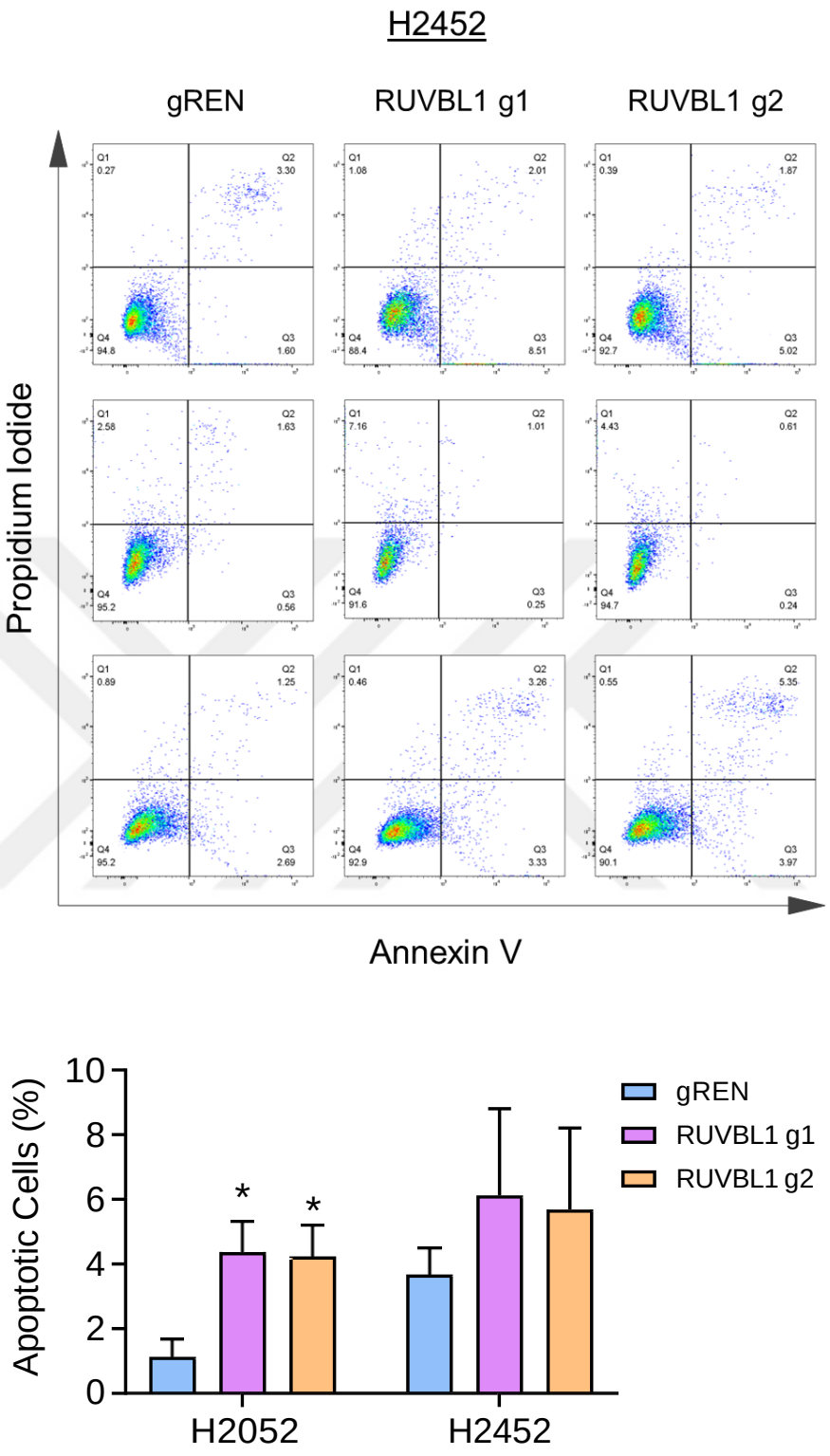
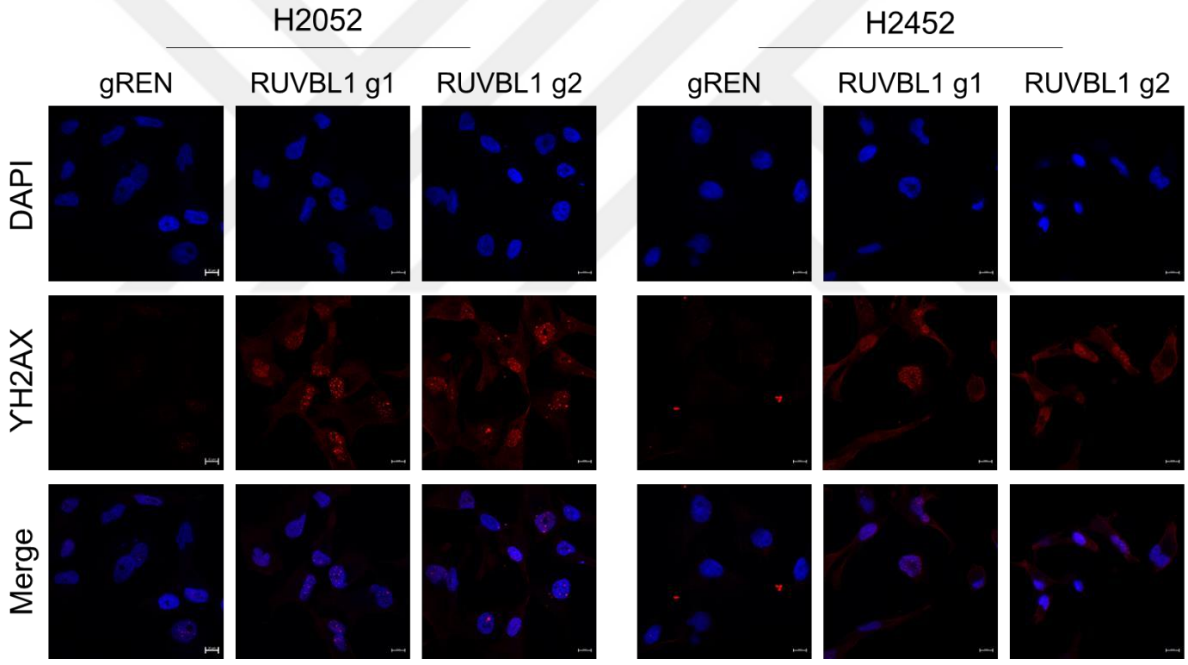


Figure 21. Apoptosis measurement by flow cytometry. Annexin V/PI staining to quantify apoptosis RUVBL1 knockout or control H2052 and H2452 cells. The total amount of apoptotic cells (early (Q3) + late (Q2)) is shown in the graph. Experiments were perfomed in triplicates.

To clarify the mechanisms underlying the association of low *RUVBL1* expression level with cell proliferation and cell cycle arrest, we checked for the presence of DNA damage response in these cells. It is well known that DNA double-strand breaks induce Histone H2AX phosphorylation at the Serine 139 residue located on the C-terminal region, resulting in the production of γH2AX (59). DNA double-strand breaks can be detected via the immunofluorescence technique using specific antibodies that recognize γH2AX. Immunofluorescent staining with γH2AX revealed significantly increased numbers of γH2AX foci in *RUVBL1* knockout cells compared to control groups (Figure 22). This indicates that *RUVBL1* ablation can induce double-stranded DNA damage in MPM cells.



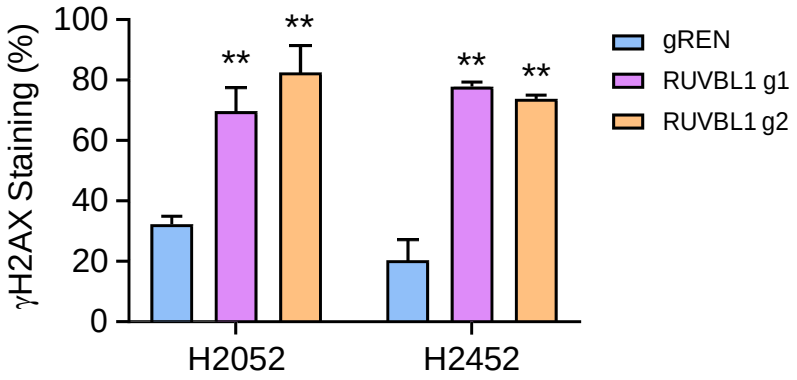


Figure 22. Immunofluorescent (IF) Staining of γH2AX. The bar graph summarizing γH2AX total nuclear staining number of RUVBL1 depleted or control MPM cells.

In addition to IF staining, we also examined whether single-strand breaks occur in the absence of *RUVBL1* via the Comet assay. This method is based on imaging DNA damage in agarose gel. If there are single strand breaks in the DNA, these break ends migrate toward the anode during electrophoresis and form a tail image. If there is no DNA damage, there will be no migration toward the anode, as the large size of fragments and the absence of free ends (60). We analyzed tail lengths of comets with OpenComet, an open-source software tool that quantifies DNA damage in comet assay images, in at least 30 photographs (50 comets) taken by the microscope randomly for each condition (61). As a result of our experiment, we observed that significantly longer tails were formed in *RUVBL1* knockout cells compared to control cells (Figure 23).

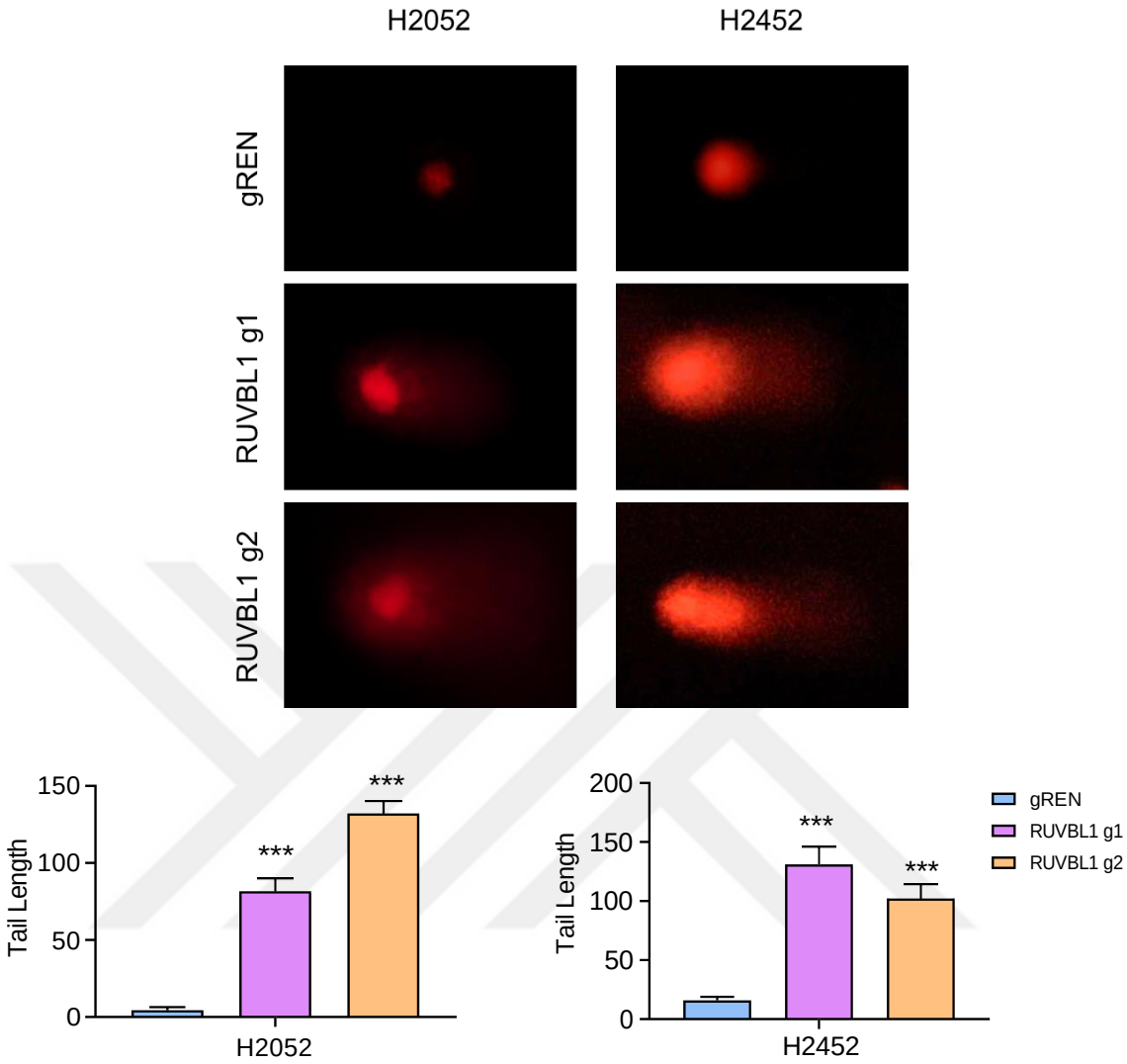


Figure 23. Alkaline Comet Assay of RUVBL1 depleted or Control MPM cells. Comet images of the MPM cells stained with PI staining were observed under fluorescent microscope (magnification 10x). Comet tail length was calculated by using ImageJ software/OpenComet tool. The graph shows mean tail length of comets.

6.6. The Impact of *RUVBL1* Depletion on Cancer Aggressive Phenotypes: Motility, Invasion and Migration Capacity

After demonstrating the effects of *RUVBL1* on cell proliferation and its relevance to the underlying mechanisms, we aimed to examine the effect on aggressive phenotypes in MPM cells. For this purpose, we seeded 150,000 MPM cells in each well of 6-well cell culture dishes, and the wound area was created with the help of the 200 µl tip 24 hours after seeding. We measured the wound area at 24-hours periods and calculated the %

wound amount relative to the first day. The results presented that the depletion of *RUVBL1* reduces cell motility (Figure 24).

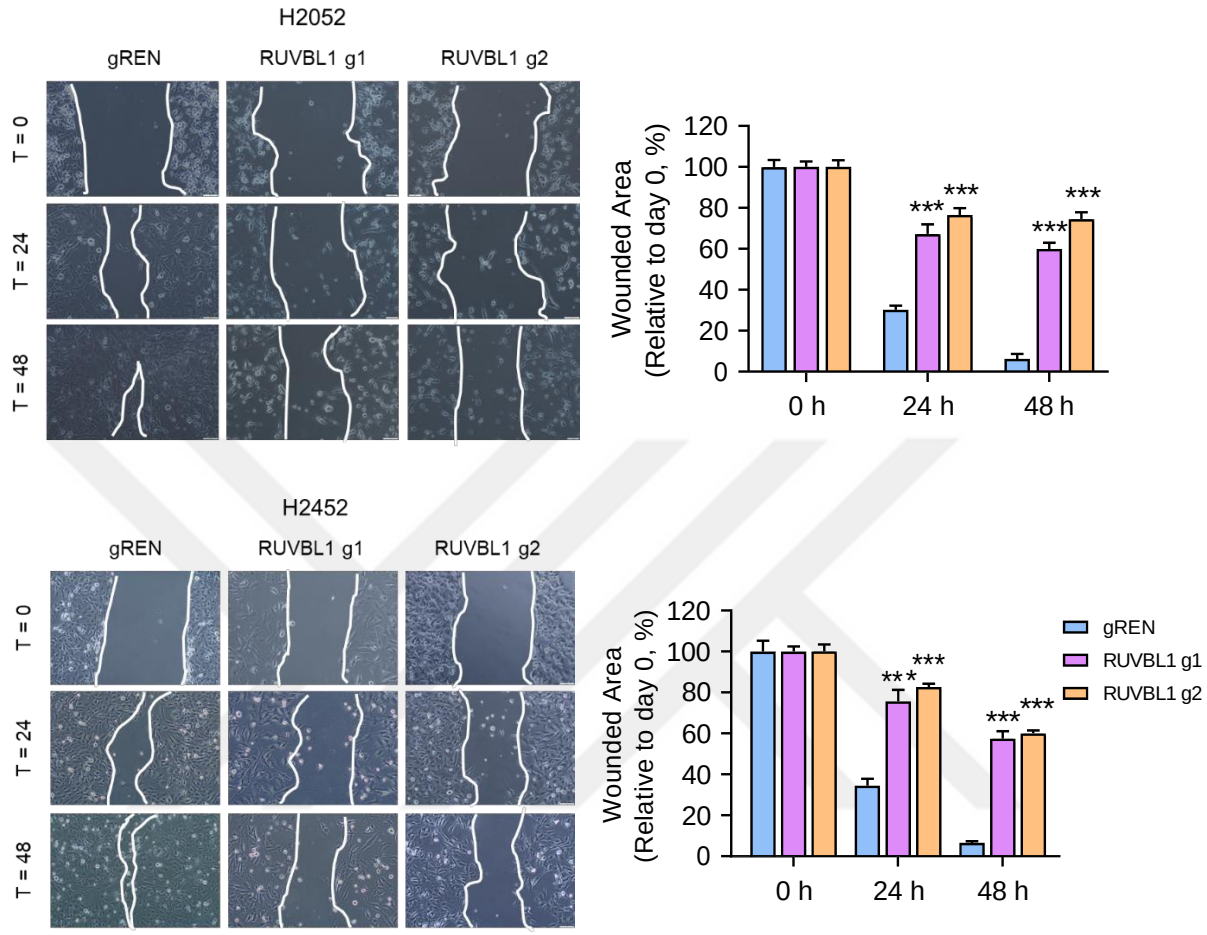


Figure 24. Wound healing assay of RUVBL1 knockout or control MPM cells. Images were taken every 24 hours and representative images were shown from three technical replicates. Wounded areas were measured by ImageJ software/ MR_Wound_Healing tool. The graphs present percentage of wounded areas of following days relative to day 0. 10X magnification, scale bar represents 100 µm.

We then tested the migration and invasion capabilities of MPM cells in the absence of RUVBL1. To this end, we seeded cells into matrigel-free and matrigel-coated Boyden chambers for migration and invasion assays, respectively. After 48 hours, we followed the staining protocol and analyzed the results. We found that the migration and invasion capacities of both cell lines were significantly reduced in the absence of RUVBL1 (Figure 25).

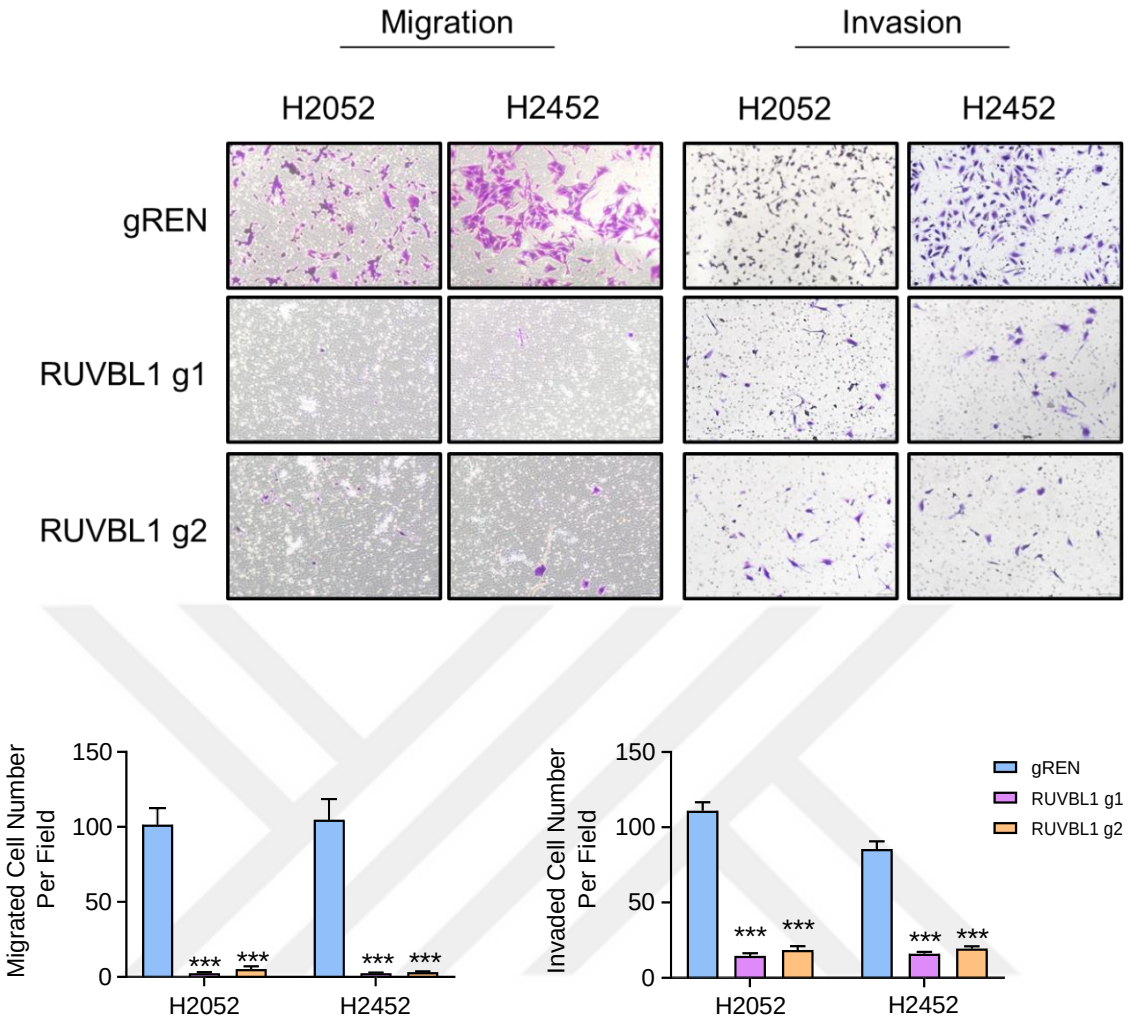


Figure 25. Representative images and quantification of Migration and invasion capacity of RUVBL1 knockout and control MPM cells. Experiments were performed in duplicate. Invaded/migrated cells were counted from randomly selected 5 area. 10X magnification, scale bar represents 100 µm.

6.7. Overexpression of *RUVBL1* in MPM Cell Lines

Having established a causal role for *RUVBL1* gene in MPM cell proliferation, growth and cancer aggressive phenotypes, we sought to corroborate these findings by overexpressing *RUVBL1* gene in the same cell lines. On this account, we cloned Venus (control, improved version of YFP) and *RUVBL1* coding sequences into the pLV-EF1a-IRES-Puro backbone. Then we performed the packaging of lentiviral particles and infection of H2052 and H2452 cell lines, followed by puromycin selection. To validate the overexpression, we performed Western blot analysis with the lysates harvested at post infection day 7 (Figure 26).

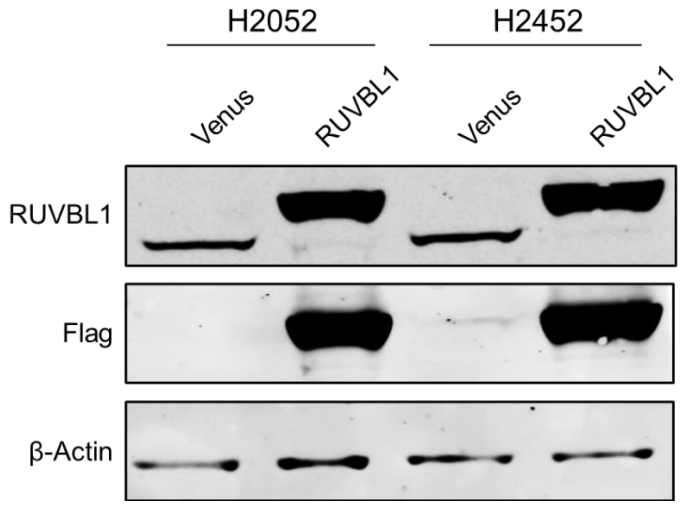


Figure 26. Western blot results of clones infected with Venus or RUVBL1 inserted vector.

.

As a result of the Western Blot, which we checked with both RUVBL1 and Flag antibodies, we observed that endogenous RUVBL1 was somehow lost in both cell lines in which we overexpressed RUVBL1. We interpreted this situation as the saturation of the RUVBL1 band due to the high infection rate causing the disappearance of the endogenous RUVBL1 band. To test this, we infected both cell lines at different dilutions and examined the presence of endogenous RUVBL1. Interestingly, we found that as the virus dilution increased, the expression of endogenous RUVBL1 in cells decreased.

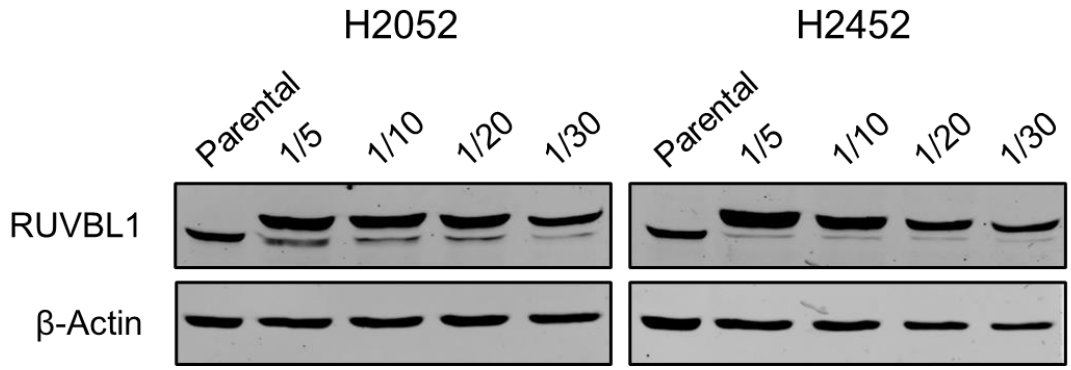


Figure 27. Western blot results of clones infected with RUVBL1 inserted vector with 4 different dilutions.

6.8. Overexpression of *RUVBL1* does not Affect the Proliferation of MPM Cells

To examine the potential effect of increased *RUVBL1* expression on MPM cell survival and growth, we initially analyzed the cell proliferation rates following the BrdU assay. We revealed that BrdU incorporation is increased in RUVBL1 overexpressed cells, that is, the proliferation rate is higher than in control cells (Figure 28). These results supported the reduction of the proliferation of MPM cells by knockout of *RUVBL1*.

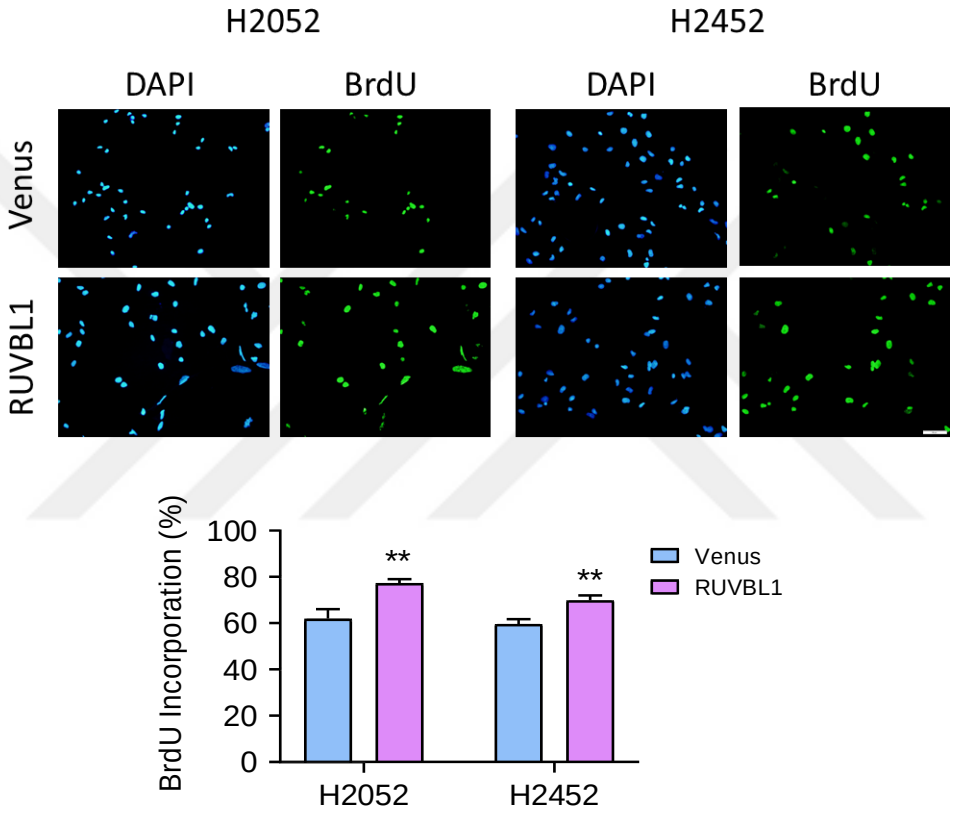


Figure 28. BrdU labeling results RUVBL1 overexpressing and control MPM cells. From cells labeled with 10 mM BrdU for 12 hours, cells stained with DAPI and/or BrdU in 7 randomly selected regions for each condition were counted. The number of BrdU-labeled cells was proportioned to cells stained with DAPI. 20X magnification, scale bar represents 50 µm.

6.9. *RUVBL1* Overexpression Augments 3D Anchorage-Independent Growth of MPM cells

Next, we performed the Soft Agar Colony formation assay to evaluate the effect of increased RUVBL1 expression level on the three-dimensional (3D) anchorage-independent growth capacity of MPM cells. We seeded cells in 12-well cell culture

dishes in Noble agar and incubated them for 21 days under normal cell culture conditions. After 21 days, we examined the colonies under the light microscope (Figure 29).

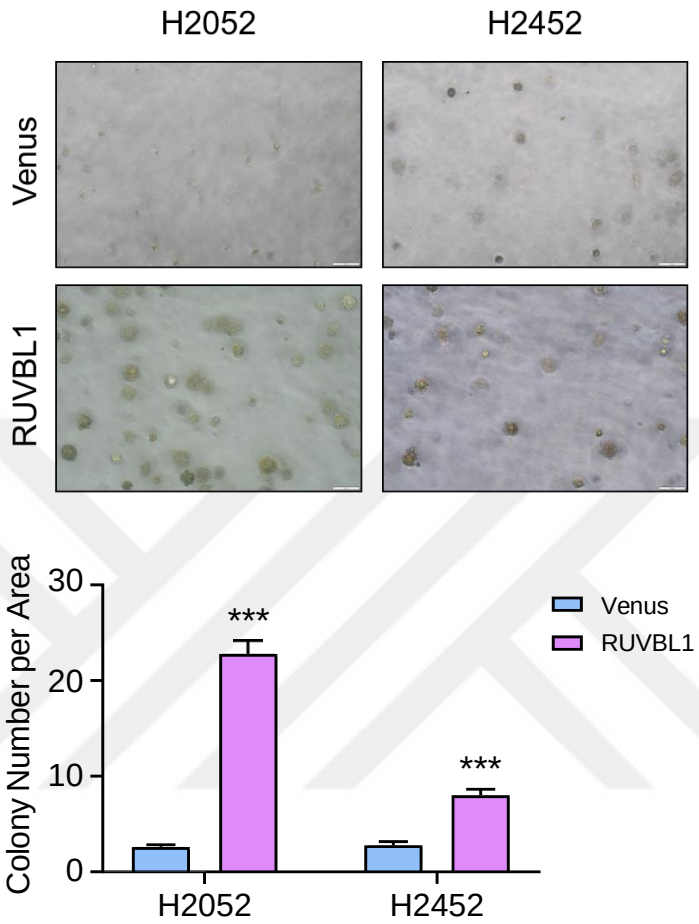


Figure 29. Effect of RUVBL1 overexpression on Anchorage-independent growth of MPM cells. Images were taken 21 days after the cell seeding. Randomly selected 5 areas were photographed by light microscope (10X magnification). Colonies were measured by ImageJ and colonies with a diameter larger than 50 µm were counted. Scale bar represents 100 µm

We photographed 5 random fields (10X magnification) from each cell group and identified colonies larger than 50 µm in diameter with the ImageJ program. In both cell lines, we found that the 3D colony-forming capacity of MPM cells with ectopic RUVBL1 expression was significantly increased.

6.10. Upregulation of *RUVBL1* Enhances Cell Motility and Invasion Capacity of MPM Cells

Our previous results suggest that *RUVBL1* depletion inhibits aggressive phenotypes of MPM cells. To test whether there would be an opposite effect when we upregulate *RUVBL1*, we first analyzed the cell motility by following the Wound healing protocol. Indeed, we found that cells with *RUVBL1* overexpression closed the wound area significantly faster than the control group, suggesting that these cells had higher motility (Figure 30)

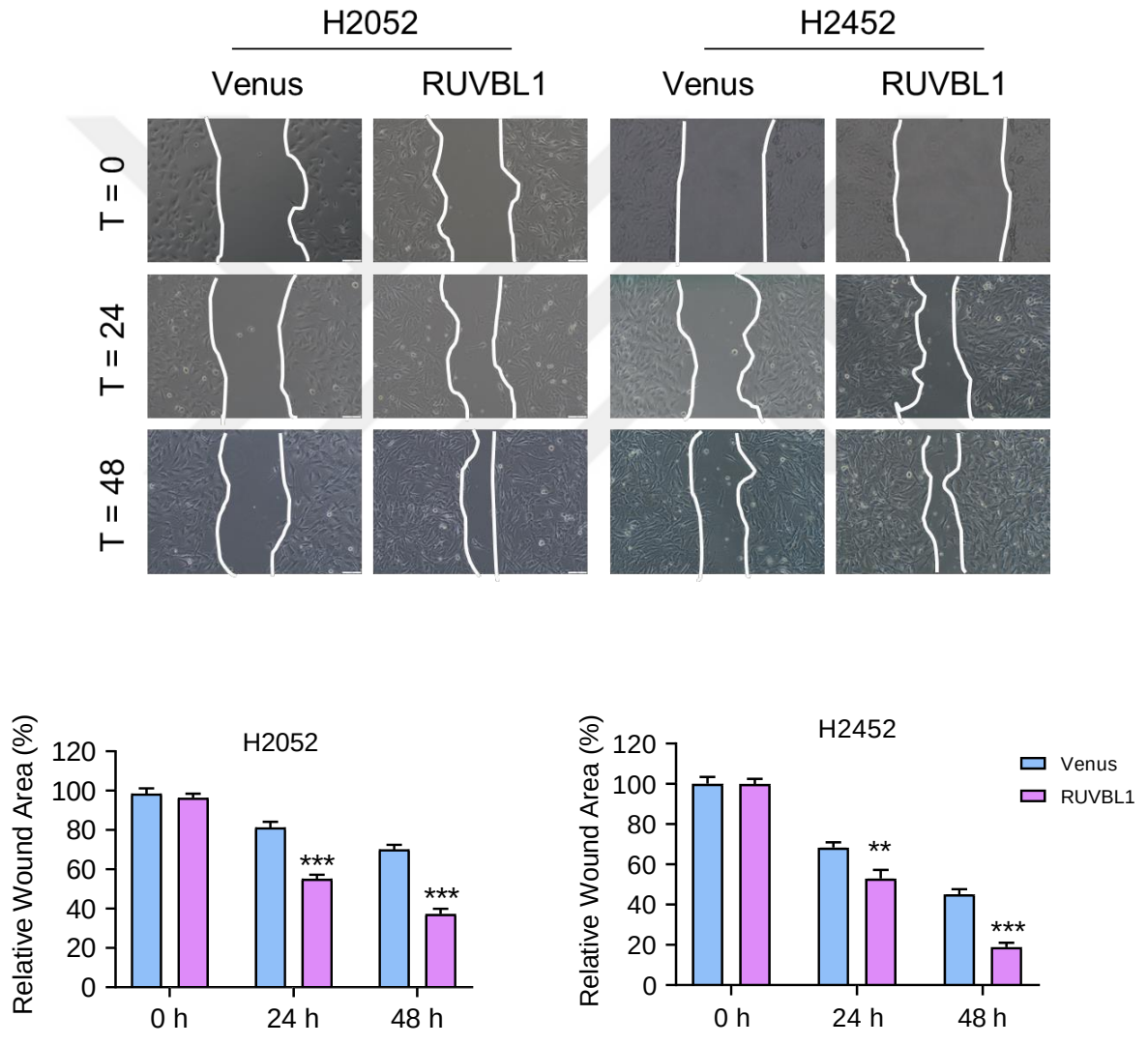


Figure 30. Wound healing assay of RUVBL1 overexpressed and control MPM cells. Images were taken every 24 hours and representative images were shown from three technical replicates. Wounded areas were measured by ImageJ software/ MR_Wound_Healing tool. The graphs present percentage of wounded areas of following days relative to day 0. 10X magnification, scale bar represents 100 µm.

We then tested the invasion capacity of *RUVBL1* overexpressed cells. In this line, we seeded *RUVBL1* upregulated cells into matrigel-coated transwells for invasion assay. After 48 hours, we followed the staining protocol and analyzed the results (Figure 31).

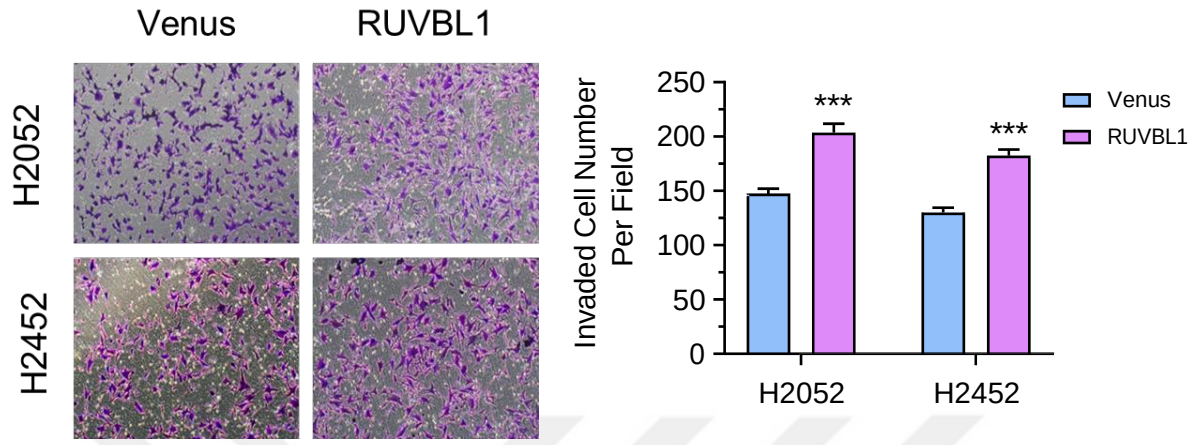


Figure 31. Representative images and quantification of invasion capacity of RUVBL1 upregulated and control MPM cells. Experiments were performed in duplicate. Invaded cells were counted from randomly selected 5 area (10X magnification).

We found that the invasion capacity was significantly increased in both cell lines with increased *RUVBL1* expression level. All these results supported the tumorigenic/metastatic role of RUVBL1 in the tested H2052 and H2452 cell lines.

6.11. Upregulation of *RUVBL1* is Associated with Epithelial Mesenchymal Transition

While examining the effects of RUVBL1 overexpression in MPM cells, we observed that RUVBL1 upregulated cells exhibited mesenchymal-like morphology (Figure 32). This made us think that RUVBL1 may be associated with Epithelial Mesenchymal Transition (EMT).

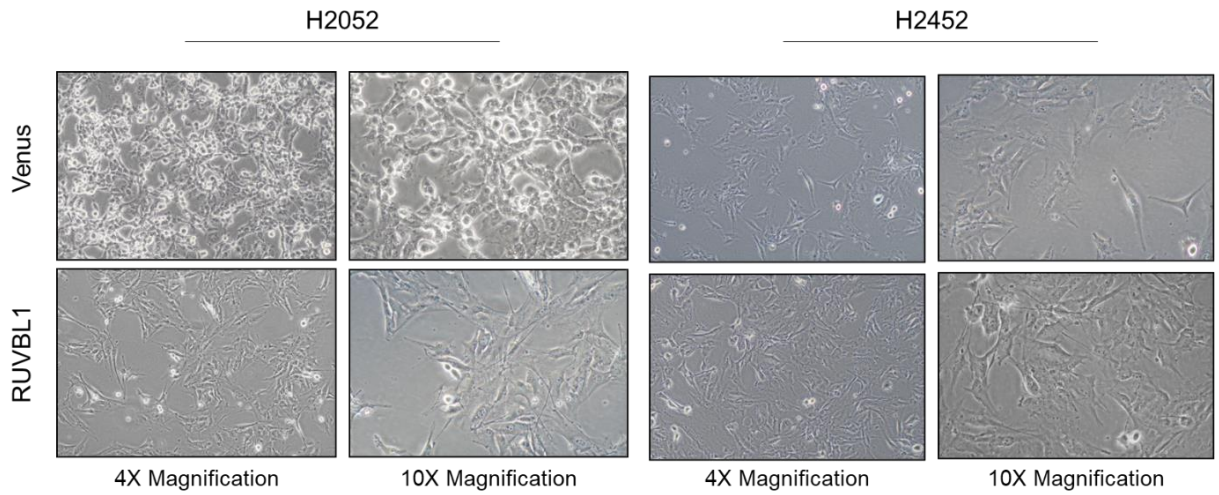


Figure 32. Representative images of RUVBL1 upregulated and control MPM cells. Photos were taken by the phase contrast microscope, 4X and 10X magnification.

Phalloidin, which can bind to all actin filament variants, is a highly selective bicyclic peptide used for microscope imaging of F-actin (62). In this direction, we first performed IF staining with a Phalloidin antibody to visualize the morphological alterations. We found that H2052 cells, which have a relatively more epithelial morphology, acquired robust mesenchymal features with the increased expression level of RUVBL1. The morphological change in H2452 cells with more mesenchymal features, was limited to the increase in their cell protrusions (Figure 33).

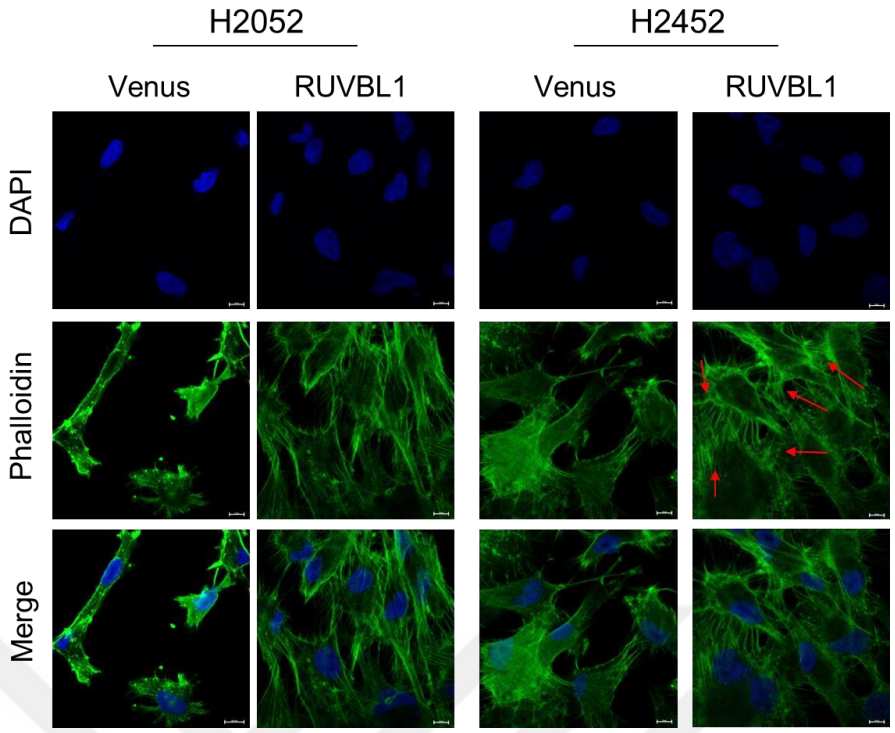


Figure 33. Immunofluorescent staining of RUVBL1 upregulated or control MPM cells with Phalloidin. Phalloidin and DAPI were observed under confocal microscope (magnification 63x). The red arrows show Phalloidin localized in cell protrusions.

Next, we examined the expression of mesenchymal marker genes, N-Cadherin and Vimentin, in cells overexpressing RUVBL1 by western blot. Like IF results, we showed that the overexpression of *RUVBL1* increased the expression of N-Cadherin and Vimentin in H2052 cells, yet we found no significant changes in H2452 cells (Figure 34).

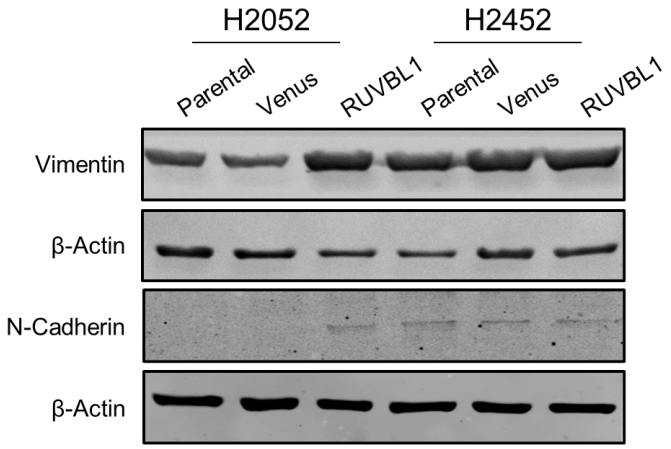


Figure 34. The expression level of Vimentin and N-cadherin in cells with and without upregulation of RUVBL1.

Finally, we examined the relative expression levels of marker genes in the EMT panel with qRT-PCR in H2052 cells with significant morphological change depending on RUVBL1 expression level. In the panel, N-Cadherin, Vimentin, Snail, Zeb1, Zeb2, Twist1 and Twist2 represent the mesenchymal marker genes, while E-Cadherin and Ocln (Occludin) are epithelial marker genes. Indeed, we showed that there was a decrease in the expression level of epithelial marker genes, while the expression of mesenchymal marker genes was significantly increased (Figure 35).

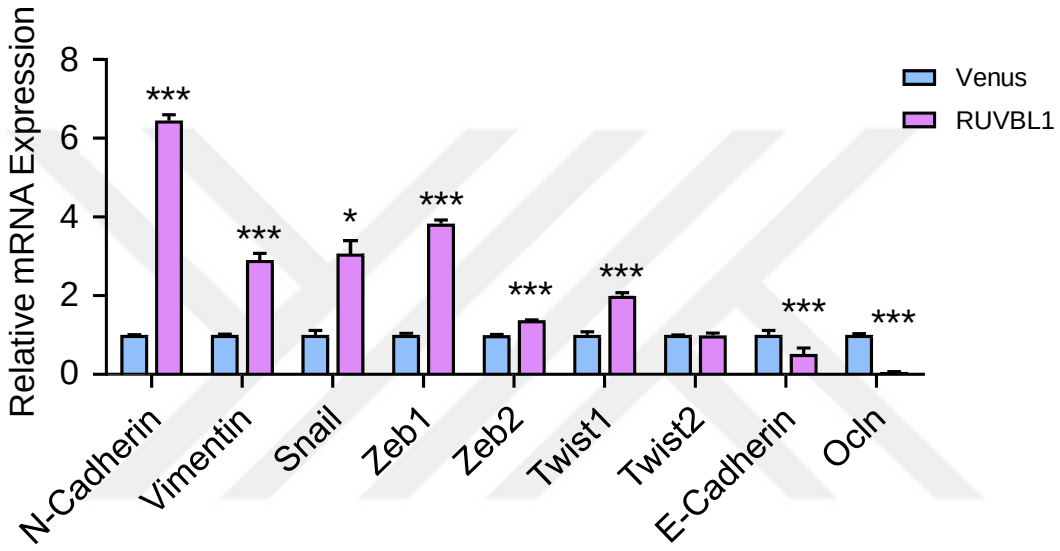


Figure 35. Relative fold change representation of gene expression of EMT marker genes by qRT-PCR analysis. All the experiments were carried out in triplicate. RPL41 was used as an internal control.

There is substantial evidence that RUVBL1 can modulate EMT in several cancers and solid tumors (63,64). To understand whether RUVBL1 is broadly associated with EMT in MPM, we performed GSEA comparing RUVBL1 mRNA levels with the EMT gene set in three publicly available GEO datasets from clinical cohorts of MPM patients. The analysis revealed that RUVBL1 expression is positively correlated with EMT, suggesting that RUVBL1 may be involved in the regulation of EMT in MPM (Figure 36).

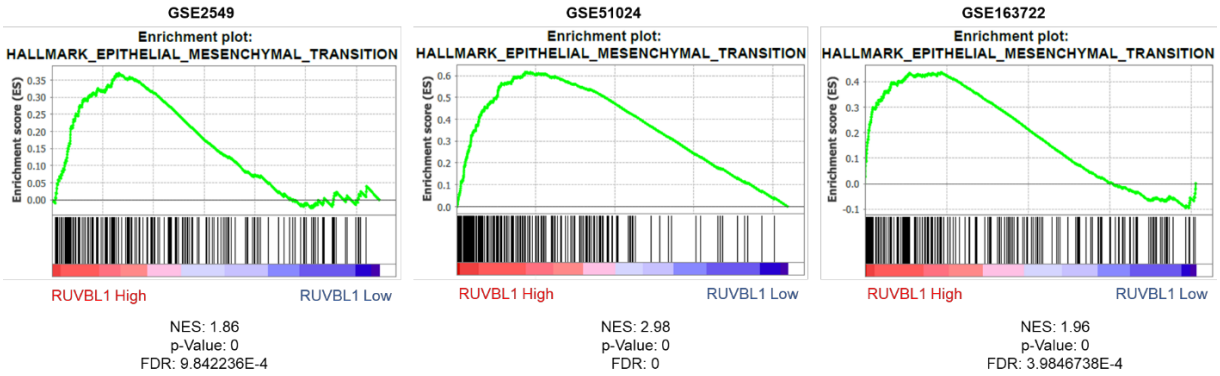


Figure 36. Gene set enrichment analysis of target genes regulating the EMT phenotype in RUVBL1 low and high MPM samples. The median value of the scores was used to divide cohorts into high and low groups for within each cohort. Enrichment plots along with normalized enrichment score (NES) and false discovery rate (FDR) are shown for both Hallmark gene sets for which enriched expression is seen in the high compared to the low group in three GEO Datasets.

6.12. CB-6644 Inhibits the Proliferation and 2D Growth Capacity of MPM Cells

Our findings, so far, indicate that the pharmacological inhibition of RUVBL1 may represent a viable therapeutic avenue for treating MPM. CB-6644 is an allosteric small-molecule inhibitor of RUVBL1 with demonstrated anti-cancer activity. As a result of the study with 123 cancer cell lines, it has been proven that this molecule specifically interacts with the RUVBL1/2 complex and inhibits ATPase activity in cancer cells. (65). To examine the effect of CB-6644 inhibitor in MPM cells, we first performed MTT analysis to determine the IC50 values in H2052 and H2452 cell lines. For this, we seeded H2052 and H2452 cells in 96-well cell culture plates in 6 replicates per dose. The next day, we treated cells with 5 different doses of CB-6644 inhibitor, 50 nM, 100 nM, 200 nM, 400 nM, and 800 nM (Control group was supplemented with DMSO only). We incubated cells with inhibitor for 3 days and performed the MTT protocol to calculate cell viability of inhibitor treated cells, compared to the control group. The drug dose that exhibited 50% reduction in cell viability was calculated in the GraphPad program (Figure 37).

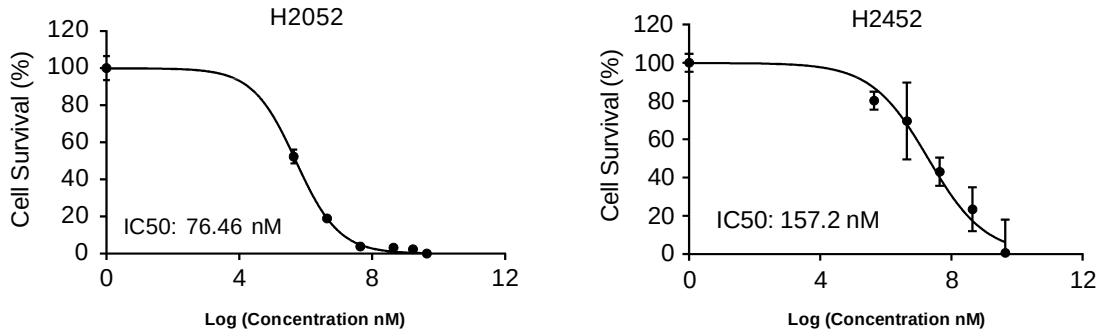
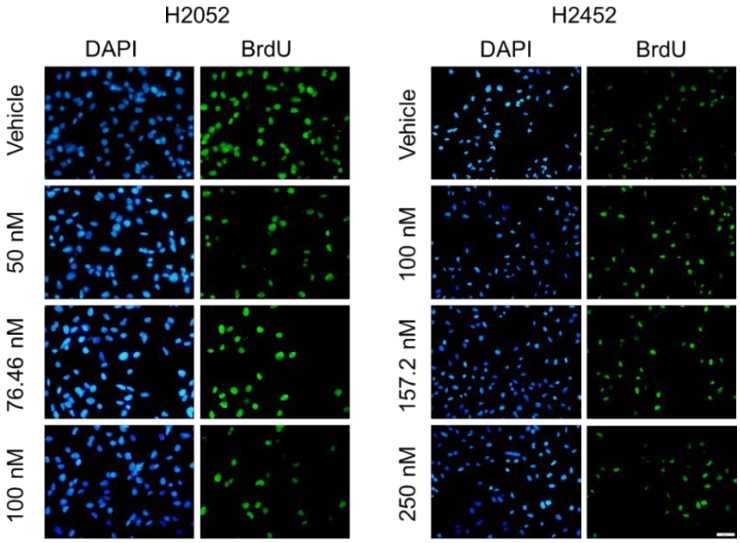


Figure 37. Half maximal inhibitory concentration (IC50) values of CB-6644 in H2052 and H2452 cell lines. The inhibitory doses of CB-6644 on MPM cell growth after 72 hours of treatment were shown in the graphs.

After determining the IC50 concentrations (H2052: 76.46 nM; H2452: 157.2 nM), we examined the effects of CB-6644 on cell proliferation using 3 different doses, i.e., the IC50, and one below, and one above of the IC50 curve. For this, we seeded 10.000 cells/well in 24-well cell culture dishes as triplicates for 4 different conditions (H2052: control, 50 nM, 76.46 nM, 100 nM; H2452: control, 100 nM, 157.2 nM, 250 nM). The next day, we treated the cells with the determined doses of inhibitor. After 3 days of incubation, we discarded the medium containing inhibitor and added the fresh RPMI containing BrdU reagent. After 12 hours of labeling, we followed the BrdU incorporation protocol. Our results revealed that cell proliferation decreased in parallel to the dose of inhibitor administered to H2052 cells increased. In H2452 cells, on the other hand, we could not see any effect at the 100 nM inhibitor treatment, but we saw the same effect at 157.2 nM and 250 nM (Figure 38).



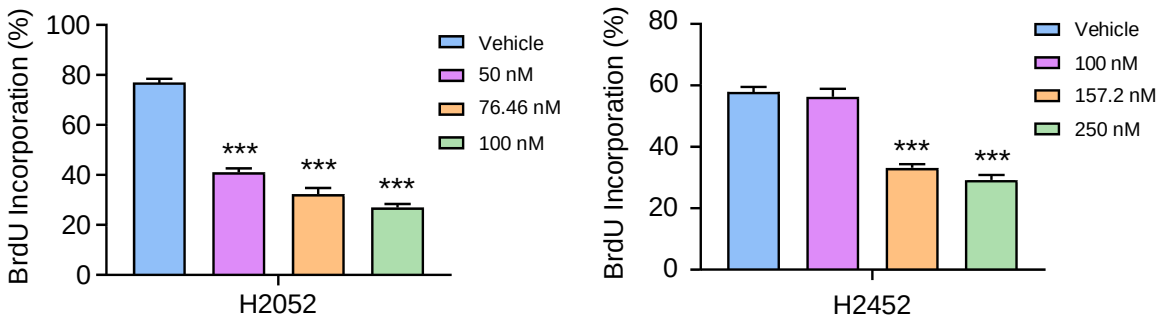


Figure 38. Demonstration of the inhibitory effect of different doses of CB-6644 on MPM cell proliferation by BrdU assay. Cells were treated with CB-6644 for 72 hours. From cells labeled with 10 mM BrdU for 12 hours, cells stained with DAPI and/or BrdU in 7 randomly selected regions for each condition were counted. The number of BrdU-labeled cells was proportioned to cells stained with DAPI. Control cells (Vehicle) treated with DMSO. 20X magnification, scale bar represents 50 µm.

Next, we analyzed the effect of inhibitor in colony-forming capacity of MPM cell lines. For this, we plated 1000 cells per well in 6-well cell culture plates with triplicates for 4 conditions. The next day, we gave the cells a medium containing the determined inhibitor doses. We changed the medium including CB-6644 of the cells every 3 days. After 10 days, we found a significant reduction in colony-forming capacity in both cell lines, including the lowest dose inhibitor treatment. While we observed a pattern of decreasing colony-forming capacity as the inhibitor dose increased in the H2452 cell line, we observed that the same effect occurred in all inhibitor doses in the H2052 cell line (Figure 39).

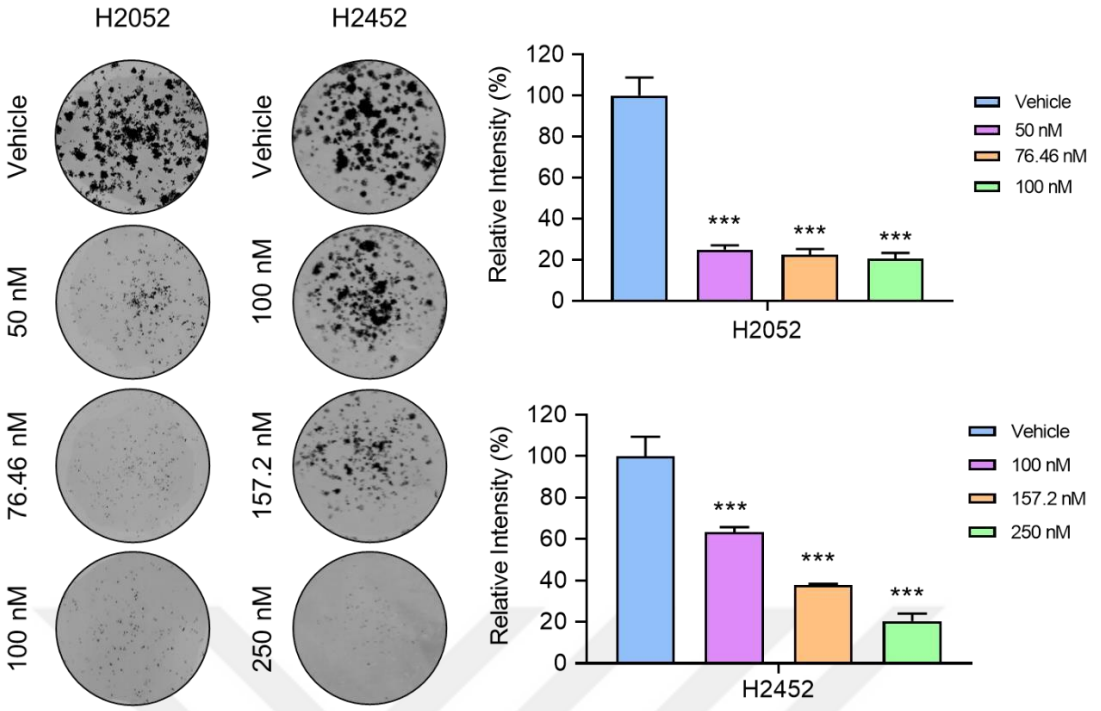


Figure 39. Cell survival results of CB-6644 treated cells reflected by colony formation assay. CB-6644 treated cells were proportioned to control cells. The experiment was performed in 3 technical replicates.

6.13. CB-6644 Reduces Cell Proliferation and Induces the Apoptosis of MPM Cells

We performed cell cycle analysis to examine the effect of the inhibitor on cell cycle progression. As a result of these experiments, cells displayed G2 phase arrest in H2052 cells, especially at IC50 and one above dose. On the other hand, H2452 cells displayed S arrest at IC50 and the one above dose. These results also supported the RUVBL1 knockout experiments (Figure 40).

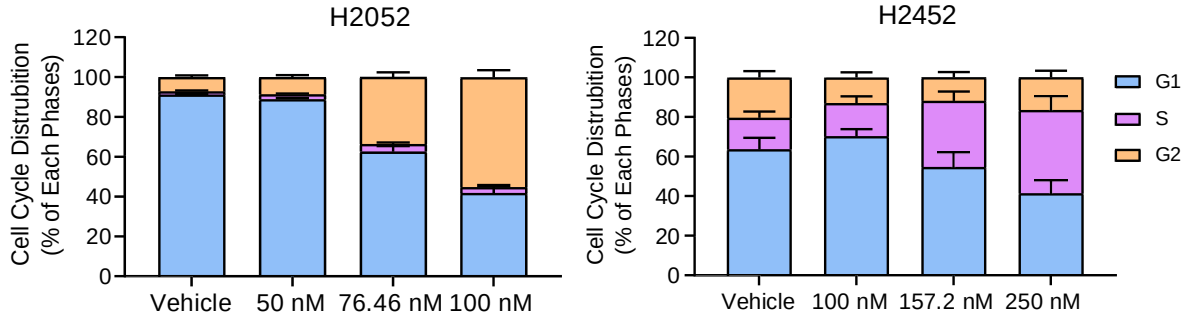
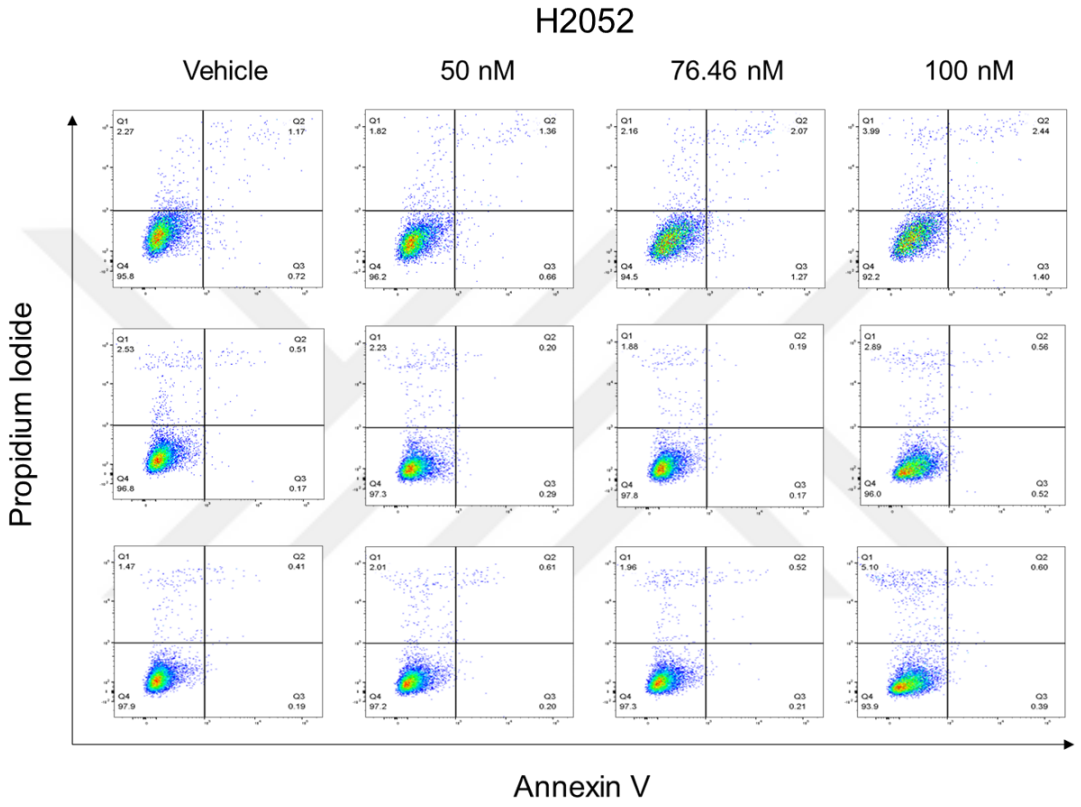


Figure 40. Cell cycle distribution of CB-6644 treated and control MPM cells. The experiments were performed in 3 biological replicates.

Using Annexin V/propidium iodide, we then examined whether RUVBL1 inhibitor treatment induces apoptosis in MPM cells. As a result of the experiment, which we carried out with 3 biological replicates, we observed an increase in the mean rate of apoptotic cells after RUVBL1 inhibition in both cell lines. However, this increase was not significant due to the deviation between biological repeats (Figure 41).



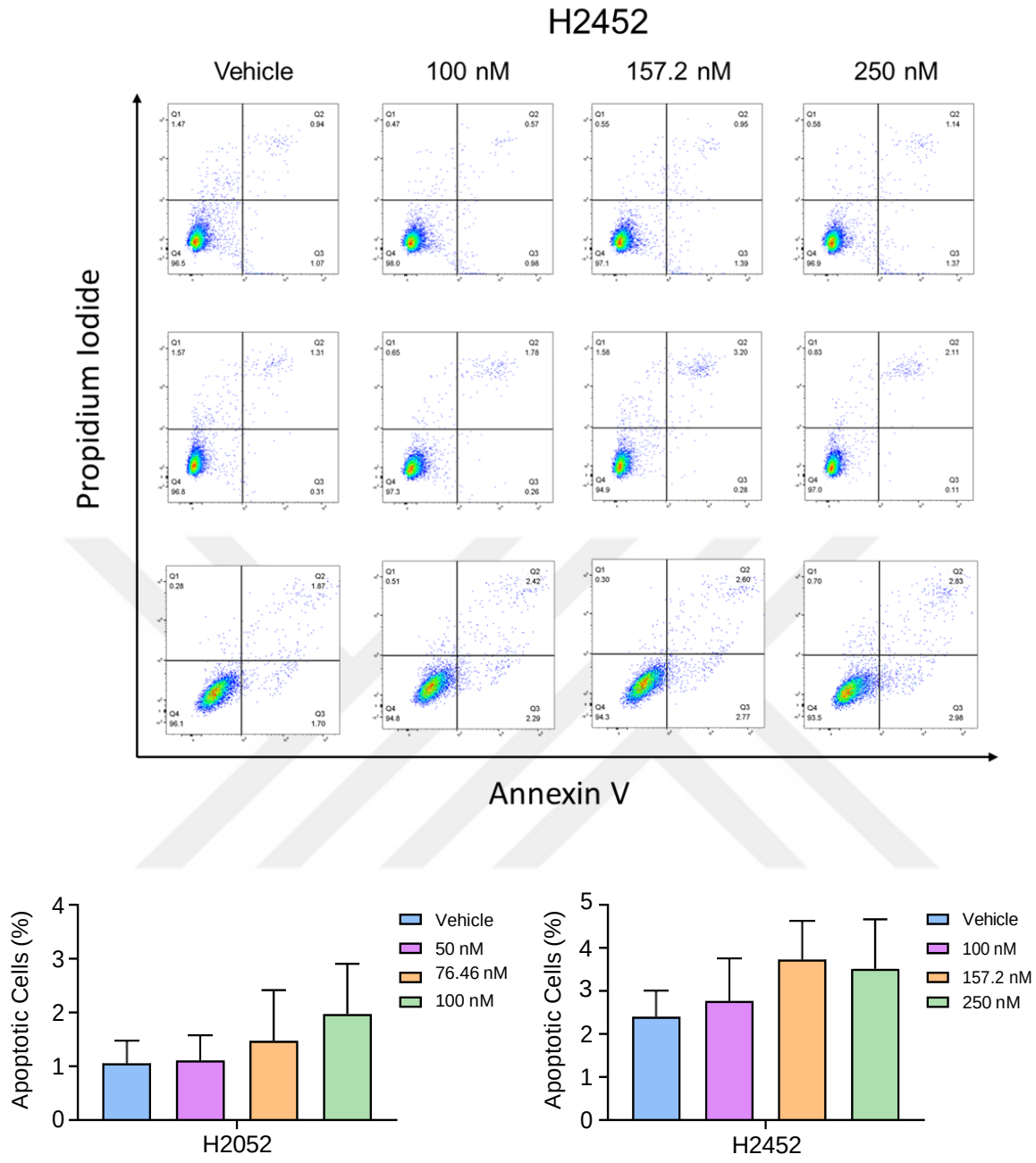
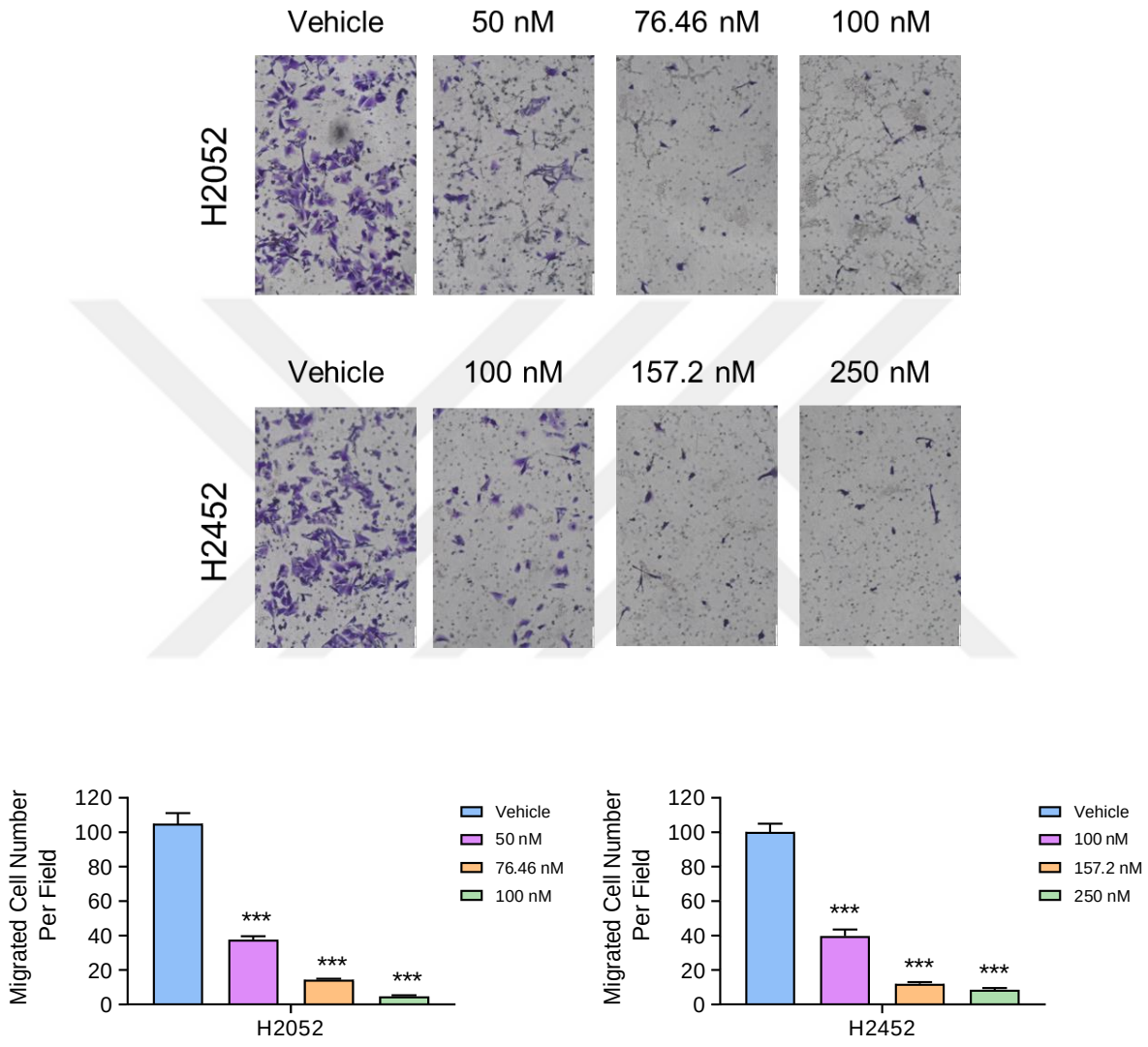


Figure 41. Apoptosis measurement of apoptosis by flow cytometry. Flow cytometry Annexin V/PI staining to quantify apoptosis CB-6644 treated or control MPM cells. The total amount of apoptotic cells (early (Q3) + late (Q2)) is shown in the graph. Experiments were performed in triplicates.

6.14. CB-6644 Inhibits Cell Migration and Invasion Capacity of MPM Cells

We then evaluated the migration and invasion capabilities of MPM cells in the absence of RUVBL1. We seeded H2052 and H2452 cells into a 6-well plate and the next day, we treated the cells with certain concentrations of CB-6644 inhibitor for 3

days. Then, we seeded cells into matrigel-coated and matrigel-free Boyden chambers for invasion and migration assays, respectively. After 48 hours, we followed the staining protocol and analyzed the results. We found that the invasion and migration capacities of both cell lines were significantly reduced in the absence of RUVBL1 (Figure 42).



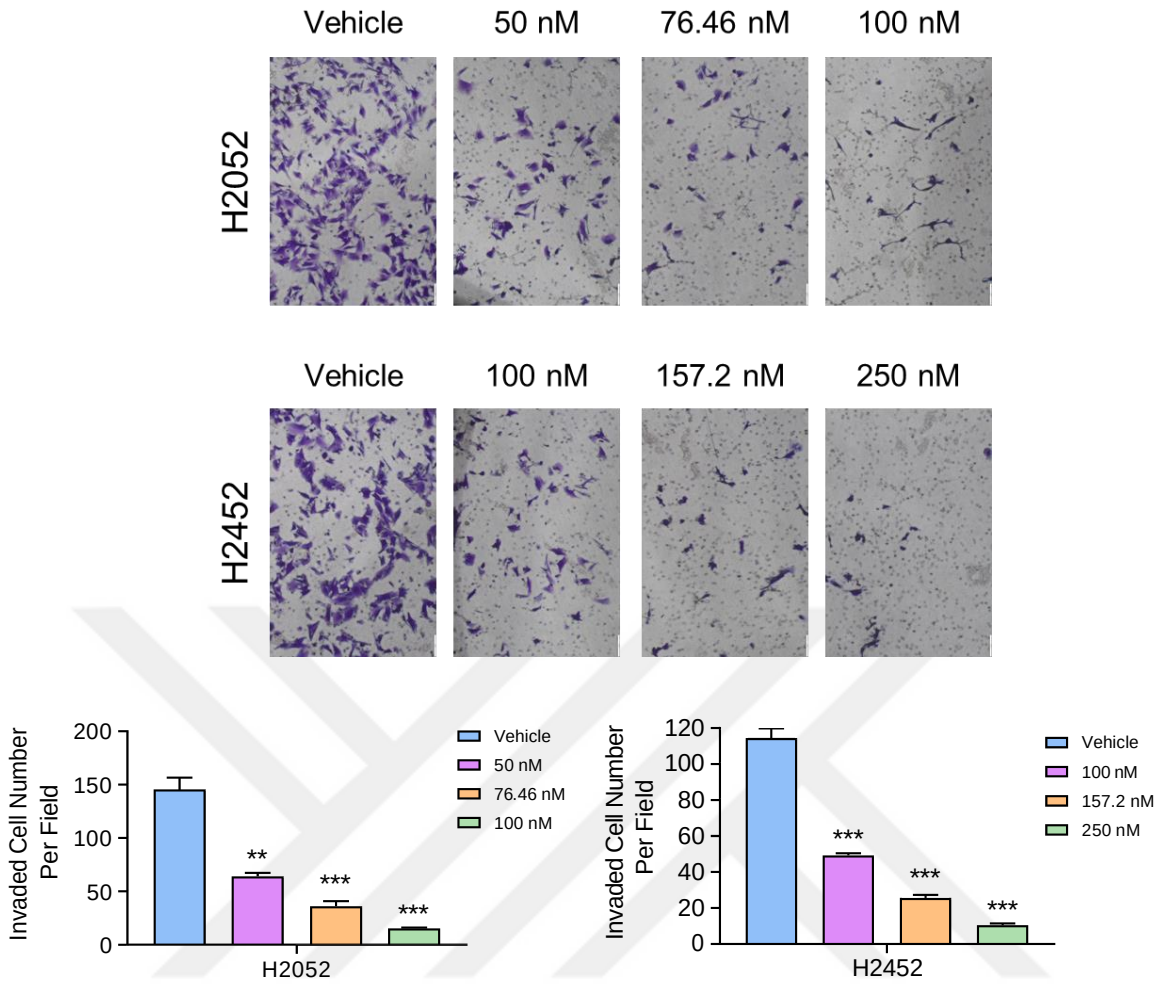


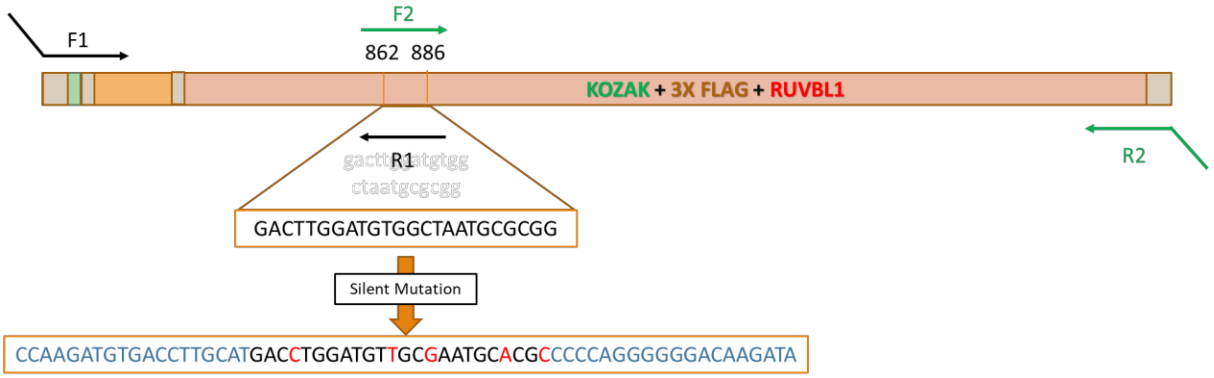
Figure 42. Representative images and quantification of Migration and invasion capacity of CB-6644 treated and control MPM cells. Experiments were performed in duplicate. Invaded/migrated cells were counted from randomly selected 5 area. 10X magnification, scale bar represents 100 µm.

6.14. Development of *RUVBL1* gRNA Resistant MPM Cells

6.14.1. Engineering of Mutant *RUVBL1* (mRUVBL) Construct

To develop gRNA resistant cells, we created silent mutations in the region where the RUVBL1 g2 oligonucleotide binds and in the first nucleotide of the PAM sequence (NGG). We designed a total of 62 nucleotides forward and reverse (RUVBL1 F2 and RUVBL1 R1) primers covering this 24-nucleotides region. We used the first and last 23 nucleotide regions of the sequence of the RUVBL1 gene as forward and reverse (RUVBL1 F1 and RUVBL1 R2) primers to generate the fragments shown in the Figure 43a.

a)



b)

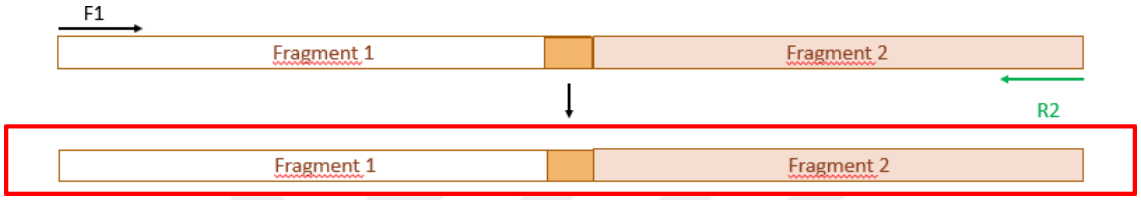


Figure 43. Schematic representation of the generation of RUVBL1 g2-resistant MPM cells. a) Creation of silent mutations in the RUVBL1 g2 binding region of RUVBL1 coding sequence. b) Synthesis of mRUVBL1 sequence by PCR.

We synthesized Fragment 1 with primers RUVBL1 F1 and RUVBL1 R1 in one test tube and Fragment 2 with primers RUVBL1 F2 and RUVBL1 R2 in the other test tube by PCR using the pLV-EF1a-3XFlag-Pontin-IRES-Puro vector as a template. We performed the gel electrophoresis with PCR product and recovered the relevant bands from the gel using the Gel Purification Kit. Then, using these fragments and RUVBL1 F1 and RUVBL1 R2 primers, we synthesized the mRUVBL1 by PCR (Figure 43b). After performing the gel electrophoresis with this PCR product, we recovered the relevant band from the gel and cloned it into the pLV-EF1a-IRES-Puro lentiviral vector.

6.14.2. Validation of mRUVBL1 in MPM Cells

We performed virus packaging of pLV-EF1a-Venus-IRES-Puro and pLV-EF1a-mRUVBL1-IRES-Puro lentiviral vectors and infection of H2052 and H2452 cell lines, followed by puromycin selection. We then infected these cells with virus particles containing gREN and RUVBL1 g2 and completed the puromycin selection. Since the vectors we use in both infections have puromycin selection markers, we saturated the

second infection with RUVBL1 g2 and gREN viral particles. Thus, after the second infection, we aimed to minimize the number of non-infected cells with gRNA as much as possible. We performed western blot analysis with the lysates collected on the 7th day of infection (Figure 44).

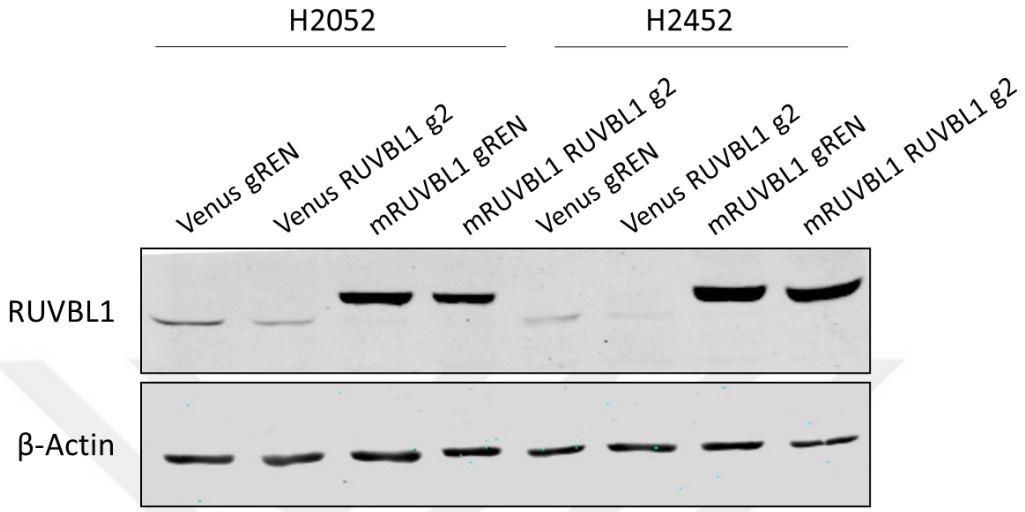


Figure 44. Validation of RUVBL1 g2-resistant H2052 and H2452 clones by western blot.

As expected, there was a decrease in the amount of RUVBL1 when cells infected with Venus were subsequently infected with RUVBL1 g2. In addition, we observed an increase in mRUVBL1-infected cells compared to Venus, followed by no change in RUVBL1 expression level when infected with RUVBL1 g2. These results proved that we developed cells resistant to RUVBL1 g2.

6.14.3. gRNA Resistant MPM Cells Display Rescued 2D Growth Capacity

To check whether there is a change in colony-forming capacity in mRUVBL1-infected cells after RUVBL1 g2 infection, we performed a 2D colony formation assay simultaneously with the clones we validated by Western blot (Figure 45).

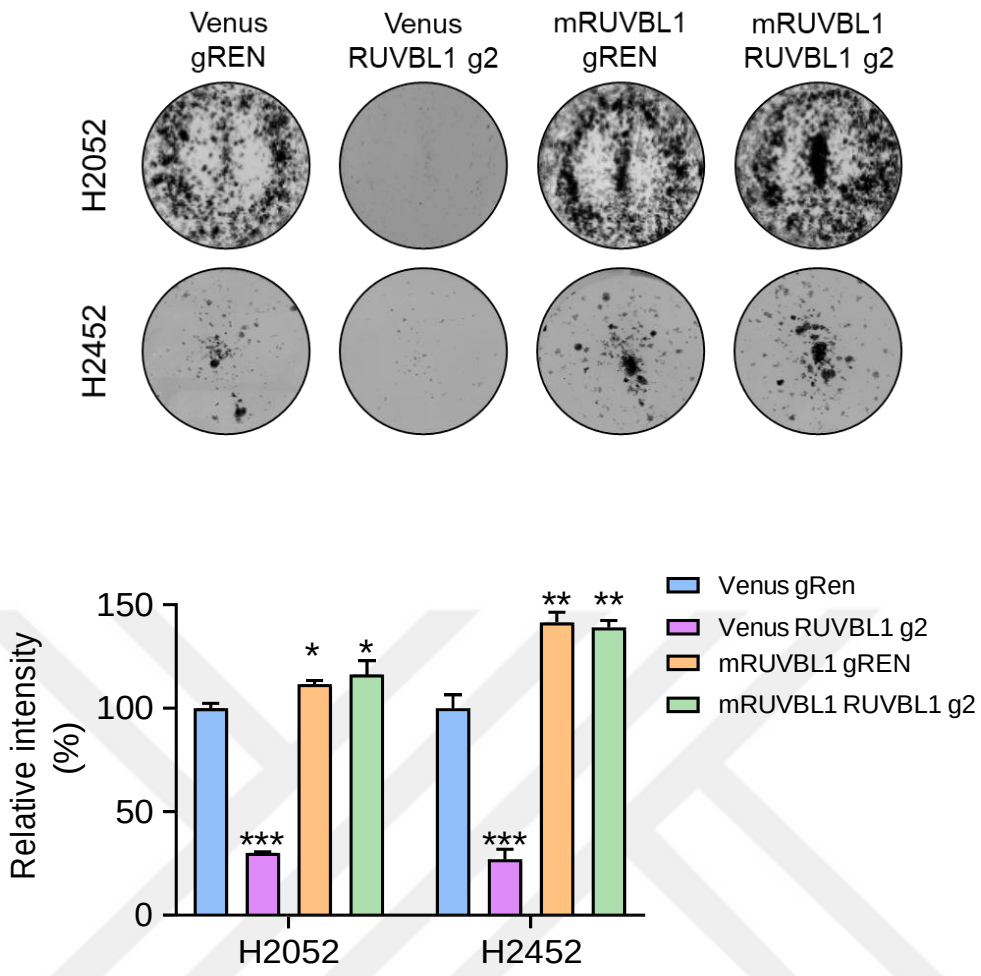


Figure 45. Colony formation analysis of gRNA resistant MPM cells. The experiment was performed in 3 technical replicates. H2052 cells were seeded into the 6-well plates; H2452 cells were seeded into the 12-well plates.

Chapter 2

6.15. Validation of Inducible System

Functional studies for genes associated with cancer cell survival are generally compromised by the depletion of an essential gene. We have shown that cell proliferation significantly decreased when RUVBL1 was depleted. In this respect, we conducted proof-of-concept experiments with the goal of developing an inducible knockout system for future studies.

6.15.1. Obtaining Cell Clones That Express Inducible Cas9

To obtain the cell clones that express inducible Cas9, we first infected H2052 and H2452 cells with virus particles in which we packaged the pCW-Cas9 lentiviral vector with Cas9 coding sequence at different dilutions (1/5, 1/10, 1/15). We then selected the cells with puromycin for 3 days and stocked the cells after 2 days of recovery. Subsequently, western blot was performed to confirm Cas9 expression in these cells by administering 1 µg/mL Doxycycline for 3 days and using monoclonal Flag-M2 antibody (Cas9 is expressed with an N-terminal 3xFlag tag) (Figure 46).

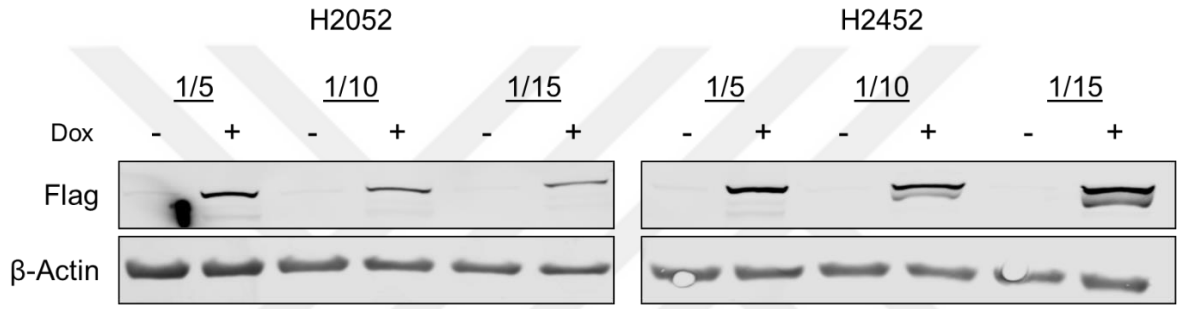


Figure 46. Validation of inducible Cas9 expressing cells by western blot analysis.

6.15.2. Obtaining *RUVBL1* Knockout Cell Clones

In parallel, we cloned the gRNAs targeting the *RUVBL1* gene and the Renilla gRNA not targeting the human genome into the pLentiGuide-Hygro-dTomato lentiviral vector and packaged the virus. Next, we infected cells in which we demonstrated inducible Cas9 expression (virus-infected clones at 1/10 dilution were selected) with these lentiviruses carrying gRNA and left the cells to selection for 4 days with 150 µg/mL Hygromycin. Thus, we developed polyclonal cell models that express inducible Cas9 and constitutively gRNA. Next, we conducted a series of functional experiments by administering 1 µg/mL Doxycycline to these models for specific periods of time to test whether the inducible genome editing system was working effectively. Specifically, we performed MTT analysis and colony formation assays, which can be quickly tested as an expected indicator of possible *RUVBL1* depleting in experiments, using cell clones with and without doxycycline (Figure 47).

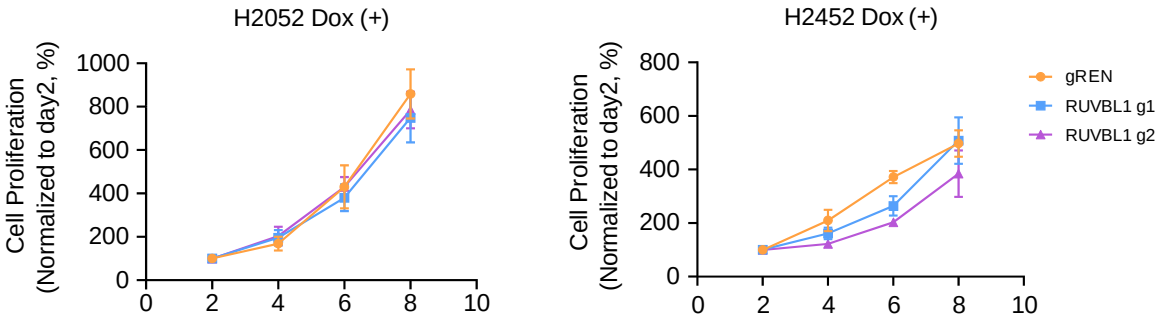


Figure 47. Comparison of the viability of H2052 and H2452 cells infected with gREN and RUVBL1 gRNAs. Cells were treated with 1 µg/mL Doxycycline for three days, then seeded to 96-well plates. The first measurements were made after 2 days of cell seeding and these values were normalized to 100. The following days' measurement results were proportioned to the first day. The experiment was performed in 6 technical replicates.

When we evaluated the MTT results of cells given doxycycline alone, we found no significant difference in the proliferation of cells targeted to the *RUVBL1* gene compared to Renilla. In addition, we observed a partial suppression effect on cell proliferation in H2452 cells on days 4 and 6, but this was not permanent and sustained as the effect was largely lost at day 8 measurements (Figure 48).

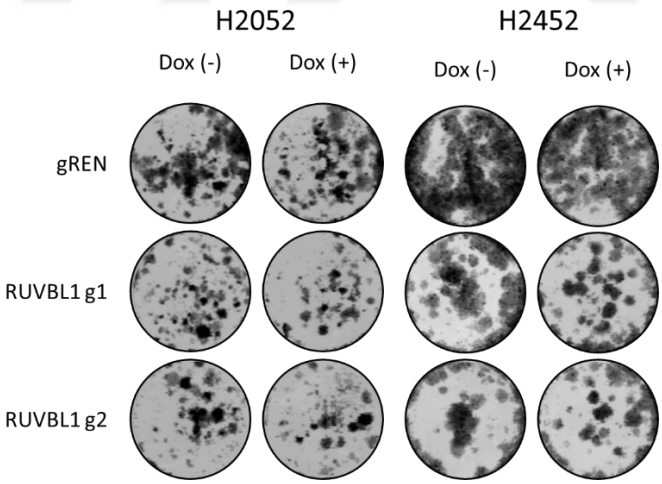


Figure 48. Cell survival results of RUVBL1 gRNAs or gREN infected cells reflected by colony formation assay. Cells were treated with1 µg/mL Doxycycline continuously. End of the 10 days cells were stained with crystal violet. The experiment was performed in 3 technical replicates.

When we look at the results of the experiment in which we set up simultaneously and measured the colony-forming capacity of the cells, we observed that the colony-

forming capacity of the cells given doxycycline and targeting the *RUVBL1* gene decreased compared to the Renilla control clone. However, in this experiment, we saw that a similar effect occurred in cells that were not given doxycycline. In this respect, we examined the time-dependent change in *RUVBL1* expression (protein isolation was performed on days 6 and 9) in the clones we used in MTT and colony formation experiments by western blot (Figure 49). However, we were unable to produce conclusive and final results that we could interpret and evaluate by associating changes in *RUVBL1* expression with doxycycline administration in both cell lines.

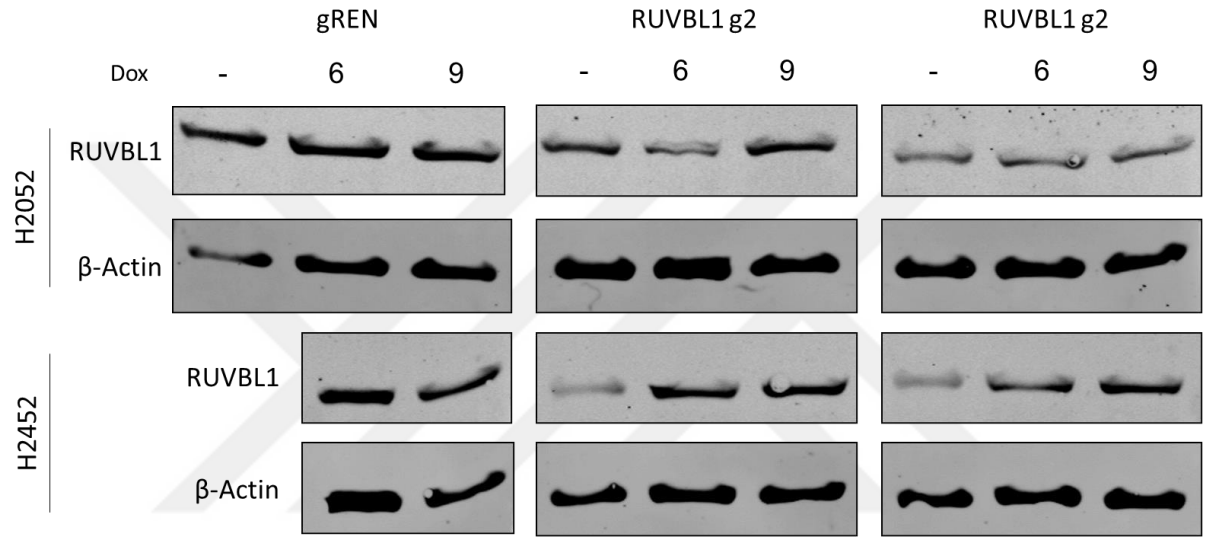


Figure 49. Western blot analysis of time-dependent change of RUVBL1 expression in gREN or RUVBL1 gRNAs infected cells.

6.15.3. Validation of the Inducible Cas9-Expressing and *RUVBL1* Knockout Cell Clones

We developed new clones in line with the primary findings in our preliminary studies. As such, we used pCW-Cas9 lentivirus particles at lower dilutions (1/20, 1/30, 1/40) (Figure 50). In this study, in which we found a great similarity with the previous results, this time we froze the cells that express inducible Cas9 we developed with 1/40 virus dilution to take stock.

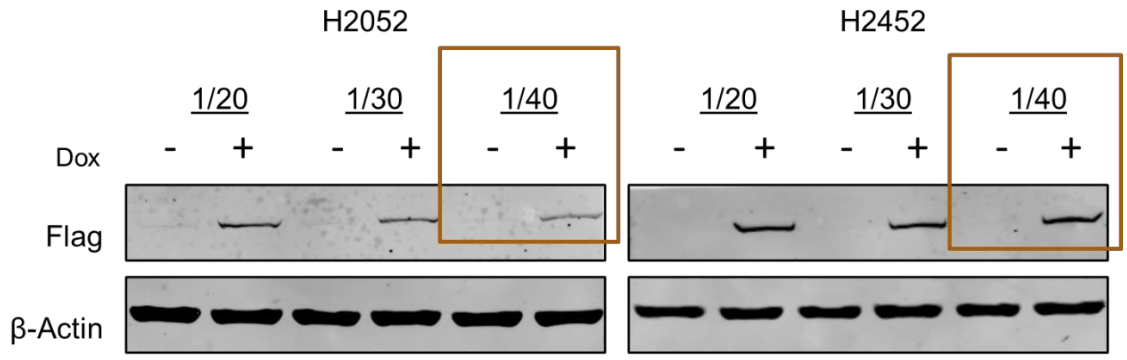
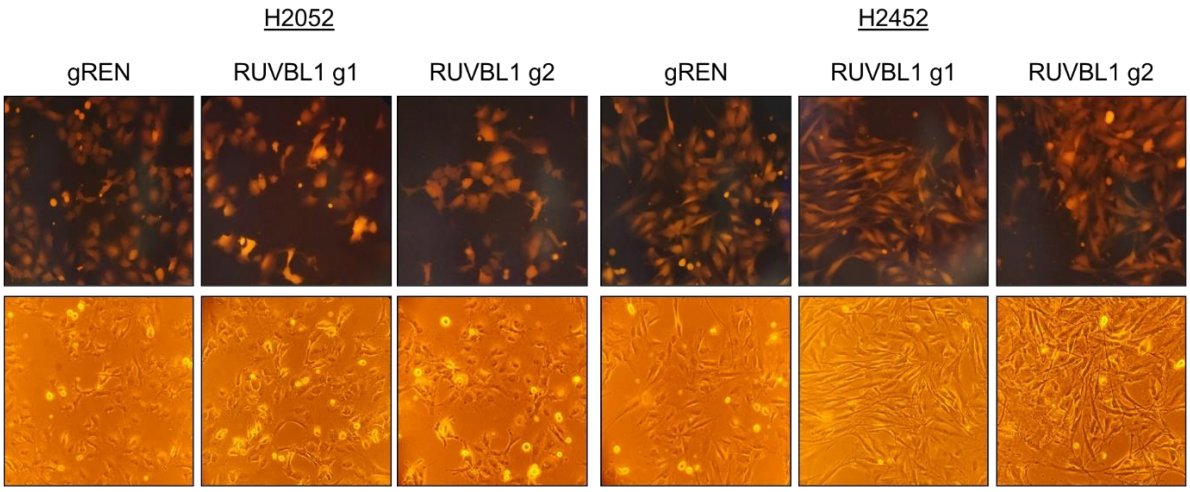


Figure 50. Validation of inducible Cas9 expressing cells by western blot analysis.

In addition, we infected the same clones with gRNA-cloned pLentiGuide-Hygro-dTomato lentiviral vectors using the optimal dose of virus particles. This time, we selected infected cells by FACS to greatly enrich dTomato + (positive) cells to obtain a clone (inducible Cas9 + gRNA) and stock (Figure 51a). Before moving on to functional studies, we carried out some control experiments. First, we administered 1 µg/mL Doxycycline to the cells for 9 days and controlled the change in RUVBL1 expression over time. Western blot results showed a decrease in RUVBL1 protein expression in H2452 cells after 9 days of Doxycycline treatment, while no change was observed in H2052 cells (Figure 51b).

a)



b)

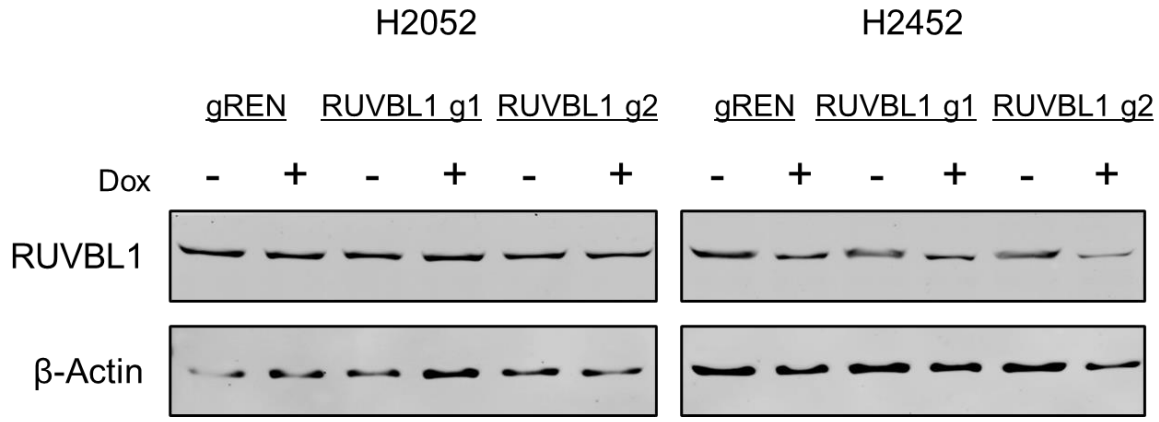
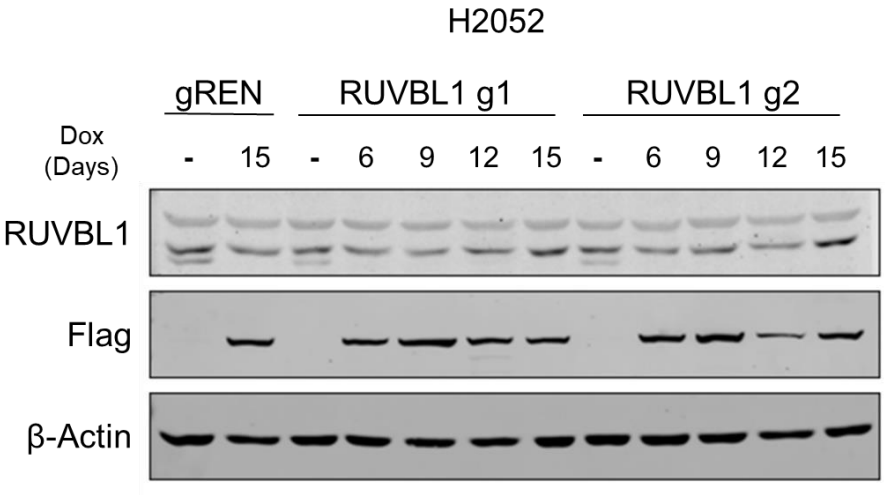


Figure 51. Western blot analysis of RUVBL1 expression in gREN or RUVBL1 gRNAs infected MPM cells.

We thought that the inducible genome editing system might have different spatiotemporal dynamics in the relevant MPM cell lines, and in this context, we decided to conduct a detailed analysis. For this, we extended the 1 µg/mL Doxycycline treatment to 15 days. In this process, we examined the time-dependent change in Ruvbl1 expression in protein samples collected on different days (Figure 52).



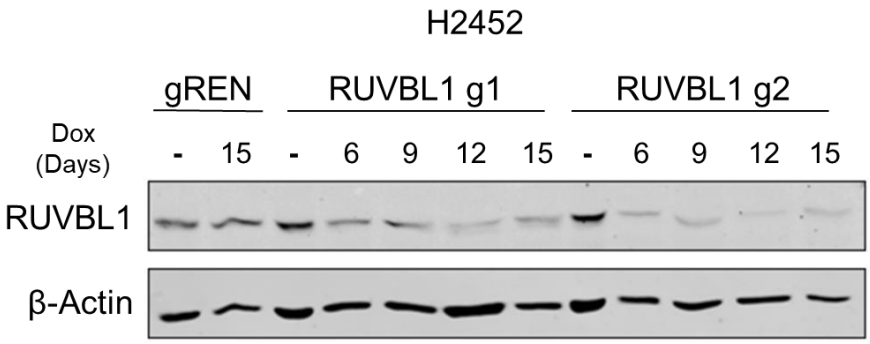


Figure 52. Western blot analysis of time-dependent change of RUVBL1 expression in gREN or RUVBL1 gRNAs infected cells.

When we evaluated the results, we easily saw that the expression of RUVBL1 in the H2452 cell line decreased with time with 2 different gRNA targeting. This shows that we can successfully operate the inducible system in this cell line after detailed optimization studies. However, the same was not true for the H2052 cell line. Of note, in western blot studies with lysates from H2052 cells, the RUVBL1 antibody occasionally gives multiple bands. We know that the main band is the prominent band in the middle. To understand whether this could be explained by Cas9 expression, we examined Cas9 expression in H2052 samples using the Flag antibody. We found that Cas9 induction worked as expected in all samples given doxycycline, but that this was not reflected in *RUVBL1* silencing.

At this point, it is safe to conclude that optimization studies should continue in order to use the inducible genome editing system jointly in both cell lines and to solve the problem especially observed in H2052.

7. DISCUSSION

MPM, arising in the pleural membrane of the lung, is a very aggressive and rarely treatable disease. Although the worldwide incidence of MPM varies depending on asbestos exposure, which is the main etiological factor, its incidence is expected to increase in the coming years due to the uncontrolled production and use of asbestos in underdeveloped countries (5,6). Therefore, it is very important to develop new

treatment strategies for MPM. There is no proven treatment beyond first-line therapy for MPM for which no curative treatment has yet been found (66). In order to develop treatments for MPM, a highly heterogeneous cancer, the underlying molecular mechanisms need to be clarified.

Today, CRISPR/Cas9-mediated focused or genome wide screen studies are one of the most effective approaches used for gene function studies. Gene pools obtained by genome wide CRISPR screen can be used to identify genes that may be cancer targets in the relevant cell (67). Thanks to these studies, signaling pathways and genes that regulate cellular and molecular mechanisms in many cancers have been identified. In this study, we performed molecular and functional studies of the *RUVBL1* gene, one of the MPM cell survival-related genes, which was identified as a result of the whole genome CRISPR/Cas9 screen performed in our lab to elucidate the mechanisms involved in MPM carcinogenesis in 2 cell lines.

Depending on whether RUVBL1 is localized in the nucleus or cytoplasm, it is involved in DNA damage repair, chromatin remodeling, and telomerase biogenesis, as well as its ATPase and ATP-dependent helicase activities (47,50,68). Studies of the function of RUVBL1 in cancer have shown that decreased expression level is associated with cancer cell survival such as epithelial ovarian cancer, non-small cell lung cancer, head and neck squamous cancers (48,69,70). In addition, previous studies have reported that nuclear β-catenin is significantly reduced after RUVBL1 depletion(64) and promotes EMT in cells through decreased E-Cadherin expression and increased Vimentin expression (63). However, there are no studies on its molecular role in MPM carcinogenesis.

In this study, we aim to perform CRISPR/Cas9 mediated genetic ablation, overexpression, and pharmacological inhibition-based studies on the molecular role of the *RUVBL1* gene in MPM, which we know is inversely related to MPM survival. For this purpose, firstly, CRISPR/Cas9-mediated silencing of the *RUVBL1* gene in H2052 and H2452 cell lines was achieved and its effects on cell proliferation, two- and three-dimensional colony formation capacity, cell cycle, DNA damage, invasion, and migration were explained. Then, by overexpressing the gene, its effects on cell proliferation, invasion and migration, its three-dimensional colony-forming capacity, and its relationship with EMT were investigated. Finally, the effects of pharmacological

inhibition of *RUVBL1* on cell proliferation, 2D colony forming capacity, invasion and migration were studied.

We started our studies by showing the association of the *RUVBL1* gene with MPM cell survival. For this, we infected MPM cells with *RUVBL1* gRNAs that we cloned into the pECPV vector and performed a 12-day competition assay. We then cloned the same oligos into the pLentiCRISPR v2 vector and performed MTT analysis, BrdU labeling, and 2D and 3D Colony Formation experiments showing their relationship to MPM cell proliferation. All the results we obtained supported that the proliferation rate of the cells in which we silenced the *RUVBL1* gene slowed down. Then, we investigated the reasons for the slowing down of cell proliferation by performing cell cycle analysis, SA-β-GAL staining, and Annexin V analysis. H2052 and H2452 cells showed arrest at different phases of the cell cycle. We plan to carry out further studies to investigate the reasons for this. When *RUVBL1* was depleted, we observed senescence phenotype in both cell lines. In addition, we showed that after depleting the *RUVBL1* gene, there was an increase in the rate of apoptotic cells after *RUVBL1* depletion in both cell lines. However, in the H2452 cell line the results were not significant due to the deviation between the biological repeats we made. We then performed γH2AX staining and comet assays to detect DNA damage to elucidate the underlying mechanisms of reduction of proliferation and cell cycle arrest. We found DNA damage in cells in which the *RUVBL1* gene was depleted in both experiments showing double-strand and single-strand breaks, respectively. Finally, we performed wound healing, invasion, and migration experiments to investigate the effect of the *RUVBL1* gene on aggressive phenotypes. We found that the invasion, migration, and motility abilities of the cells decreased in both cell lines in which we silenced the *RUVBL1* gene.

According to elucidating results, we investigated whether we would see the opposite effect when we overexpress the *RUVBL1* gene in the same cell lines. For this, we first infected cells with the lentiviral expression vector including the *RUVBL1* sequence and validated the overexpression by western blot analysis. After overexpression of 3X Flag-tagged RUVBL1, RUVBL1 bands displayed higher molecular weight than expected bands on the membrane. The reason of that maybe PAGE transports proteins according to their denatured hydrodynamic radii, so if the protein with the Flag-Tag is not fully denatured from folding, the protein may stay higher than expected. Besides, Flag-tag is very rich in aspartates, which leads to the high negative charge of the tag.

Any additional negative charge can lead to a different migration of the same protein, so a slightly higher than expected band can be seen on SDS-PAGE. In addition, western blot analysis after overexpression with the pCDNA 3XFlag Pontin plasmid from Addgene showed a shift similar to our results (71). Next, we performed BrdU labeling to examine effect of *RUVBL1* overexpression on cell proliferation. We revealed that BrdU incorporation is increased in *RUVBL1* overexpressed cells, that is, the proliferation rate is higher than in control cells. Next, we performed a 3D colony formation assay and reported that the colony-forming capacity was significantly increased in cells where *RUVBL1* was upregulated. Then, we examined the effects on aggressive phenotypes with wound healing and invasion experiments. We showed that cell motility and invasion capacity increased in both cell lines in which we overexpressed *RUVBL1*. Finally, considering the information in the literature (63,64), we performed Phalloidin staining, western blot, and qRT-PCR with EMT marker genes to show the association between the overexpression of *RUVBL1* and the EMT profile, and we found that the cells went to EMT by overexpression of *RUVBL1* in the H2052 cell line.

Finally, we examined the effects on MPM cells by treating cells with CB-6644, a pharmacological inhibitor of RUVBL1 (65,72). For this, we first determined the IC50 value of the inhibitor in both cell lines. Then, we performed BrdU analysis and 2D colony formation assay to examine the effects of the inhibitor on cell proliferation. With these experiments, we found that CB-6644 has a proliferation inhibitory effect in both cell lines. We then examined the effect of the inhibitor on the invasion and migration capacities of cells. We showed that cells given CB-6644 significantly reduced their capacity to invade and migrate, like when we silenced the *RUVBL1* gene with CRISPR.

Concurrent with our functional studies to examine the molecular role of the *RUVBL1* gene in MPM we performed experiments to develop the inducible system. Although we have reached a certain point in these studies, where we aim to prevent biological variation in experiments by inducing a single clone, optimization studies should continue. In order to avoid variation with the pLentiCRISPR v2 vector, we started experiments simultaneously after infection.

8. CONCLUSION AN FUTURE PERSPECTIVE

We showed that depletion of *RUVBL1* significantly reduced cell proliferation in H2052 and H2452 cells, in which we knocked out the *RUVBL1* gene with 2 different gRNAs from the Brunello library. We then examined the effect of *RUVBL1* on cancer-aggressive phenotypes in these cells. We found that when *RUVBL1* was depleted, the migration and invasion capacity of cells decreased. Our experiments with CB-6644, a pharmacological inhibitor of RUVBL1, also supported these results. We conducted further studies to understand the underlying mechanisms of the association of *RUVBL1* with cell proliferation and cell cycle arrest. We detected DNA damage in cells in which we depleted *RUVBL1*. We then showed that *RUVBL1* overexpression increased proliferation in cells. We observed that the morphologies of the cells in which we had increased *RUVBL1* expression turned into mesenchymal. To confirm this, we performed IF staining with phalloidin and western blot analysis with N-Cadherin and Vimentin antibodies. We found an increase in N-cadherin and Vimentin expression and increased protrusions in H2052 cells with increased *RUVBL1* expression. Then, we proved the transformation from epithelium to mesenchymal in H2052 cells by qRT-PCR analysis with EMT marker genes. We examined the correlation between low and high expression of *RUVBL1* and the expression of target genes E2F, MYC, and EMT with the GSE analyses in 3 different cohorts. GSE analyses supported our experimental studies. Finally, we developed cells resistant to RUVBL1 g2 gRNA and performed rescue experiments. In these experiments, we expected that the cells that we rendered resistant to gRNA would become unresponsive when infected with RUVBL1 g2. We showed that there is no change in the colony formation capacity of gRNA-resistant cells after gRNA infection with the 2D colony formation assay with gRNA-resistant cells, which we validated by Western blot. In future studies, it is planned to examine the cell cycle progression in MPM cells with RUVBL1 depletion. In addition, the mechanism should be better elucidated by examining other signaling pathways associated with RUVBL1. Once these mechanisms are better understood, mouse tumor models targeting RUVBL1 with inhibitor and CRISPR can be developed. After the positive results of these studies, nanoparticles that directly target carcinogenic cells in MPM patients can be designed to contribute to targeted therapy studies.

9. REFERNCES

1. Baas P, Fennell D, Kerr KM, Van Schil PE, Haas RL, Peters S, et al. Malignant pleural mesothelioma: ESMO Clinical Practice Guidelines for diagnosis, treatment and follow-up. Ann Oncol Off J Eur Soc Med Oncol. 2015 Sep;26 Suppl 5:v31-39.

2. Sung H, Ferlay J, Siegel RL, Laversanne M, Soerjomataram I, Jemal A, et al. Global Cancer Statistics 2020: GLOBOCAN Estimates of Incidence and Mortality Worldwide for 36 Cancers in 185 Countries. CA Cancer J Clin. 2021 May;71(3):209–49.

3. Betti M, Aspesi A, Ferrante D, Sculco M, Righi L, Mirabelli D, et al. Sensitivity to asbestos is increased in patients with mesothelioma and pathogenic germline variants in BAP1 or other DNA repair genes. Genes Chromosomes Cancer. 2018 Nov;57(11):573–83.

4. Sinn K, Mosleh B, Hoda MA. Malignant pleural mesothelioma: recent developments. Curr Opin Oncol. 2021 Jan;33(1):80–6.

5. McCambridge AJ, Napolitano A, Mansfield AS, Fennell DA, Sekido Y, Nowak AK, et al. Progress in the Management of Malignant Pleural Mesothelioma in 2017. J Thorac Oncol Off Publ Int Assoc Study Lung Cancer. 2018 May;13(5):606–23.

6. Opitz I, Scherpereel A, Berghmans T, Psallidas I, Glatzer M, Rigau D, et al. ERS/ESTS/EACTS/ESTRO guidelines for the management of malignant pleural mesothelioma. Eur J Cardio-Thorac Surg Off J Eur Assoc Cardio-Thorac Surg. 2020 Jul 1;58(1):1–24.

7. Brcic L, Kern I. Clinical significance of histologic subtyping of malignant pleural mesothelioma. Transl Lung Cancer Res. 2020 Jun;9(3):924–33.

8. Suzuki Y. Pathology of human malignant mesothelioma--preliminary analysis of 1,517 mesothelioma cases. Ind Health. 2001 Apr;39(2):183–5.

9. Classification and Histologic Features of Mesotheliomas. In: Pathology of Malignant Mesothelioma [Internet]. London: Springer London; 2006 [cited 2023 Feb 13]. p. 68–131. Available from: https://link.springer.com/10.1007/978-1-84628-012-2_8

10. Zhou JG, Zhong H, Zhang J, Jin SH, Roudi R, Ma H. Development and Validation of a Prognostic Signature for Malignant Pleural Mesothelioma. Front Oncol. 2019;9:78.

11. Verma V, Ahern CA, Berlind CG, Lindsay WD, Shabason J, Sharma S, et al. Survival by Histologic Subtype of Malignant Pleural Mesothelioma and the Impact of Surgical Resection on Overall Survival. Clin Lung Cancer. 2018 Nov;19(6):e901–12.

12. Kindler HL, Ismaila N, Armato SG, Bueno R, Hesdorffer M, Jahan T, et al. Treatment of Malignant Pleural Mesothelioma: American Society of Clinical

Oncology Clinical Practice Guideline. J Clin Oncol Off J Am Soc Clin Oncol. 2018 May 1;36(13):1343–73.

13. Vigneswaran WT, Kircheva DY, Ananthanarayanan V, Watson S, Arif Q, Celauro AD, et al. Amount of Epithelioid Differentiation Is a Predictor of Survival in Malignant Pleural Mesothelioma. Ann Thorac Surg. 2017 Mar;103(3):962–6.

14. Harling L, Kolokotroni SM, Nair A, Smelt J, King J, Routledge T, et al. Differential Survival Characteristics of Sarcomatoid Subtype in Biphasic Pleural Mesothelioma. Ann Thorac Surg. 2019 Mar;107(3):929–35.

15. Paajanen J, Laaksonen S, Ilonen I, Wolff H, Husgafvel-Pursiainen K, Kuosma E, et al. Computed tomography in the evaluation of malignant pleural mesothelioma—Association of tumor size to a sarcomatoid histology, a more advanced TNM stage and poor survival. Lung Cancer. 2018 Feb;116:73–9.

16. Ferrante D, Mirabelli D, Tunesi S, Terracini B, Magnani C. Pleural mesothelioma and occupational and non-occupational asbestos exposure: a case-control study with quantitative risk assessment. Occup Environ Med. 2016 Mar;73(3):147–53.

17. Dubois F, Bazille C, Levallet J, Maille E, Brosseau S, Madelaine J, et al. Molecular Alterations in Malignant Pleural Mesothelioma: A Hope for Effective Treatment by Targeting YAP. Target Oncol. 2022 Jul;17(4):407–31.

18. Cakiroglu E, Senturk S. Genomics and Functional Genomics of Malignant Pleural Mesothelioma. Int J Mol Sci. 2020 Sep 1;21(17):6342.

19. Hjerpe A, Own SA, Dobra K. Integrative approach to cytologic and molecular diagnosis of malignant pleural mesothelioma. Transl Lung Cancer Res. 2020 Jun;9(3):934–43.

20. Bueno R, Stawiski EW, Goldstein LD, Durinck S, De Rienzo A, Modrusan Z, et al. Comprehensive genomic analysis of malignant pleural mesothelioma identifies recurrent mutations, gene fusions and splicing alterations. Nat Genet. 2016 Apr;48(4):407–16.

21. Churg A, Galateau-Salle F, Roden AC, Attanoos R, von der Thusen JH, Tsao MS, et al. Malignant mesothelioma in situ: morphologic features and clinical outcome. Mod Pathol. 2020 Feb;33(2):297–302.

22. Guo G, Chmielecki J, Goparaju C, Heguy A, Dolgalev I, Carbone M, et al. Whole-Exome Sequencing Reveals Frequent Genetic Alterations in *BAP1* , *NF2* , *CDKN2A* , and *CUL1* in Malignant Pleural Mesothelioma. Cancer Res. 2015 Jan 15;75(2):264–9.

23. Hmeljak J, Sanchez-Vega F, Hoadley KA, Shih J, Stewart C, Heiman D, et al. Integrative Molecular Characterization of Malignant Pleural Mesothelioma. Cancer Discov. 2018 Dec 1;8(12):1548–65.

24. Quetel L, Meiller C, Assié JB, Blum Y, Imbeaud S, Montagne F, et al. Genetic alterations of malignant pleural mesothelioma: association with tumor heterogeneity and overall survival. Mol Oncol. 2020 Jun;14(6):1207–23.

25. Illei PB, Rusch VW, Zakowski MF, Ladanyi M. Homozygous deletion of CDKN2A and codeletion of the methylthioadenosine phosphorylase gene in the majority of pleural mesotheliomas. Clin Cancer Res Off J Am Assoc Cancer Res. 2003 Jun;9(6):2108–13.

26. de Reyniès A, Jaurand MC, Renier A, Couchy G, Hysi I, Elarouci N, et al. Molecular classification of malignant pleural mesothelioma: identification of a poor prognosis subgroup linked to the epithelial-to-mesenchymal transition. Clin Cancer Res Off J Am Assoc Cancer Res. 2014 Mar 1;20(5):1323–34.

27. Bott M, Brevet M, Taylor BS, Shimizu S, Ito T, Wang L, et al. The nuclear deubiquitinase BAP1 is commonly inactivated by somatic mutations and 3p21.1 losses in malignant pleural mesothelioma. Nat Genet. 2011 Jun 5;43(7):668–72.

28. Scherpereel A, Wallyn F, Albelda SM, Munck C. Novel therapies for malignant pleural mesothelioma. Lancet Oncol. 2018 Mar;19(3):e161–72.

29. Buikhuisen WA, Hiddinga BI, Baas P, van Meerbeeck JP. Second line therapy in malignant pleural mesothelioma: A systematic review. Lung Cancer. 2015 Sep;89(3):223–31.

30. Zauderer MG, Kass SL, Woo K, Sima CS, Ginsberg MS, Krug LM. Vinorelbine and gemcitabine as second- or third-line therapy for malignant pleural mesothelioma. Lung Cancer. 2014 Jun;84(3):271–4.

31. Zalcman G, Mazieres J, Margery J, Greillier L, Audigier-Valette C, Moro-Sibilot D, et al. Bevacizumab for newly diagnosed pleural mesothelioma in the Mesothelioma Avastin Cisplatin Pemetrexed Study (MAPS): a randomised, controlled, open-label, phase 3 trial. Lancet Lond Engl. 2016 Apr 2;387(10026):1405–14.

32. Shalem O, Sanjana NE, Hartenian E, Shi X, Scott DA, Mikkelsen TS, et al. Genome-Scale CRISPR-Cas9 Knockout Screening in Human Cells. Science. 2014 Jan 3;343(6166):84–7.

33. Berns K, Hijmans EM, Mullenders J, Brummelkamp TR, Velds A, Heimerikx M, et al. A large-scale RNAi screen in human cells identifies new components of the p53 pathway. Nature. 2004 Mar 25;428(6981):431–7.

34. Tsujino T, Komura K, Inamoto T, Azuma H. CRISPR Screen Contributes to Novel Target Discovery in Prostate Cancer. Int J Mol Sci. 2021 Nov 26;22(23):12777.

35. Kanemaki M, Kurokawa Y, Matsu-ura T, Makino Y, Masani A, Okazaki K ichiro, et al. TIP49b, a New RuvB-like DNA Helicase, Is Included in a Complex Together with Another RuvB-like DNA Helicase, TIP49a. J Biol Chem. 1999 Aug;274(32):22437–44.

36. Puri T, Wendler P, Sigala B, Saibil H, Tsaneva IR. Dodecameric structure and ATPase activity of the human TIP48/TIP49 complex. J Mol Biol. 2007 Feb 9;366(1):179–92.

37. Muñoz-Hernández H, Pal M, Rodríguez CF, Fernandez-Leiro R, Prodromou C, Pearl LH, et al. Structural mechanism for regulation of the AAA-ATPases RUVBL1-

RUVBL2 in the R2TP co-chaperone revealed by cryo-EM. Sci Adv. 2019 May;5(5):eaaw1616.

38. Nano N, Houry WA. Chaperone-like activity of the AAA+ proteins Rvb1 and Rvb2 in the assembly of various complexes. Philos Trans R Soc Lond B Biol Sci. 2013 May 5;368(1617):20110399.

39. Houry WA, Bertrand E, Coulombe B. The PAQosome, an R2TP-Based Chaperone for Quaternary Structure Formation. Trends Biochem Sci. 2018 Jan;43(1):4–9.

40. Jha S, Gupta A, Dar A, Dutta A. RVBs Are Required for Assembling a Functional TIP60 Complex. Mol Cell Biol. 2013 Mar 15;33(6):1164–74.

41. Jónsson ZO, Jha S, Wohlschlegel JA, Dutta A. Rvb1p/Rvb2p Recruit Arp5p and Assemble a Functional Ino80 Chromatin Remodeling Complex. Mol Cell. 2004 Nov;16(3):465–77.

42. Wong MM, Cox LK, Chrivia JC. The Chromatin Remodeling Protein, SRCAP, Is Critical for Deposition of the Histone Variant H2A.Z at Promoters. J Biol Chem. 2007 Sep;282(36):26132–9.

43. Izumi N, Yamashita A, Iwamatsu A, Kurata R, Nakamura H, Saari B, et al. AAA+ Proteins RUVBL1 and RUVBL2 Coordinate PIKK Activity and Function in Nonsense-Mediated mRNA Decay. Sci Signal [Internet]. 2010 Apr 6 [cited 2022 Dec 9];3(116). Available from: https://www.science.org/doi/10.1126/scisignal.2000468

44. Guo H, Zhang XY, Peng J, Huang Y, Yang Y, Liu Y, et al. RUVBL1, a novel C-RAF-binding protein, activates the RAF/MEK/ERK pathway to promote lung cancer tumorigenesis. Biochem Biophys Res Commun. 2018 Apr;498(4):932–9.

45. Munoz DM, Cassiani PJ, Li L, Billy E, Korn JM, Jones MD, et al. CRISPR Screens Provide a Comprehensive Assessment of Cancer Vulnerabilities but Generate False-Positive Hits for Highly Amplified Genomic Regions. Cancer Discov. 2016 Aug 1;6(8):900–13.

46. Yuan XS, Wang ZT, Hu YJ, Bao FC, Yuan P, Zhang C, et al. Downregulation of RUVBL1 inhibits proliferation of lung adenocarcinoma cells by G1/S phase cell cycle arrest via multiple mechanisms. Tumor Biol. 2016 Dec;37(12):16015–27.

47. Yenerall P, Das AK, Wang S, Kollipara RK, Li LS, Villalobos P, et al. RUVBL1/RUVBL2 ATPase Activity Drives PAQosome Maturation, DNA Replication and Radioresistance in Lung Cancer. Cell Chem Biol. 2020 Jan;27(1):105-121.e14.

48. Li H, Tong X, Xu Y, Wang M, Dai H, Shi T, et al. Functional genetic variants of RUVBL1 predict overall survival of Chinese patients with epithelial ovarian cancer. Carcinogenesis. 2019 Oct 16;40(10):1209–19.

49. Sun Q, Li F, Yu S, Zhang X, Shi F, She J. Pontin Acts as a Potential Biomarker for Poor Clinical Outcome and Promotes Tumor Invasion in Hilar Cholangiocarcinoma. BioMed Res Int. 2018;2018:1–9.

50. Hristova RH, Stoynov SS, Tsaneva IR, Gospodinov AG. Deregulated levels of RUVBL1 induce transcription-dependent replication stress. Int J Biochem Cell Biol. 2020 Nov;128:105839.

51. Doench JG, Fusi N, Sullender M, Hegde M, Vaimberg EW, Donovan KF, et al. Optimized sgRNA design to maximize activity and minimize off-target effects of CRISPR-Cas9. Nat Biotechnol. 2016 Feb;34(2):184–91.

52. Gungor MZ, Uysal M, Ozturk M, Senturk S. Systematic Analysis of Cytostatic TGF-Beta Response in Mesenchymal-Like Hepatocellular Carcinoma Cell Lines. J Gastrointest Cancer [Internet]. 2021 Aug 31 [cited 2021 Oct 5]; Available from: https://link.springer.com/10.1007/s12029-021-00704-z

53. Livak KJ, Schmittgen TD. Analysis of Relative Gene Expression Data Using Real-Time Quantitative PCR and the 2−ΔΔCT Method. Methods. 2001 Dec;25(4):402–8.

54. UALCAN [Internet]. 2023. Available from: http://ualcan.path.uab.edu/

55. GEPIA [Internet]. 2023. Available from: http://gepia.cancer-pku.cn/

56. Senturk S, Shirole NH, Nowak DG, Corbo V, Pal D, Vaughan A, et al. Rapid and tunable method to temporally control gene editing based on conditional Cas9 stabilization. Nat Commun. 2017 Feb 22;8:14370.

57. Crane AM, Bhattacharya SK. The use of bromodeoxyuridine incorporation assays to assess corneal stem cell proliferation. Methods Mol Biol Clifton NJ. 2013;1014:65–70.

58. He X, Wang L, Riedel H, Wang K, Yang Y, Dinu CZ, et al. Mesothelin promotes epithelial-to-mesenchymal transition and tumorigenicity of human lung cancer and mesothelioma cells. Mol Cancer. 2017 Mar 14;16(1):63.

59. Itahana K, Campisi J, Dimri GP. Methods to detect biomarkers of cellular senescence: the senescence-associated beta-galactosidase assay. Methods Mol Biol Clifton NJ. 2007;371:21–31.

60. Rogakou EP, Pilch DR, Orr AH, Ivanova VS, Bonner WM. DNA Double-stranded Breaks Induce Histone H2AX Phosphorylation on Serine 139. J Biol Chem. 1998 Mar;273(10):5858–68.

61. Olive PL, Banáth JP. The comet assay: a method to measure DNA damage in individual cells. Nat Protoc. 2006 Jun;1(1):23–9.

62. Gyori BM, Venkatachalam G, Thiagarajan PS, Hsu D, Clement MV. OpenComet: an automated tool for comet assay image analysis. Redox Biol. 2014;2:457–65.

63. Small JV, Rottner K, Hahne P, Anderson KI. Visualising the actin cytoskeleton. Microsc Res Tech. 1999 Oct 1;47(1):3–17.

64. Mao YQ, Houry WA. The Role of Pontin and Reptin in Cellular Physiology and Cancer Etiology. Front Mol Biosci. 2017 Aug 24;4:58.

65. Zhang X, Ren J, Yan L, Tang Y, Zhang W, Li D, et al. Cytoplasmic Expression of Pontin in Renal Cell Carcinoma Correlates with Tumor Invasion, Metastasis and Patients' Survival. Sun LZ, editor. PLOS ONE. 2015 Mar 9;10(3):e0118659.

66. Assimon VA, Tang Y, Vargas JD, Lee GJ, Wu ZY, Lou K, et al. CB-6644 Is a Selective Inhibitor of the RUVBL1/2 Complex with Anticancer Activity. ACS Chem Biol. 2019 Feb 15;14(2):236–44.

67. Wadowski B, De Rienzo A, Bueno R. The Molecular Basis of Malignant Pleural Mesothelioma. Thorac Surg Clin. 2020 Nov;30(4):383–93.

68. Wang T, Wei JJ, Sabatini DM, Lander ES. Genetic screens in human cells using the CRISPR-Cas9 system. Science. 2014 Jan 3;343(6166):80–4.

69. Taniuchi K, Furihata M, Iwasaki S, Tanaka K, Shimizu T, Saito M, et al. RUVBL1 directly binds actin filaments and induces formation of cell protrusions to promote pancreatic cancer cell invasion. Int J Oncol. 2014 Jun;44(6):1945–54.

70. Lin D, Lin B, Bhanot H, Riou R, Abt NB, Rajagopal J, et al. RUVBL1 is an amplified epigenetic factor promoting proliferation and inhibiting differentiation program in head and neck squamous cancers. Oral Oncol. 2020 Dec;111:104930.

71. Durślewicz J, Jóźwicki J, Klimaszewska-Wiśniewska A, Zielińska A, Antosik P, Grzanka D, et al. High expression of RUVBL1 and HNRNPU is associated with poor overall survival in stage I and II non-small cell lung cancer patients. Discov Oncol. 2022 Oct 15;13(1):106.

72. Venteicher AS, Meng Z, Mason PJ, Veenstra TD, Artandi SE. Identification of ATPases pontin and reptin as telomerase components essential for holoenzyme assembly. Cell. 2008 Mar 21;132(6):945–57.

73. Sun F, Wang X, Hu J, Liu J, Wang X, Jia W, et al. RUVBL1 promotes enzalutamide resistance of prostate tumors through the PLXNA1-CRAF-MAPK pathway. Oncogene. 2022 Jun 3;41(23):3239–50.

10. APPENDIX

İZMİR BİYOTIP VE GENOM MERKEZİ
GİRİŞİMSEL OLMAYAN ARAŞTIRMALAR ETİK KURULU (İBG-GOEK)
KARARI

Toplantı Tarihi	: 24/09/2021	**Toplantı Günü**	: Cuma
Toplantı Sayısı	: 10	**Toplantı Saati**	: 10:30

Sayın Doç. Dr. Şerif ŞENTÜRK,

2021-033 Protokol No'lu; sorumlusu olduğunuz "RUVBL-1 Geninin Malign Plevral Mezotelyomadaki Moleküler Rolünün Araştırılması" başlıklı araştırmanın uygulanmasında etik açıdan sakınca olmadığına oy birliği ile karar verilmiştir.

Bilgilerinizi ve gereğini rica ederiz.

Dr. Serap ERKEK ÖZHAN
Başkan V.

Pandemi süresince online ortamda gerçekleştirilen toplantımızda alınan kararlar tek imzalı olarak düzenlenmektedir. Pandemi sona erdikten sonra ıslak imzalı karar belgesi teslim edilecektir.

İZMİR BİYOTIP VE GENOM MERKEZİ
GİRİŞİMSEL OLMAYAN ARAŞTIRMALAR ETİK KURULU (İBG-GOEK)
KARARI

Toplantı Tarihi	: 24/09/2021	**Toplantı Günü**	: Cuma
Toplantı Sayısı	: 10	**Toplantı Saati**	: 10:30

Sayın Doç. Dr. Şerif ŞENTÜRK,

2021-033 Protokol No'lu; sorumlusu olduğunuz "RUVBL-1 Geninin Malign Plevral Mezotelyomadaki Moleküler Rolünün Araştırılması" başlıklı araştırmanın uygulanmasında etik açıdan sakınca olmadığına oy birliği ile karar verilmiştir.

Bilgilerinizi ve gereğini rica ederiz.

Prof. Dr. H. Alper BAĞRIYANIK **Başkan** (Katılmadı)	**Prof. Dr. Hilmi ORHAN** **Başkan Yardımcısı** (Katılmadı)
Prof. Dr. Sedef AKGÜNGÖR **Üye**	**Prof. Dr. İnci ALACACIOĞLU** **Üye**
Prof. Dr. Gülgün OKTAY **Üye** (Katılmadı)	**Dr. Serap ERKEK ÖZHAN** **Üye**
Prof. Dr. Şermin GENÇ **Üye** (Katılmadı)	**Doç. Dr. Canan Aslı YILDIRIM** **Üye**
Doç. Dr. Can KÜÇÜK **Üye**	**Dr. Öğr. Üyesi Yavuz OKTAY** **Üye**



MEDİNE ZEYNEP GÜNGÖR

Kişisel Bilgiler

İletişim Bilgileri

İletişim Adresi

Telefon

E-posta

İnternet Sayfası

Öğrenim Bilgileri

04 Şubat 2020 - Şu Anda (3 yıl 1 ay)
Yüksek Lisans, Tezli Program, DOKUZ EYLÜL ÜNİVERSİTESİ, TÜRKİYE
İZMİR ULUSLARARASI BİYOTIP VE GENOM ENSTİTÜSÜ, MOLEKÜLER BİYOLOJİ VE GENETİK (YL) (TEZLİ) (İNGİLİZCE)
Diploma Numarası: -

03 Eylül 2014 - 19 Haziran 2019 (4 yıl 10 ay)
Lisans, Anadal/Normal Öğretim, İSTANBUL ÜNİVERSİTESİ, TÜRKİYE
FEN FAKÜLTESİ, MOLEKÜLER BİYOLOJİ VE GENETİK PR.
Diploma Numarası: 24585
Ağırlıklı Genel Not Ortalaması: 3.06 / 4.0

Bilimsel Teknolojik Faaliyet Alanları

Bilimsel Teknolojik Faaliyet Alanı Bilgileri

Temel Bilimler -- Yaşam Bilimleri -- Moleküler Biyoloji ve Genetik -- Kanser Moleküler Biyolojisi

Ar-Ge Yetkinlik

Makaleler

M. Z. GÜNGÖR, M. UYSAL & Ş. ŞENTÜRK, The Bright and the Dark Side of TGF-ß Signaling in Hepatocellular Carcinoma: Mechanisms, Dysregulation, and Therapeutic Implications, Cancers, 2022, 2072-6694, 14, 4, 940.

M. Z. GÜNGÖR, M. UYSAL & Ş. ŞENTÜRK, Systematic Analysis of Cytostatic TGF-Beta Response in Mesenchymal-Like Hepatocellular Carcinoma Cell Lines, Journal of Gastrointestinal Cancer, 2021, 1941-6628, 52, 4, 1320.

Bildiriler

M. Z. GÜNGÖR, E. ÇAKIROĞLU, B. AKDEMİR & Ş. ŞENTÜRK, The Molecular Role of Ruvbl1 Gene On Cancer Cell Phenotypes In Malignant Pleural Mesothelioma, Poster Sunumu, 33. TBS International Biochemistry Congress, 26 Ekim 2022, 30

Ekim 2022.

TÜBİTAK Burs ve Destekleri

Proje Bilgileri

221Z170, RUVBL1 Geninin Malign Plevral Mezotelyomadaki Moleküler Rolünün İncelenmesi, 1002 - Hızlı Destek, Burslu, Yürürlükte, ARDEB, KBAG - Kimya Biyoloji Araştırma Destek Grubu, Projeye Katılma/Ayrılma Tarihleri: 01.02.2022 - 01.02.2023, Proje Başlangıç/Bitiş Tarihleri: 01.02.2022 - 01.02.2023.

BİDEB Destekleri

MEDİNE ZEYNEP GÜNGÖR, Araştırma Burs ve Destekleri Müdürlüğü, 2247-C Stajyer Araştırmacı Burs Programı (STAR)- Star Lisans, Destek Sona Erdi, 2020 - 1, 01.06.2020 - 01.06.2021.

Panelistlik/İzleyicilik/Raportörlük Sayısı

Hakemlik/Panelistlik/Dış Danışmanlık Sayısı	ARDEB/BİDEB 0	TEYDEB 0	Toplam 0
İzleyicilik/Danışmanlık Sayısı	ARDEB/BİDEB 0	TEYDEB 0	Toplam 0
Raportörlük Sayısı	ARDEB/BİDEB 0	TEYDEB 0	Toplam 0

Oluşturma Zamanı: 16 Şubat 2023 12:32:20